Electronic Supplementary Material (ESI) for ChemComm.

Supporting Information

Affinity modulation of photoresponsive hosts for fullerenes. Light-gated corannulene tweezers.

Héctor Barbero, Sergio Ferrero, Lucía Álvarez-Miguel, Patricia Gómez-Iglesias, Daniel Miguel and Celedonio M. Álvarez*

GIR MIOMeT, IU CINQUIMA/Química Inorgánica, Facultad de Ciencias, Universidad de Valladolid, E-47011, Valladolid, Spain

---

Table of Contents

General Methods

All reagents were purchased from regular suppliers and used without further purification. Solvents were of analytical grade or spectrophotometric grade. They were either used as purchased or dried according to procedures described elsewhere.[1] All reactions under inert atmosphere (when needed) were performed with standard Schlenk techniques. Column chromatography separations were carried out by using Silica gel 60 (particle size 0.040-0.063 mm; 230-400 mesh; Merck, Germany) as the stationary phase and TLCs were performed on precoated silica gel plates (0.25 mm thick, 60 F_{254}, Merck, Germany) and observed under UV light. NMR spectra were recorded on Agilent DD2 500 instruments. ^{1}H and ^{13}C NMR chemical shifts are reported in parts per million (ppm) and are referenced to TMS, using solvents as an internal reference. Coupling constants (*J*) are reported in hertz (Hz). Standard abbreviations used to indicate multiplicity: s = singlet, d = doublet, t=triplet, m = multiplet. ^{1}H and ^{13}C assignments were performed by utilizing 2D NMR methods (COSY, DQCOSY, zTOCSY, band selective ROESY, band selective HSQC, band selective HMBC, and gradient crisis HMBC). Due to low solubility and fast relaxation properties, $^{13}C\{^{1}H\}$ spectra were recorded under nonstandard conditions, which were: pulse angle=90º, acquisition time=250ms, relaxation delay=5ms, number of scans=700000-850000. Even under these conditions, some quaternary carbon atoms were not detected, but they were located thanks to HMBC. In those cases the abbreviation used was *in* to denote that the carbon has been detected indirectly. All peaks reported correspond to E isomer. High resolution mass spectra were recorded at mass spectrometry service of the Laboratory of Instrumental Techniques of the University of Valladolid (L.T.I., www.laboratoriotecnicasinstrumentales.es). A MALDI-TOF system (MALDI-TOF) Bruker Autoflex Speed (N_2 laser (337 nm, pulse energy 100μJ, 1 ns), acceleration voltage 19 kV, reflector positive mode was used. Trans-2-[3-(4-tert-butylphenyl)-2-methyl-2-propenylidene]malonitrile (DCTB) and 1,8,9-anthracenetriol, 1,8-dihydroxy-9(10H)-anthracenone (dithranol) were used as matrixes. A UPLC-MS system (UPLC: Waters ACQUITY H-class UPLC; MS: Bruker Maxis Impact) by electrospray ionization (ESI positive and negative) was utilized as well. HRMS spectra were analyzed using Bruker DataAnalysis 4.1© (www.bruker.com). UV/Vis spectra were recorded in a Shimadzu UV-1603 with spectrophotometric grade solvents. UV/vis absorption wavelengths (λ) are reported in nanometers (nm), and molar absorption coefficients (ε) are reported in $M^{-1}\cdot cm^{-1}$. Photoisomerization experiments were carried out at room temperature with a PELCO UVC2 UV Cryo Chamber or a HQRP 21 LED Ultraviolet Flashlight.

Synthesis Overview

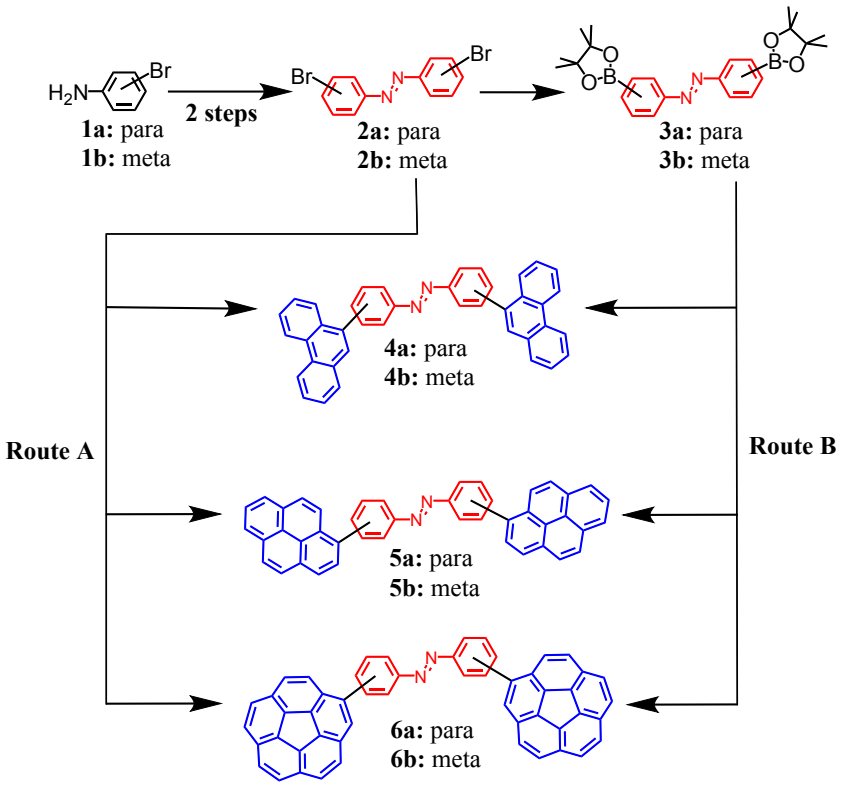

Scheme S1: Synthesis routes to achieve final azobenzene-functionalized polyaromatic hydrocarbons.

Both routes involve oxidation of *para* or *meta*-bromo aniline (**1a** and **1b**) and subsequent coupling to give azobenzene precursors **2a** and **2b**. From that point, we decided that the most straightforward method was a C-C cross coupling reaction with functionalized aromatic molecules. Pinacol boronate esters were chosen as candidates because of their well-known better stability and functional groups tolerance if compared to stannanes or Grignard reagents, for instance.[2]

Thus, there are two options to carry out Suzuki coupling in order to obtain the final compounds. One option is to functionalize the polyaromatic compound with pinacol ester (Route A) and react it with compounds **2**. However, we found several difficulties when performing chromatographic separations due to their tendency to elute along with halogenated non-reacted starting materials, thus decreasing dramatically the final yield, especially for **6a**. In contrast, the second option turned out to be a more efficient method. Instead of functionalizing the aromatic compound with pinacol ester, we decided to functionalize the azobenzene molecule (Route B), leading to compounds **3** in excellent yield. These compounds were cross-coupled with the suitable brominated aromatic molecule. In this route, yields were increased as well as the ease of their separation because starting materials and byproducts have very different retention factors.

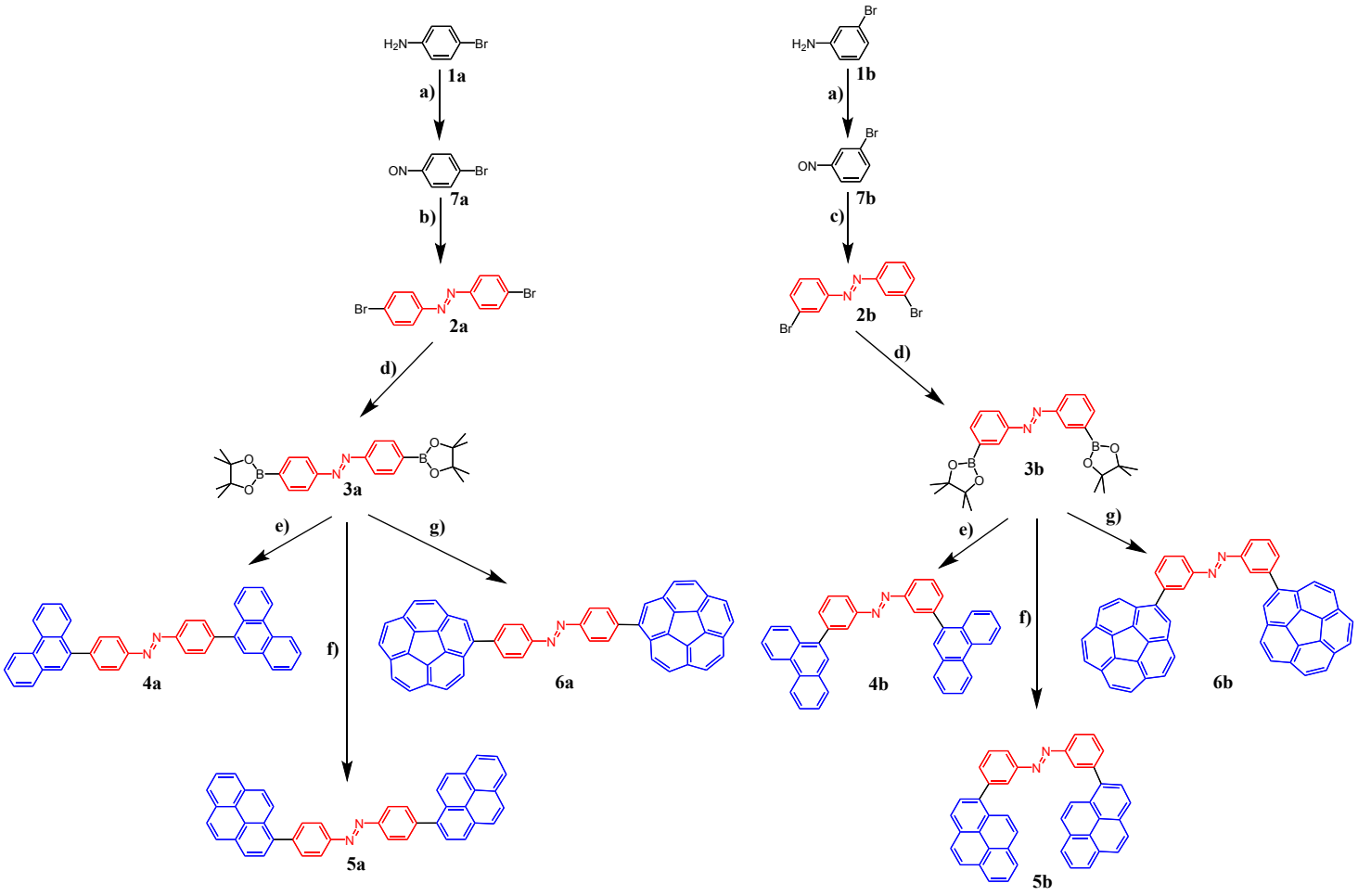

Scheme S2: Synthesis of azobenzene derivatives by Method A. Reagents and Conditions: a) Oxone®, DCM/H_2O. b) 4-bromoaniline, HAcO. c) 3-Bromoaniline, HAcO. d) $B_2(pin)_2$, [$PdCl_2$(dppf)], AcOK, dioxane. e) 9-bromophenanthrene, [$PdCl_2$(dppf)], ^{t}BuONa, toluene. f) 1-bromopyrene, [$PdCl_2$(dppf)], ^{t}BuONa, toluene. g) Bromocorannulene, [$PdCl_2$(dppf)], ^{t}BuONa, toluene.

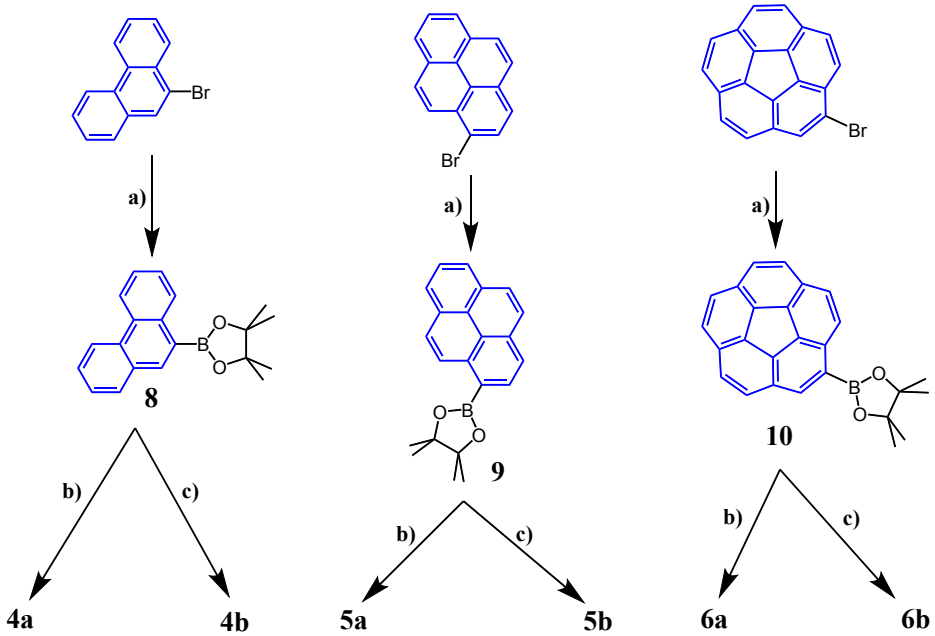

Scheme S3: Synthesis of azobenzene derivatives by Method B. Reagents and Conditions: a) $B_2(pin)_2$, [$PdCl_2$(dppf)], AcOK, dioxane. b) **2a**, [$PdCl_2$(dppf)], ^{t}BuONa, toluene. c) **2b**, [$PdCl_2$(dppf)], ^{t}BuONa, toluene.

Synthesis procedures

All nitrosoarenes and azobenzenes where prepared according to Prewisch and Rück-Braun procedure.[3]
Corannulene and bromocorannulene were prepared by using current methods. [4]

General method for boronate esters preparation:

Bromoarene (0.3mmol), bis(pinacolato)diboron (1.5eq per bromine atom), [$PdCl_2$(dppf)] (0.05eq per bromine atom) and AcOK (3eq per bromine atom) were mixed in a Schlenk flask under inert atmosphere. 3mL of dry dioxane were added and the mixture was degassed. Then, it was refluxed for 24h. Solvent was removed under vacuum before a purification by column chromatography.

General method for Suzuki coupling:

Method A: Azo compound (**3a** or **3b**) (34.7mg, 0.08mmol), bromoarene (0.17 mmol), [$PdCl_2$(dppf)] (23.4mg 0.032mmol) and ^{t}BuONa (46.1mg, 0.48mmol) were mixed in a Schlenk flask under inert atmosphere. 6mL of dry toluene were added and the mixture was degassed. Then, it was refluxed overnight and finally purified by column chromatography after evaporating off the solvent.
Method B: Azo compound (**2a** or **2b**) (27.2mg, 0.08mmol), borylated arene (**8**, **9** or **10**) (0.17 mmol), [$PdCl_2$(dppf)] (23.4mg 0.032mmol) and ^{t}BuONa (46.1mg, 0.48mmol) were mixed in a Schlenk flask under inert atmosphere. 6mL of dry toluene were added and the mixture was degassed. Then, it was refluxed overnight and finally purified by column chromatography after removing the solvent *in vacuo*.

Characterization details

Spectral data for compounds **7a**, **7b**, **2a**, **2b**, **3a**, **8**, **9** and **10** are according to those reported in literature. [5]

4a

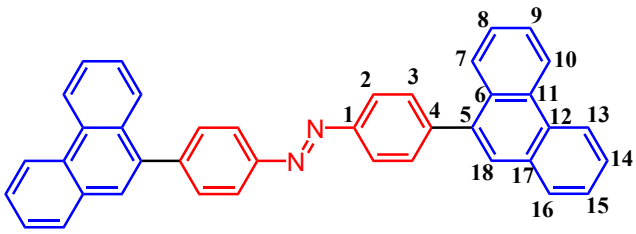

Column chromatography conditions: SiO_2 gel, hexane/$CHCl_3$ (2:1 - 1:1 - 1:2 - 1:3). Yellow solid. Yield: 95% (Method A), 90% (Method B). ^{1}H NMR (500 MHz, $CDCl_3$) δ 8.82 (d, J = 8.4 Hz, 1H, H_{10}), 8.76 (d, J = 8.3 Hz, 1H, H_{13}), 8.14 (d, J = 8.5 Hz, 2H, H_2), 8.00 (dd, J = 8.4, 1.1 Hz, 1H, H_7), 7.95 (dd, J = 8.1, 1.5 Hz, 1H, H_{16}), 7.78 (s, 1H, H_{18}), 7.76 (d, J = 8.5 Hz, 2H, H_3), 7.74 - 7.79 (m, 2H, H_9+H_{14}), 7.65 (ddd, J = 8.1, 7.0, 1.2 Hz, 1H, H_{15}), 7.59 (ddd, J = 8.4, 6.9, 1.2 Hz, 1H, H_8). ^{13}C{^{1}H} NMR (126 MHz, $CDCl_3$) δ 152.16 (C_1), 143.91 (C_4), 138.10 (C_5), 131.58 (C_{17}), 131.09 (C_3), 130.97 (C_6), 130.85 (C_{11}), 130.27 (C_{12}), 128.94 (C_{16}), 127.83 (C_{18}), 127.14 (C_{15}), 127.02 (C_{14}), 126.93 (C_7), 126.84 (C_8), 126.81 (C_9), 123.17 (C_{10}), 123.09 (C_2), 122.74 (C_{13}). HRMS (MALDI-TOF): *m/z* = 535.2178 $[M+H]^+$ (calcd. 535.2169 for $C_{40}H_{27}N_2$). UV/vis (chloroform): λ 258 (ε = 104500), 300 (ε = 29567), 361 (ε = 27867).

5a

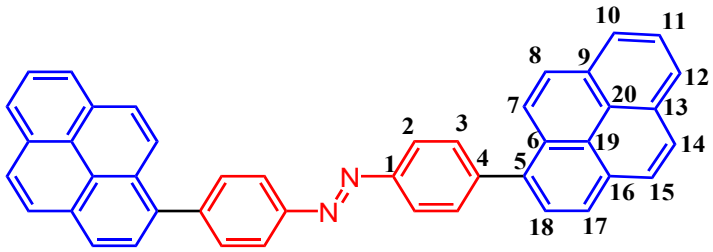

Column chromatography conditions: SiO_2 gel, hexane/$CHCl_3$ (2:1 - 1:1 - 1:2 - $CHCl_3$). Orange solid. Yield: 70% (Method A), 58% (Method B). ^1H NMR (500 MHz, $CDCl_3$) δ 8.28 (d, J = 7.9 Hz, 1H, H_{17}), 8.26 (d, J = 9.6 Hz, 1H, H_7), 8.24 (dd, J = 7.5, 1.0 Hz, 1H, H_{12}), 8.22 – 8.19 (m, 3H, H_2+H_{10}), 8.14 (s, 2H, H_{15}+H_{14}), 8.10 (d, J = 9.6 Hz, 1H, H_8), 8.08 (d, J = 7.9 Hz, 1H, H_{18}), 8.06 (t, J = 7.5 Hz, 1H, H_{11}), 7.86 (d, J = 8.3 Hz, 2H, H_3). $^{13}C\{^1H\}$ NMR (126 MHz, $CDCl_3$) δ 151.80 (C_1, *in*), 144.17 (C_4, *in*), 136.72 (C_5, *in*), 131.62 (C_3), 130.90 (C_{19}, *in*), 128.50 (C_6, *in*), 127.99 (C_8), 127.87 (C_{14} or C_{15}), 127.63 (C_{18}), 127.59 (C_{14} or C_{15}), 126.29 (C_{11}), 125.48 (C_{12}), 125.20 (C_7 + C_{10}), 124.92 (C_9, *in*), 124.85 (C_{20}, *in*), 124.89 (C_{17}), 123.17 (C_2). HRMS (MALDI-TOF): *m/z* = 582.2083 $[M]^+$ (calcd. 582.2091 for $C_{44}H_{26}N_2$). UV/vis (chloroform): λ 246 (ε = 39440), 268 (ε = 16860), 279 (ε = 20860), 327 (ε = 17240), 343 (ε = 19920), 380 (ε = 14360).

6a

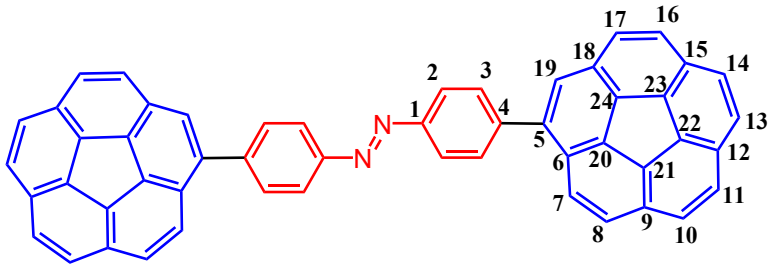

Column chromatography conditions: SiO_2 gel, hexane/$CHCl_3$ (1:1 - 1:2 - 1:5 - $CHCl_3$ - $CHCl_3$/MeOH 95:5). Orange solid. Yield: 60% (Method A), 51% (Method B). ^1H NMR (500 MHz, $CDCl_3$) δ 8.19 (d, J = 8.4 Hz, 2H, H_2), 8.00 (d, J = 8.4 Hz, 2H, H_3), 8.00 (s, 1H, H_{19}), 7.91 – 7.88 (m, 3H, H_7+H_8+H_{17}), 7.86 – 7.82 (m, 5H, H_{10}+H_{11}+H_{13}+H_{14}+H_{16}). $^{13}C\{^1H\}$ NMR (126 MHz, $CDCl_3$) δ 152.10 (C_1, *in*), 142.50 (C_5, *in*), 142.40 (C_4, *in*), 136.30 (C_6+C_{20}, *in*), 136.20 (C_{18},C_{21} or C_{23} + C_{24}, *in*), 135.85 (C_{12}, C_{15} or C_{22} + C_{12}, C_{15} or C_{22}, *in*), 135.50 (C_9, *in*), 130.95 (C_{12}, C_{15}, C_{18}, C_{21}, C_{22} or C_{23} + C_{12}, C_{15}, C_{18}, C_{21}, C_{22} or C_{23}, *in*), 130.70 (C_{19}, *in*), 127.60 (C_{10}, C_{11}, C_{13}, C_{14} or C_{16}, *in*), 127.50 (C_7, C_8 or C_{17}, *in*), 127.40 ($C_{10,}$ C_{11}, C_{13}, C_{14} or C_{16}, *in*), 127.10 ($C_{10,}$ C_{11}, C_{13}, C_{14} or C_{16} + $C_{10,}$ C_{11}, C_{13}, C_{14} or C_{16}, *in*), 127.00 ($C_{7,}$ C_8 or C_{17}, *in*), 126.90 (C_7, C_8 or C_{17} + C_{10}, C_{11}, C_{13}, C_{14} or C_{16}, *in*), 126.20 (C_3, *in*), 123.40 (C_2, *in*). HRMS (MALDI-TOF): *m/z* = 679.2248 $[M+H]^+$ (calcd. 679.2169 for $C_{52}H_{27}N_2$). UV/vis (chloroform): λ 296 (ε = 28221), 382 (ε = 25068).

3b

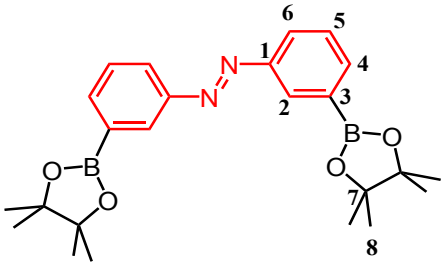

Column chromatography conditions: SiO_2 gel, hexane/AcOEt (4:1 - 2:1 - 1:1). Red solid. Yield: 95%. ^1H NMR (500 MHz, $CDCl_3$) δ 8.36 (t, J = 1.3 Hz, 1H, H_2), 8.01 (ddd, J = 7.9, 2.2, 1.3 Hz, 1H, H_6), 7.90 (dt, J = 7.9, 1.3 Hz, 1H, H_4), 7.52 (t, J =

7.9 Hz, 1H, H_5), 1.38 (s, 12H, H_8). $^{13}C\{^1H\}$ NMR (126 MHz, $CDCl_3$) δ 152.25 (C_1), 137.31 (C_4), 129.46 (C_2), 128.68 (C_5), 125.49 (C_6), 84.20 (C_7), 25.06 (C_8). HRMS (ESI-TOF): *m/z* = 435.2630 $[M+H]^+$ (calcd. 435.2629 for $C_{24}H_{33}B_2N_2O_4$). UV/vis (chloroform): λ 241 (ε = 15206), 322 (ε = 17387).

4b

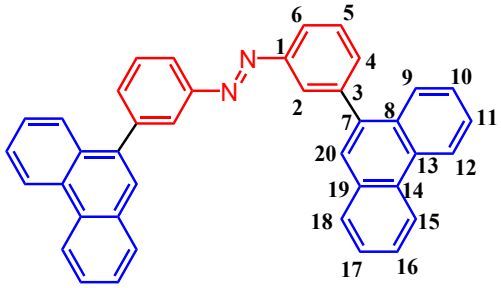

Column chromatography conditions: SiO_2 gel, hexane/$CHCl_3$ (2:1 - 1:1 - 1:2). Yellow solid. Yield: 75% (Method A), 70% (Method B). ^1H NMR (500 MHz, $CDCl_3$) δ 8.80 (d, J = 8.3 Hz, 1H, H_{12}), 8.74 (d, J = 8.3 Hz, 1H, H_{15}), 8.15 (s, 1H, H_2), 8.06 – 8.02 (m, 1H, H_4), 7.96 (dd, J = 8.3, 1.4 Hz, 1H, H_9), 7.92 (dd, J = 7.8, 0.9 Hz, 1H, H_{18}), 7.77 (s, 1H, H_{20}), 7.72 – 7.66 (m, 4H, H_5+H_6+H_{11}+H_{16}), 7.63 (ddd, J = 7.8, 7.0, 1.2 Hz, 1H, H_{17}), 7.56 (ddd, J = 8.3, 6.9, 1.2 Hz, 1H, H_{10}). $^{13}C\{^1H\}$ NMR (126 MHz, $CDCl_3$) δ 152.89 (C_1), 141.83 (C_3, *in*), 138.07 (C_7, *in*), 132.89 (C_5, C_6, C_{11} or C_{16}), 131.53 (C_{19}, *in*), 131.05 (C_8), 130.80 (C_{13}), 130.25 (C_{14}), 129.24 (C_5, C_6, C_{11} or C_{16}), 128.90 (C_{18}), 127.91 (C_{20}), 127.06 (C_{17}), 126.91 (C_5, C_6, C_{11}, C_{16} + C_9), 126.82 (C_{10}), 126.73 (C_5, C_6, C_{11} or C_{16}), 124.52 (C_2), 123.12 (C_{12}), 122.71 (C_{15}), 122.27 (C_4). HRMS (MALDI-TOF): *m/z* = 534.2126 $[M]^+$ (calcd. 534.2091 for $C_{40}H_{26}N_2$). UV/vis (chloroform): λ 260 (ε = 108767), 302 (ε = 35967), 333 (ε = 19833).

5b

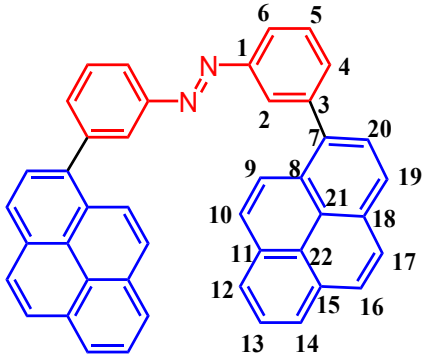

Column chromatography conditions: SiO_2 gel, hexane/$CHCl_3$ (1:1 - 1:2). Orange solid. Yield: 82% (Method A), 67% (Method B). ^1H NMR (500 MHz, $CDCl_3$) δ 8.26 (d, J = 7.9 Hz, 1H, H_{19}), 8.24 (t, J = 1.5 Hz, 1H, H_2), 8.23 (d, J = 9.3 Hz, 1H, H_9), 8.21 (dd, J = 7.6, 1.1 Hz, 1H, H_{14}), 8.18 (dd, J = 7.6, 1.1 Hz, 1H, H_{12}), 8.12 (s, 2H, H_{16}+H_{17}), 8.08 (dt, J = 7.9, 1.5 Hz, 1H, H_6), 8.06 (d, J = 7.9 Hz, 1H, H_{20}), 8.05 (d, J = 9.3 Hz, 1H, H_{10}), 8.02 (t, J = 7.6 Hz, 1H, H_{13}), 7.77 (dt, J = 7.9, 1.5 Hz, 1H, H_4), 7.73 (t, J = 7.9 Hz, 1H, H_5). $^{13}C\{^1H\}$ NMR (126 MHz, $CDCl_3$) δ 152.95 (C_1), 142.44 (C_3), 136.70 (C_7, *in*), 133.40 (C_4), 131.12 (C_{15}), 130.90 (C_{11}, *in*), 130.80 (C_8, *in*), 129.31 (C_5), 128.70 (C_{22}), 127.91 (C_{10}), 127.74 (C_{20} + C_{16} or C_{17}), 127.56 (C_{16} or C_{17}), 126.22 (C_{13}), 125.38 (C_{14}), 125.18 (C_9), 125.13 (C_2 + C_{12}), 124.85 (C_{19}), 124.76 (C_{18}), 122.02 (C_6). HRMS (MALDI-TOF): *m/z* = 582.2076 $[M]^+$ (calcd. 582.2091 for $C_{44}H_{26}N_2$). UV/vis (chloroform): λ 246 (ε = 62900), 271 (ε = 36450), 281 (ε = 52025), 350 (ε = 52100).

6b

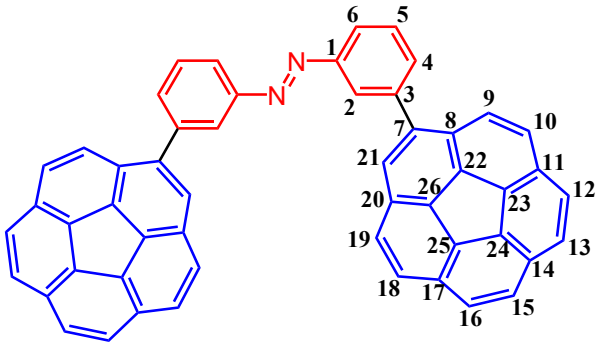

Column chromatography conditions: SiO_2 gel, hexane/$CHCl_3$ (1:1 - 1:5 - $CHCl_3$). Orange solid. Yield: 57% (Method A), 50% (Method B). ^1H NMR (500 MHz, $CDCl_3$) δ 8.38 (t, J = 1.9 Hz, 1H, H_2), 8.07 (ddd, J = 8.0, 1.9, 1.2 Hz, 1H, H_6), 7.99 (s, 1H, H_{21}), 7.94 (dt, J = 8.0, 1.2 Hz, 1H, H_4), 7.88 ($d_{ABsystem}$, J_{AB} = 8.7 Hz, 1H, H_9), 7.87 ($d_{ABsystem}$, J_{AB} = 4.6 Hz, 1H, H_{19}), 7.86 ($d_{ABsystem}$, J_{AB} = 4.6 Hz, 1H, H_{18}), 7.84 ($d_{ABsystem}$, J_{AB} = 4.6 Hz, 1H, H_{16}), 7.83 ($d_{ABsystem}$, J_{AB} = 4.6 Hz, 1H, H_{15}), 7.82 ($d_{ABsystem}$, J_{AB} = 5.1 Hz, 1H, H_{12}), 7.81 ($d_{ABsystem}$, J_{AB} = 5.1 Hz, 1H, H_{13}), 7.79 ($d_{ABsystem}$, J_{AB} = 8.7 Hz, 1H, H_{10}), 7.73 (t, J = 8.0 Hz, 1H, H_5). $^{13}C\{^1H\}$ NMR (126 MHz, $CDCl_3$) δ 153.10 (C_1, *in*), 140. 80 (C_3 + C_7), 136.38 (C_{17} or C_{26}, *in*), 136.34 (C_{20} or C_{25}, *in*), 136.28 (C_{11} or C_{22}, *in*), 136.24 (C_{17} or C_{24}, *in*), 136.22 (C_{17} or C_{26}, *in*), 135.90 (C_{11} or C_{24}, *in*), 135.80 (C_{23}, *in*), 135.70 (C_{11} or C_{24}, *in*), 135.50 (C_8, *in*), 135.40 (C_{17} or C_{25}, *in*), 132.60 (C_4), 129.46 (C_5), 127.55 (C_{13}), 127.42 (C_{19}), 127.32 (C_{15}), 127.09 (C_{10} + C_{16}), 127.00 (C_9), 126.90 (C_{12}), 126.80 (C_{18}), 126.24 (C_{21}), 124.50 (C_2) 122.00 (C_6, *in*). HRMS (MALDI-TOF): *m/z* = 678.2188 $[M]^+$ (calcd. 678.2091 for $C_{52}H_{26}N_2$). UV/vis (chloroform): λ 257 (ε = 100333), 295 (ε = 79400), 318 (ε = 43800).

Additional spectra

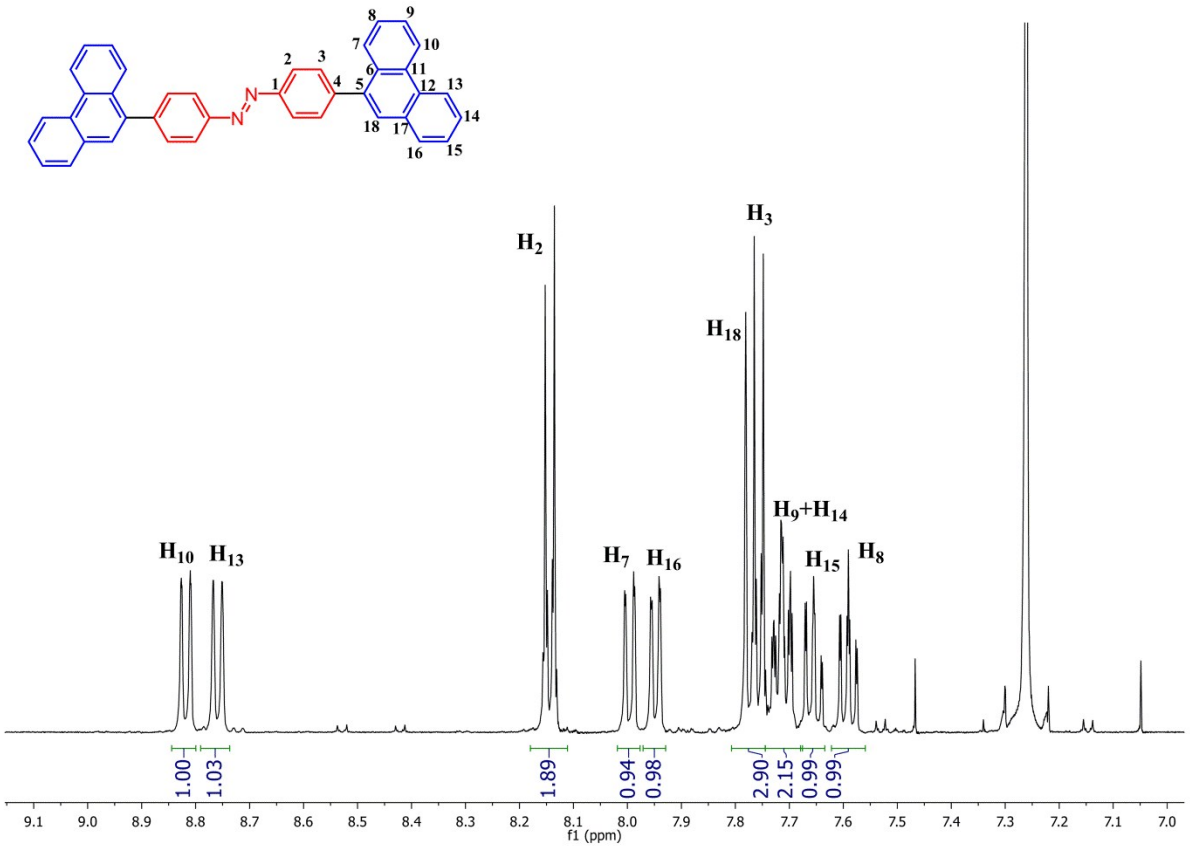

Figure S1: ^{1}H NMR (500MHz, $CDCl_3$) of **4a**.

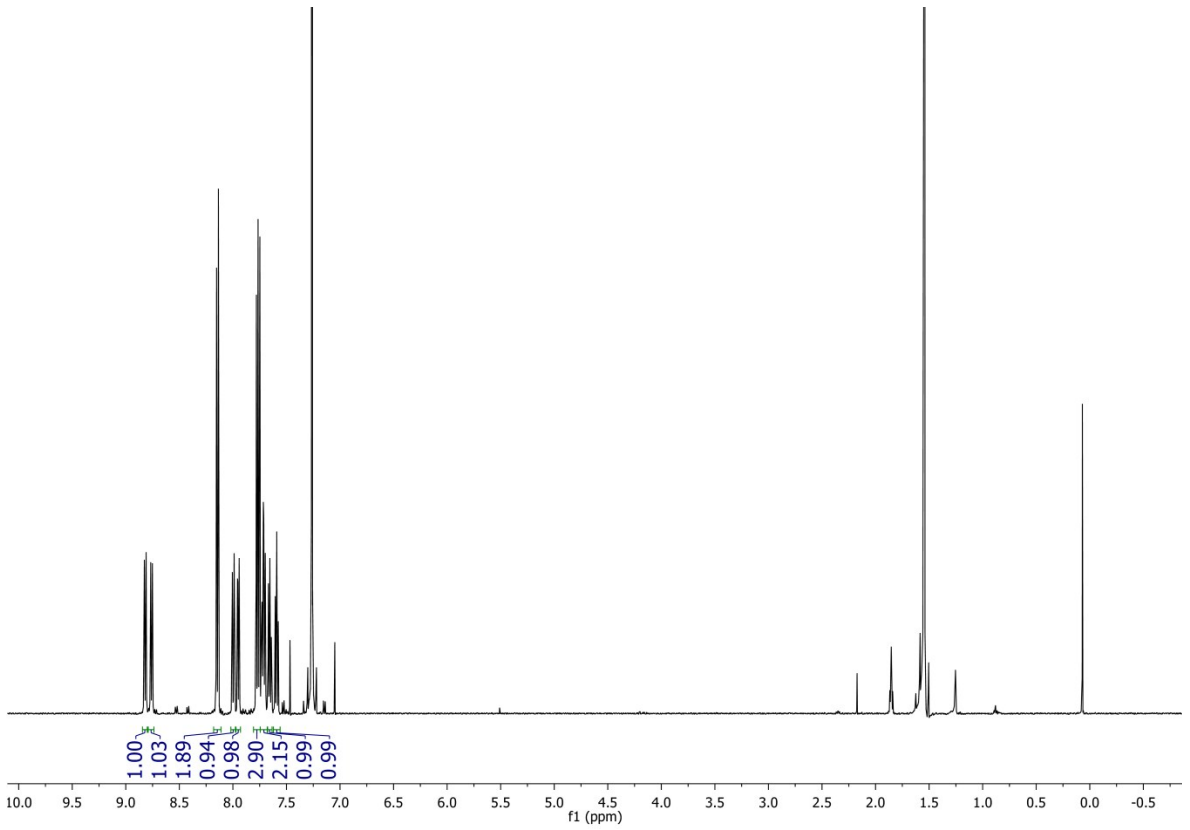

Figure S2: Full ^{1}H NMR (500MHz, $CDCl_3$) of **4a**.

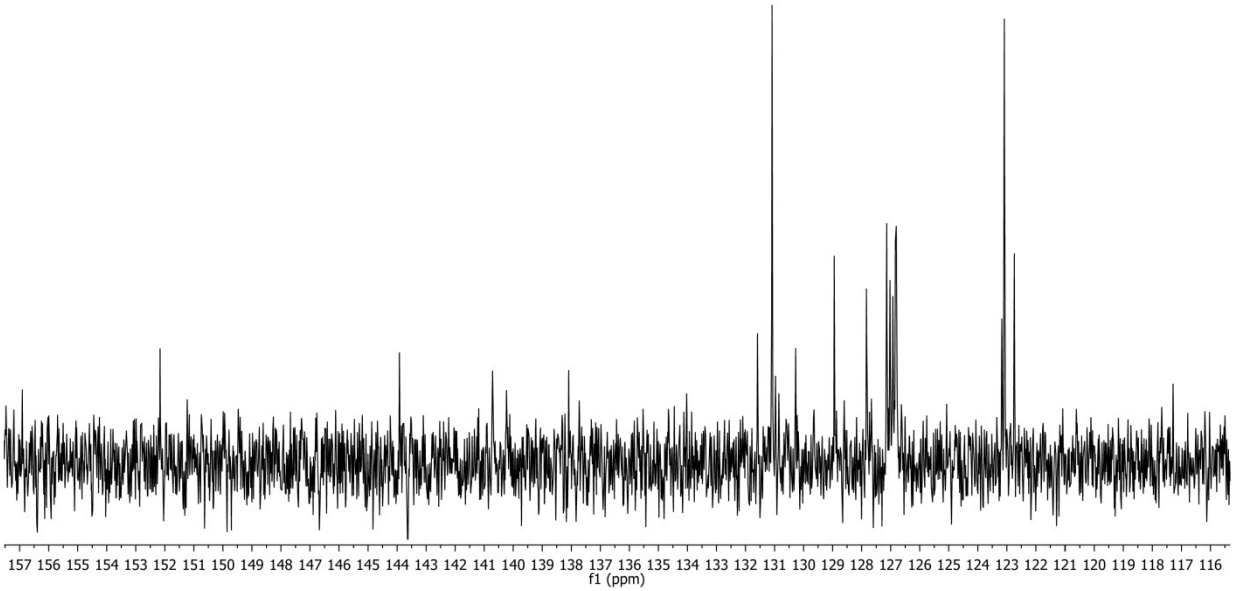

Figure S3: $^{13}C\{^{1}H\}$ NMR (126MHz, $CDCl_3$) of **4a**.

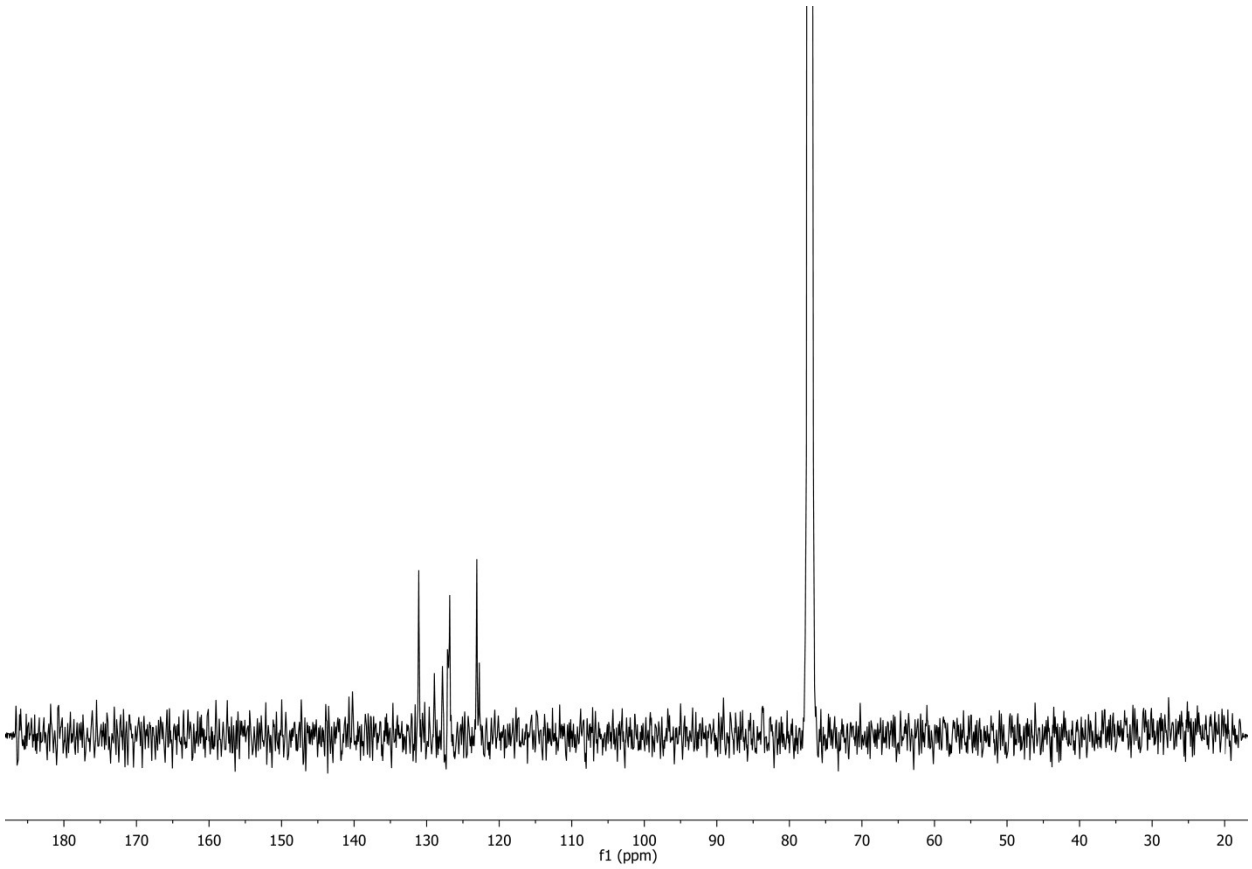

Figure S4: Full $^{13}C\{^{1}H\}$ NMR (126MHz, $CDCl_3$) of **4a**.

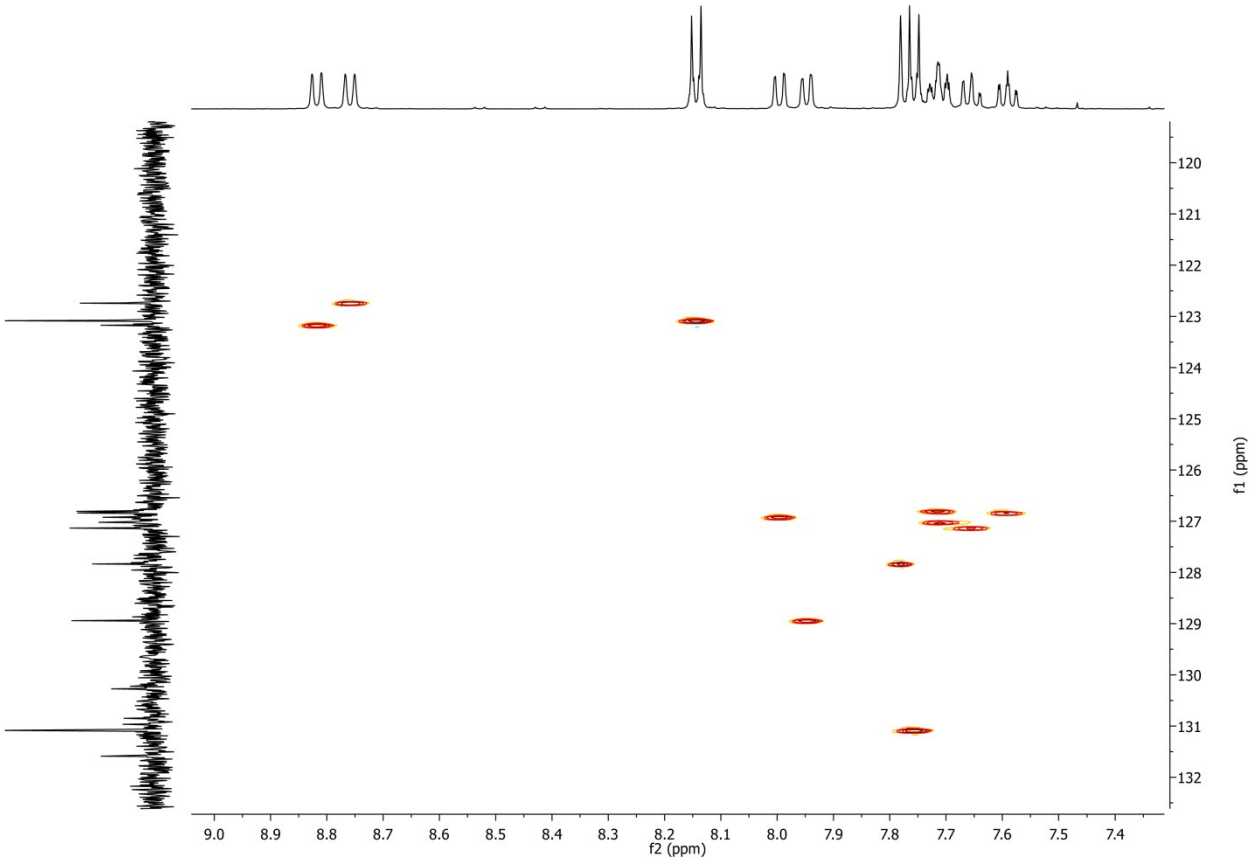

Figure S5: ^{1}H - ^{13}C band selective HSQC ($CDCl_3$) of **4a**.

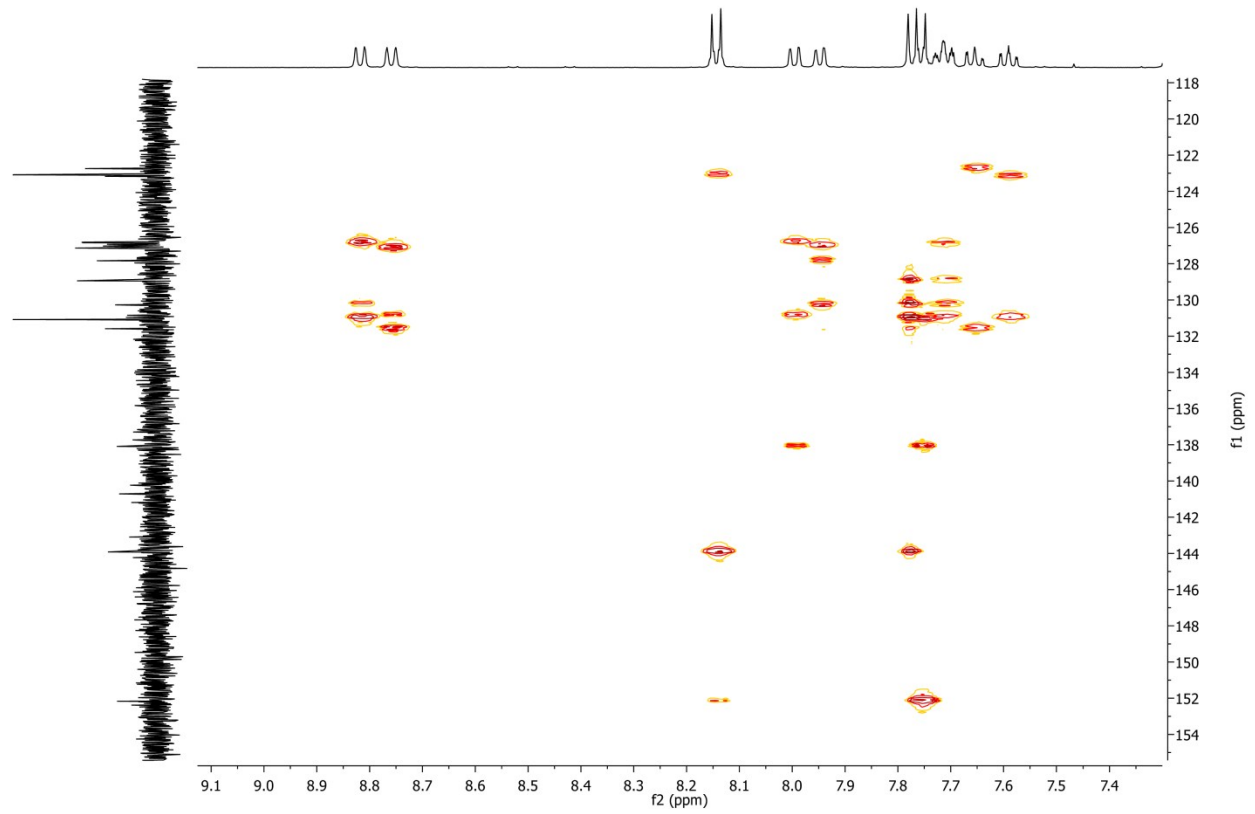

Figure S6: ^{1}H - ^{13}C band selective HMBC ($CDCl_3$) of **4a**.

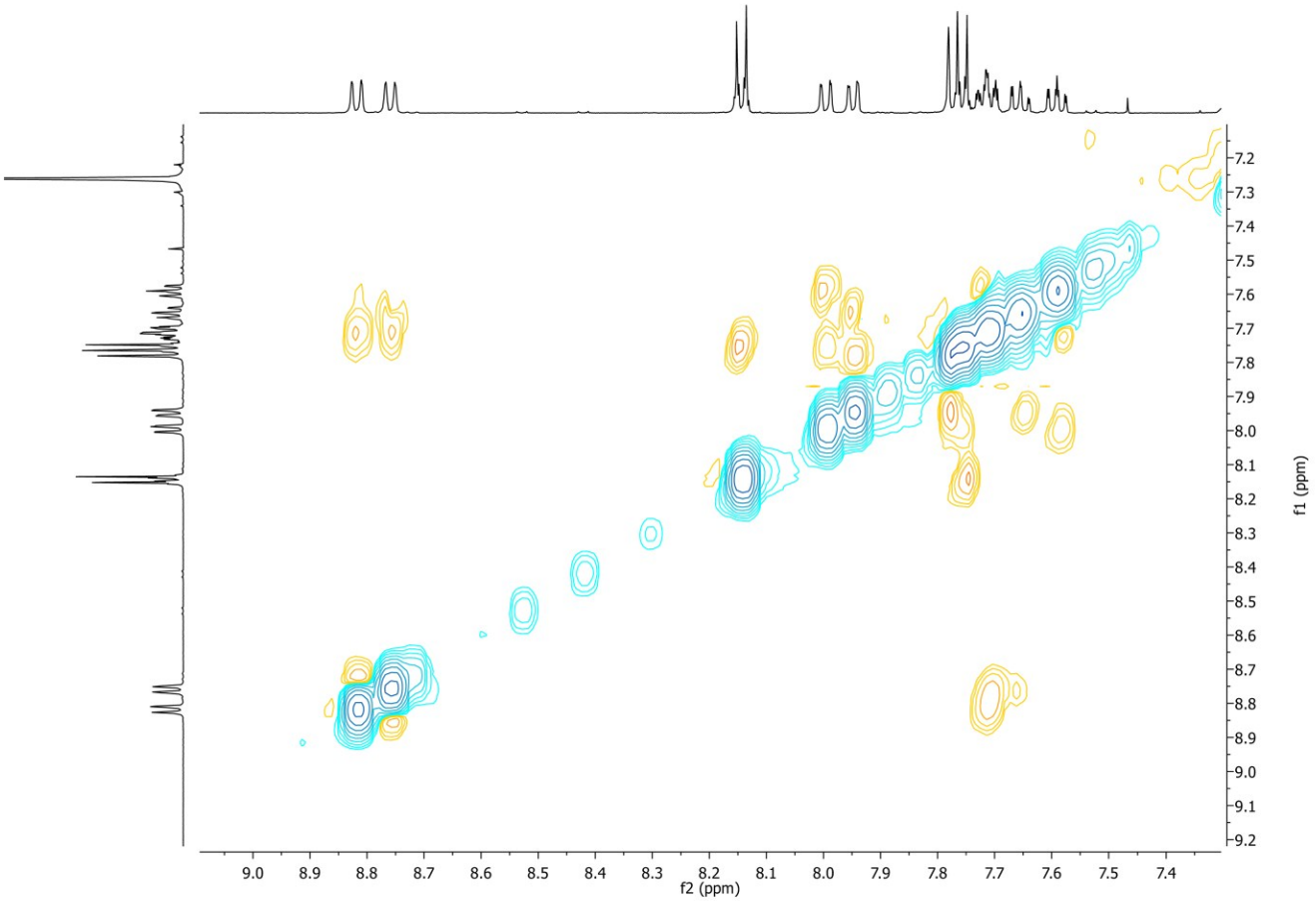

Figure S7: ^{1}H - ^{1}H NOESY ($CDCl_3$) of **4a**.

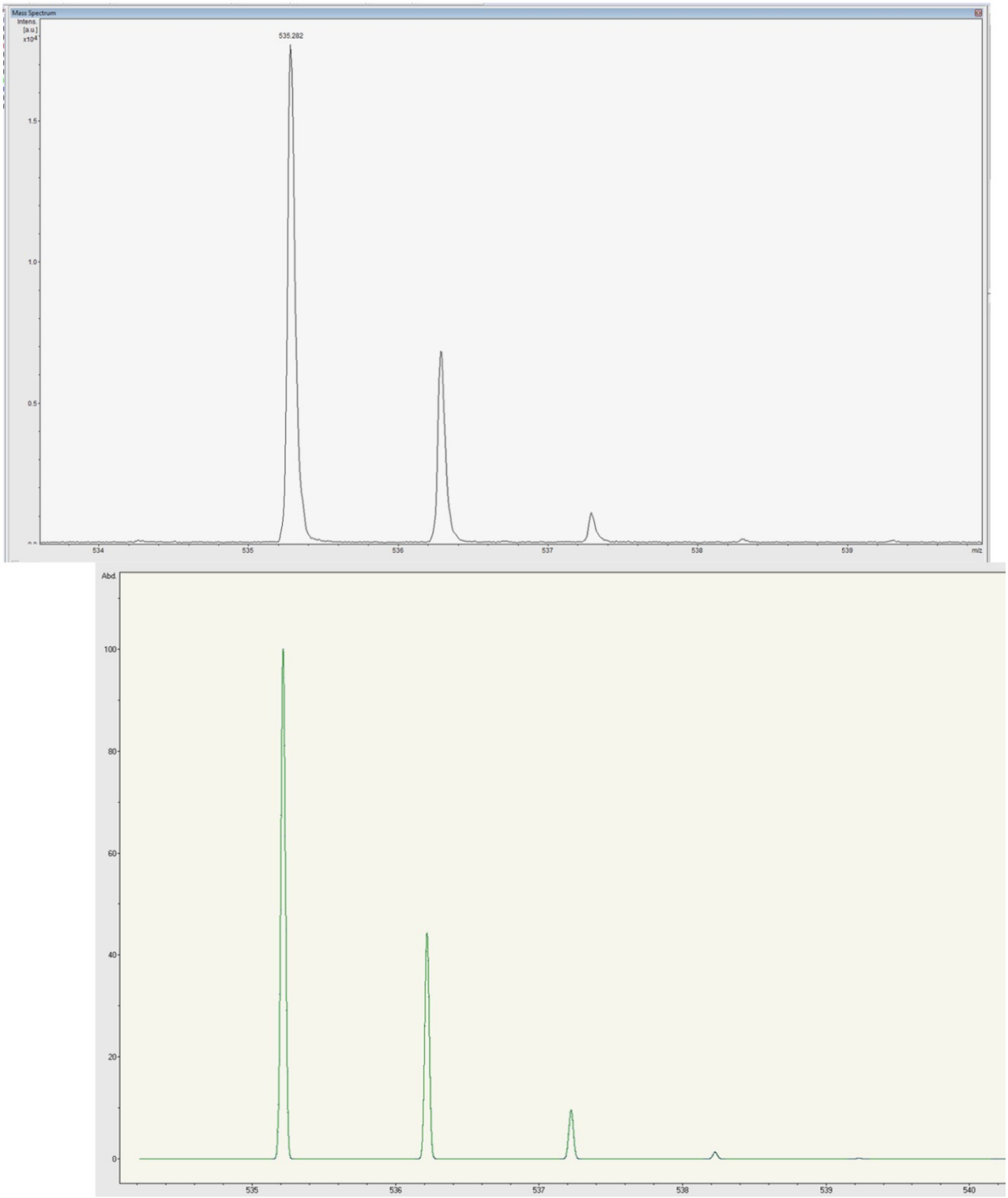

Figure S8: MS (MALDI-TOF) in dithranol of **4a** $[M+H]^+$ (up) and predicted spectrum (bottom).

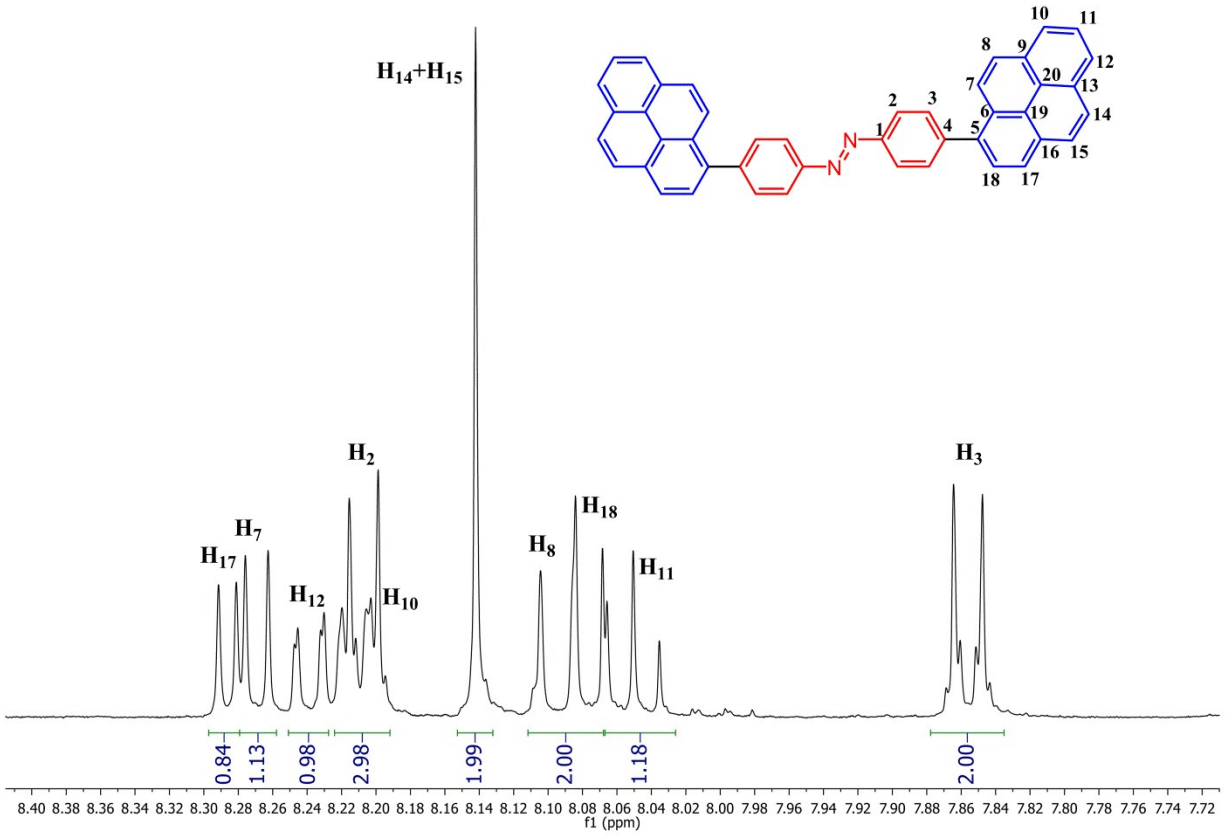

Figure S9: ^{1}H NMR (500MHz, $CDCl_3$) of **5a**.

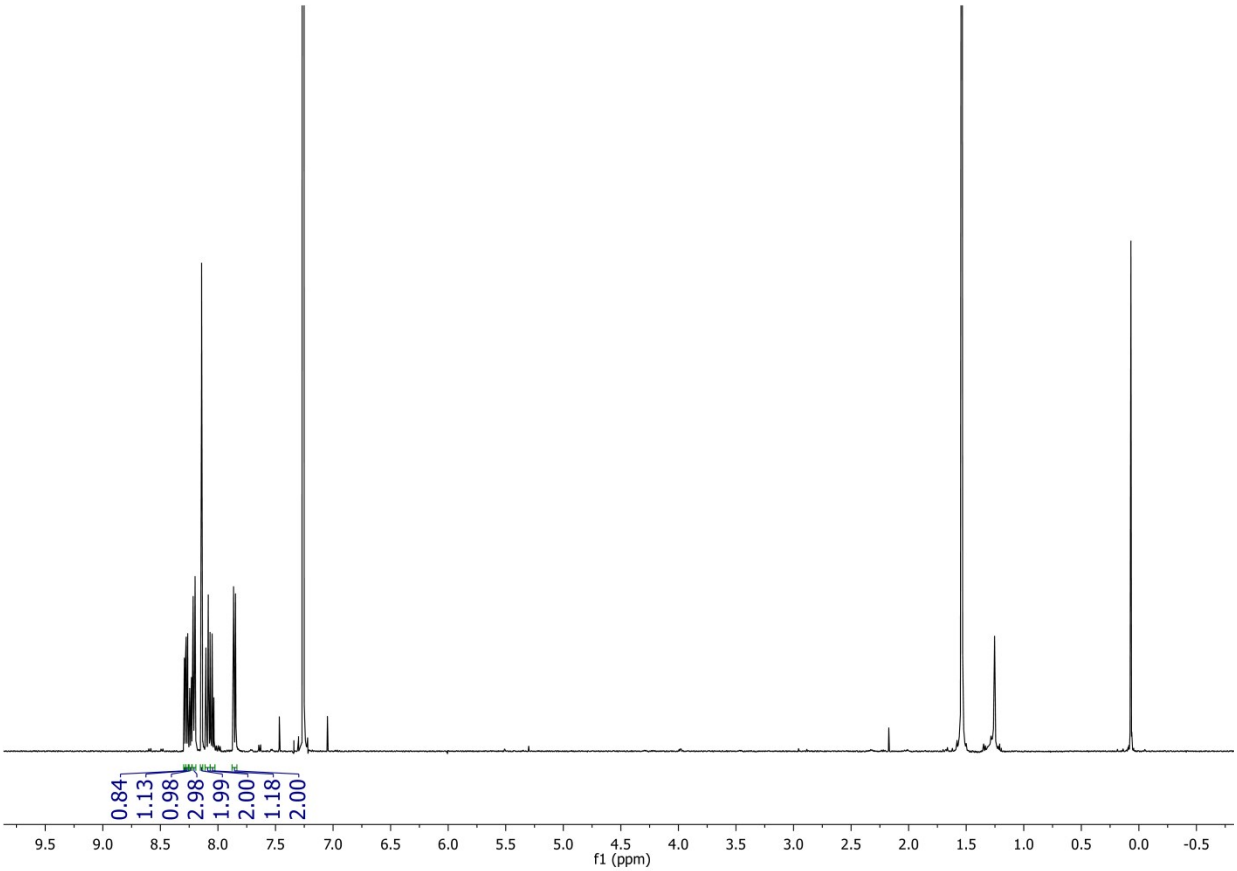

Figure S10: Full ^{1}H NMR (500MHz, $CDCl_3$) of **5a**.

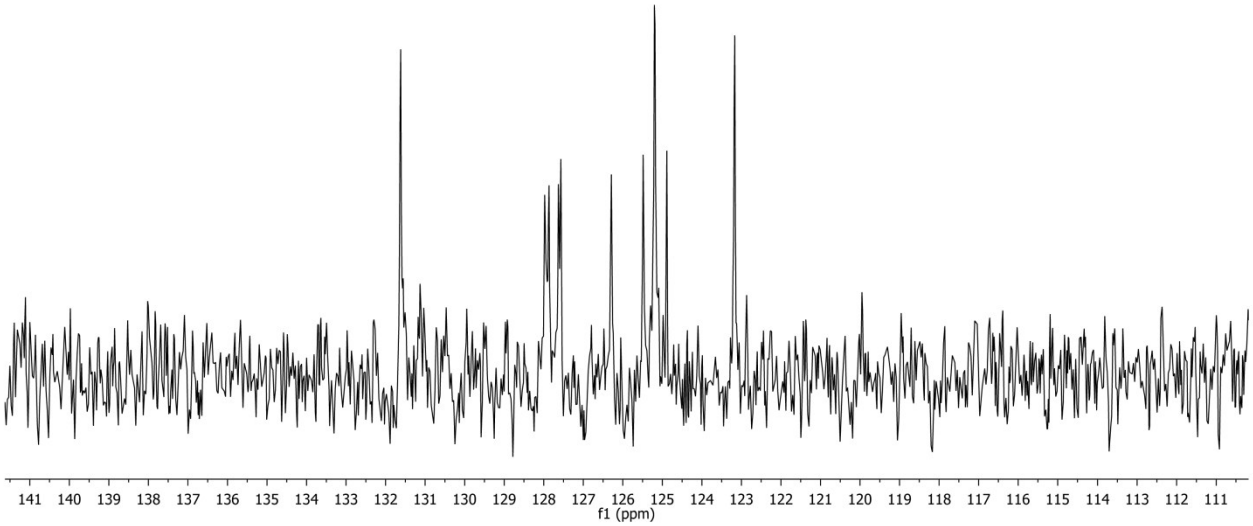

Figure S11: $^{13}C\{^{1}H\}$ NMR (126MHz, $CDCl_3$) of **5a**.

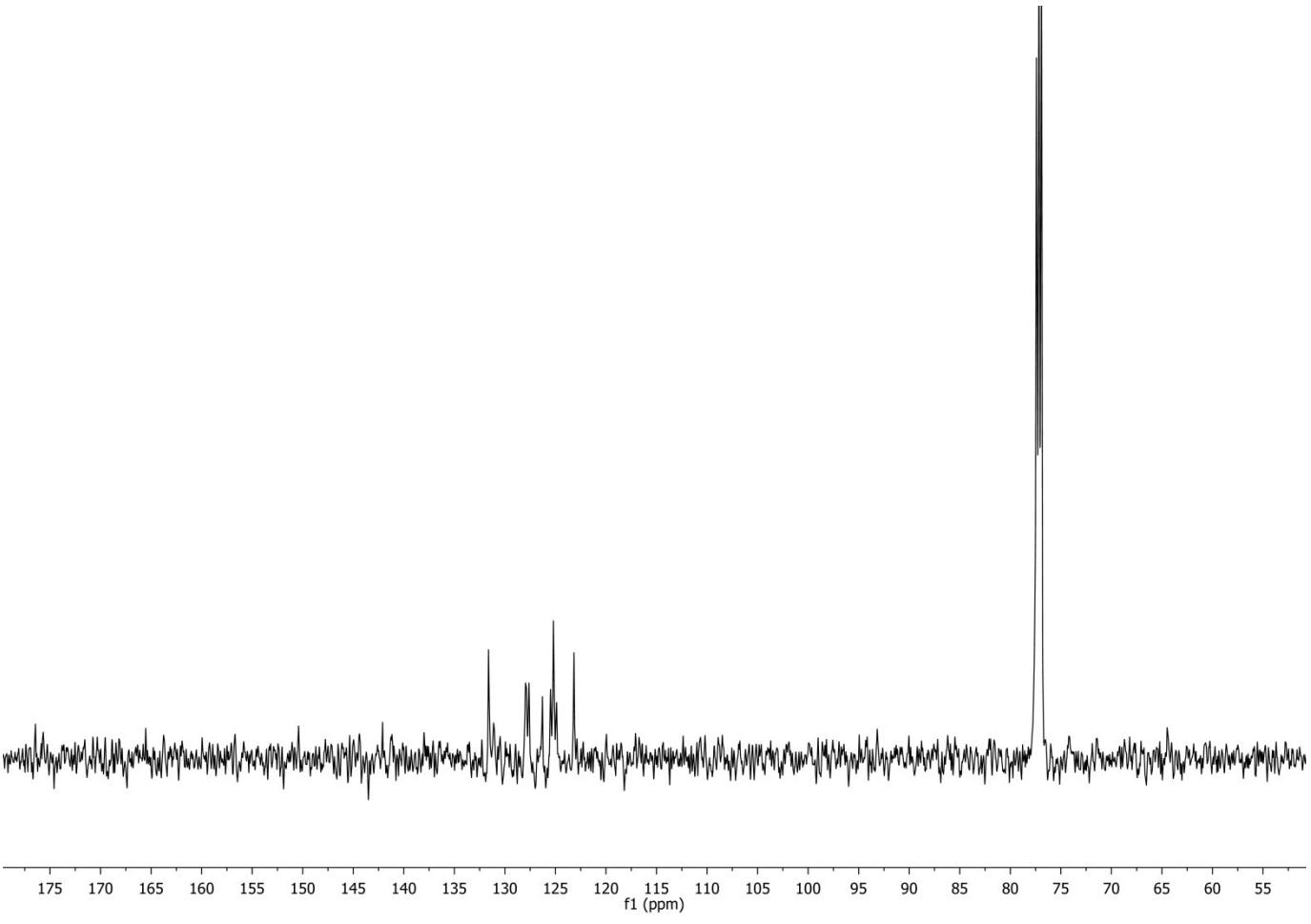

Figure S12: Full $^{13}C\{^{1}H\}$ NMR (126MHz, $CDCl_3$) of **5a**.

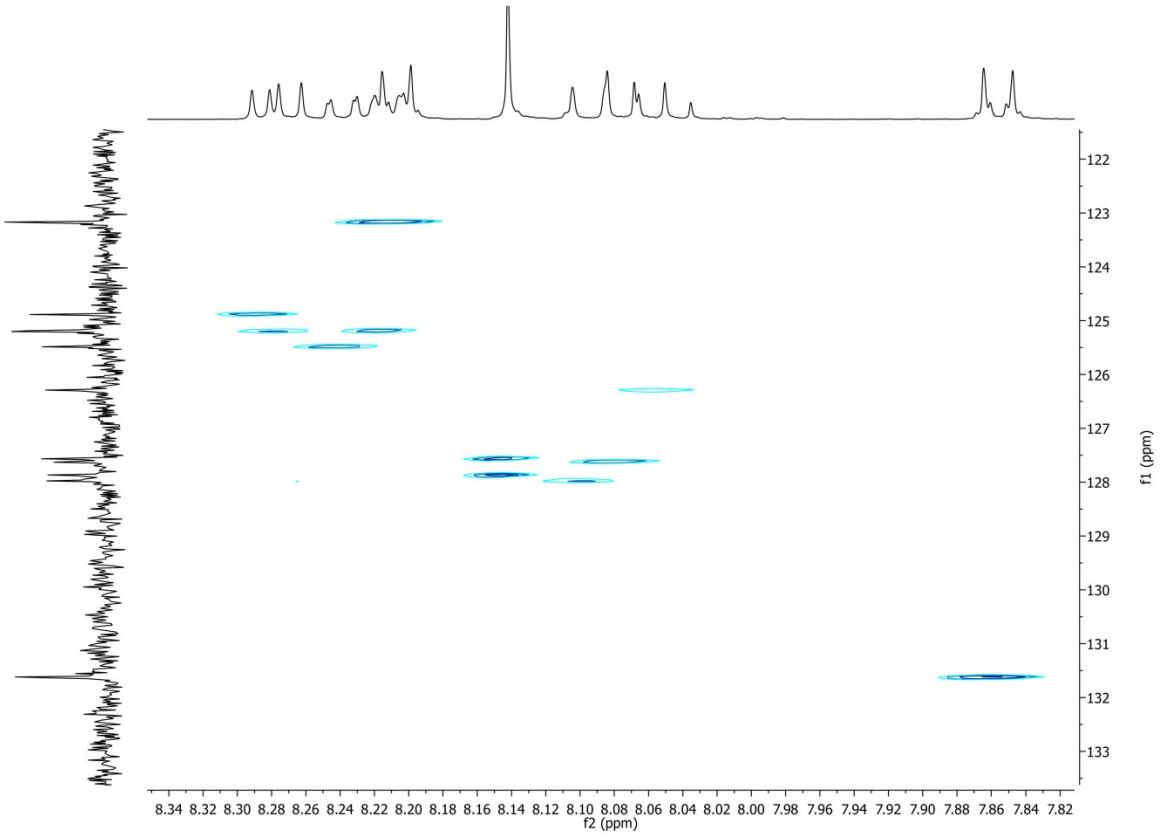

Figure S13: ^{1}H - ^{13}C band selective HSQC ($CDCl_3$) of **5a**.

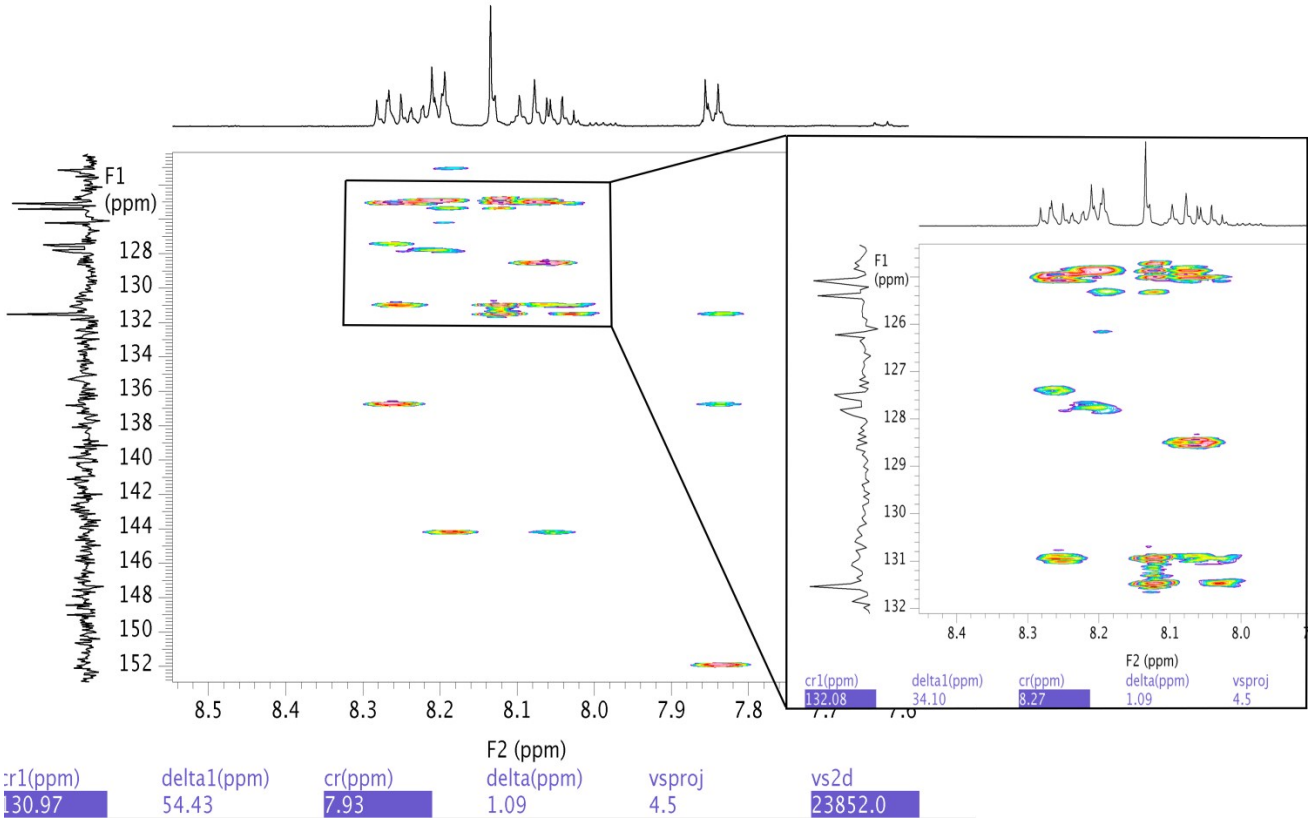

Figure S14: ^{1}H - ^{13}C band selective HMBC ($CDCl_3$) of **5a**.

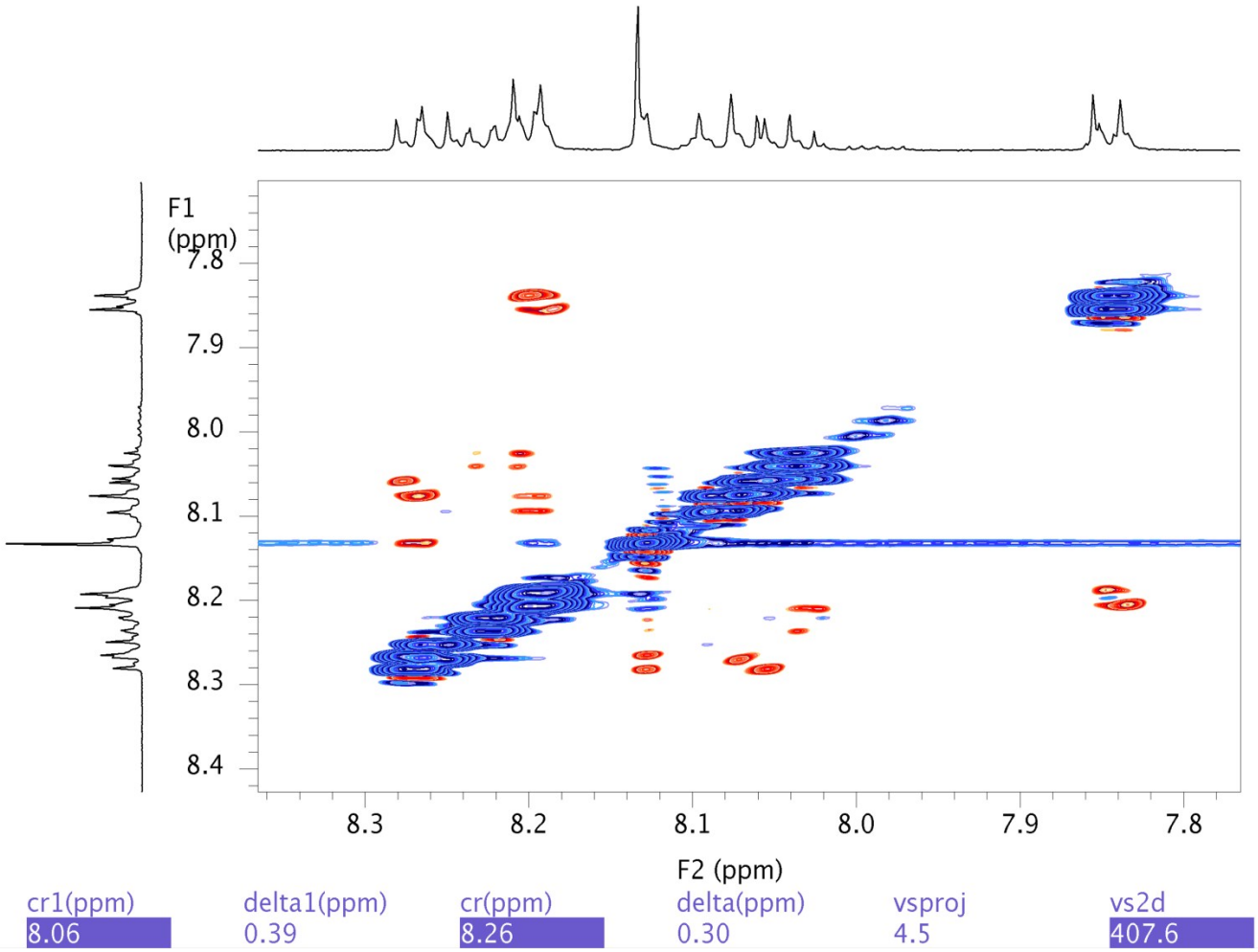

Figure S15: ^{1}H - ^{1}H band selective ROESY ($CDCl_3$) of **5a**.

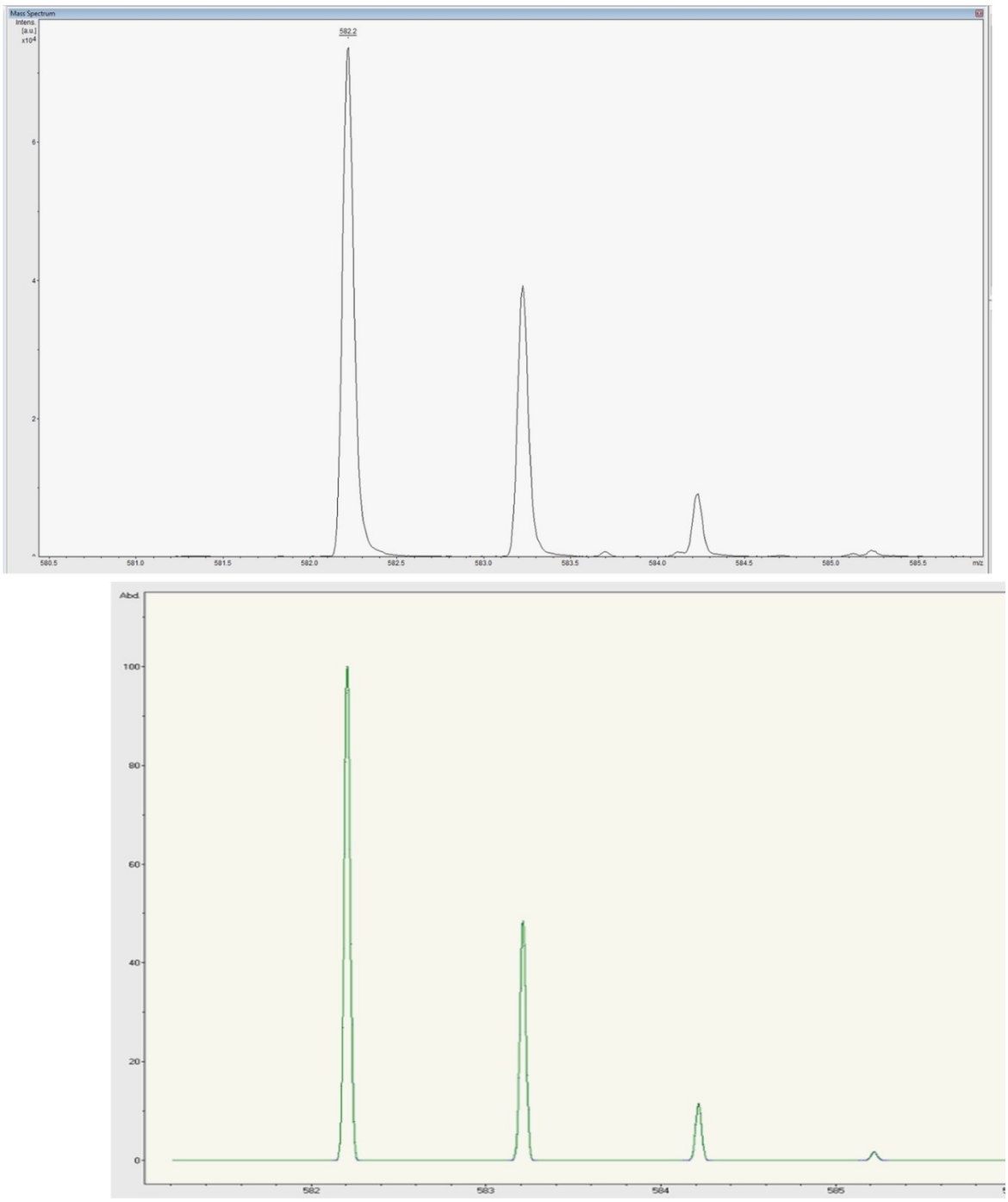

Figure S16: MS (MALDI-TOF) in DCTB of **5a** $[M]^+$ (up) and predicted spectrum (bottom).

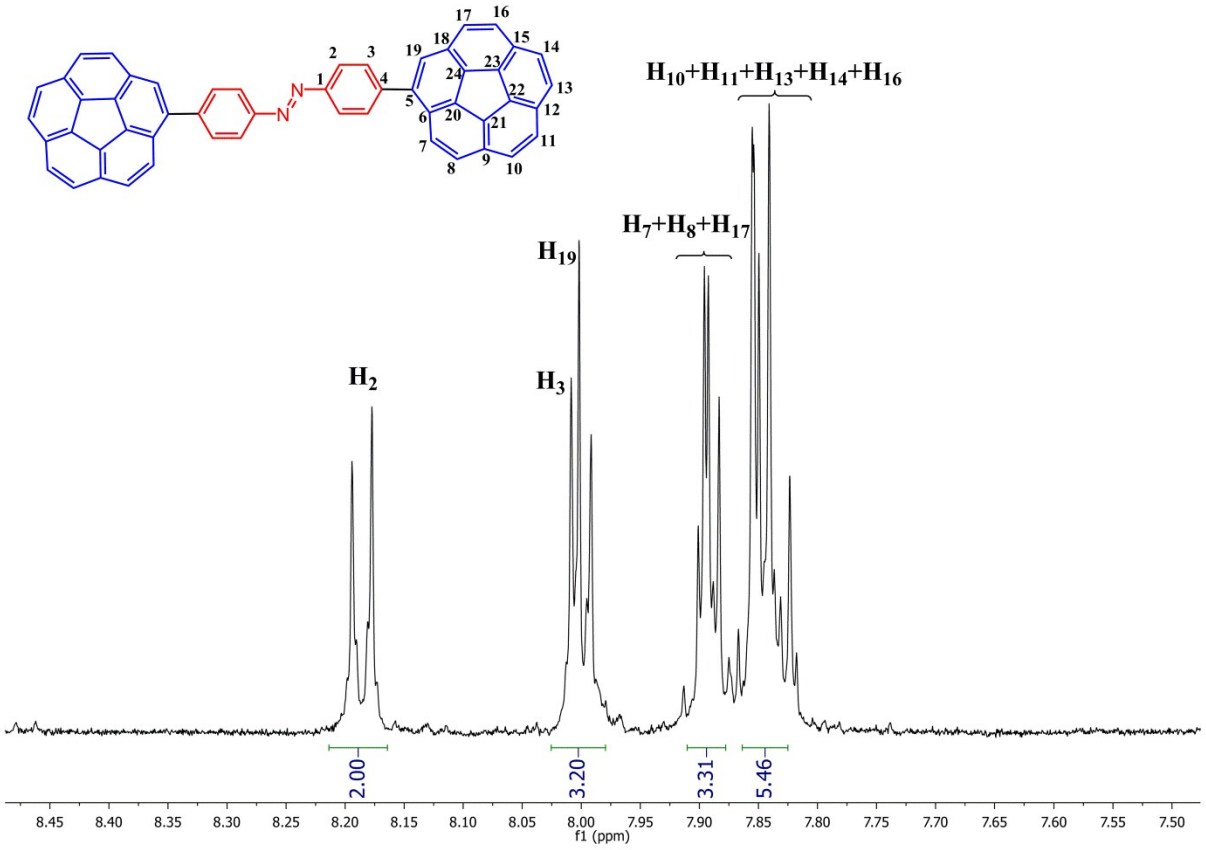

Figure S17: ^{1}H NMR (500MHz, $CDCl_3$) of **6a**.

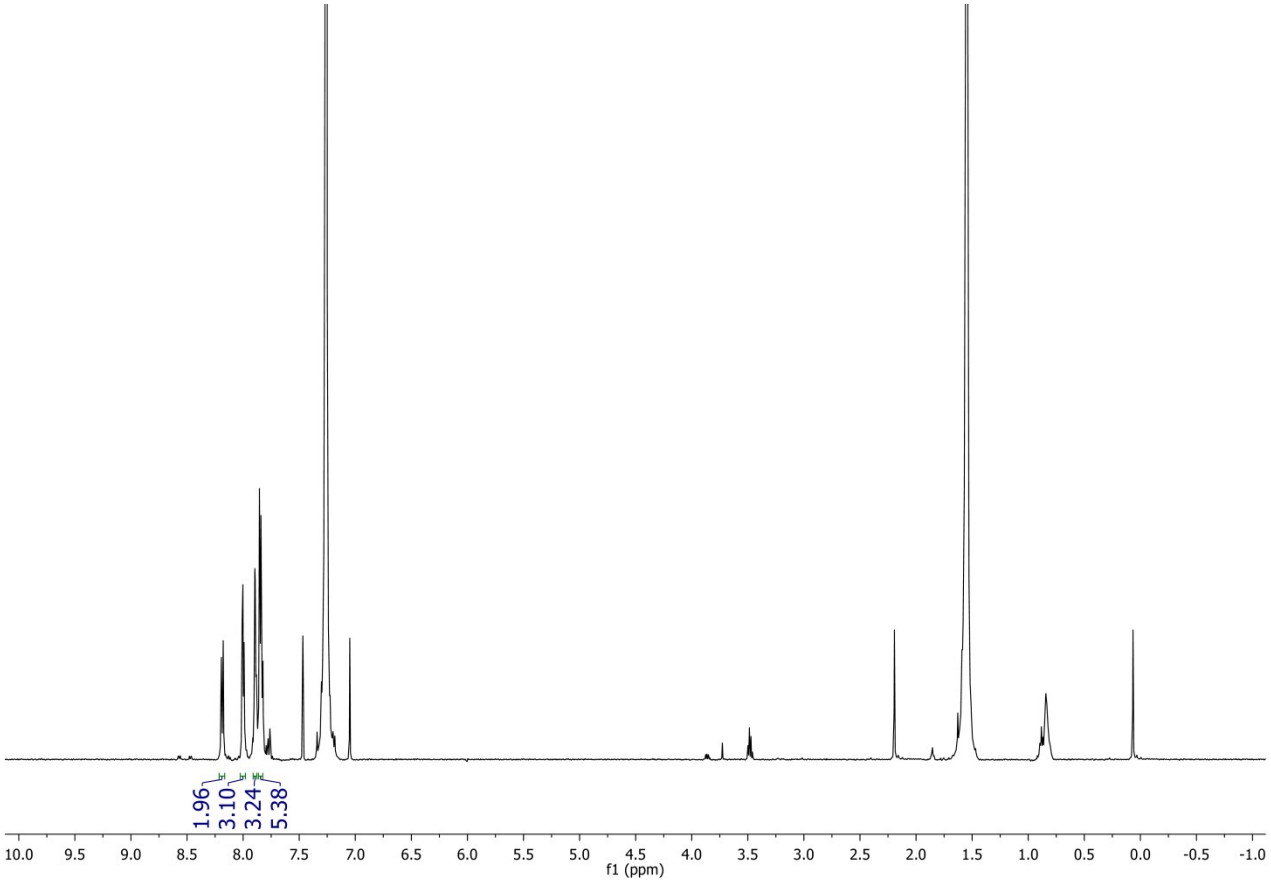

Figure S18: Full ^{1}H NMR (500MHz, $CDCl_3$) of **6a**.

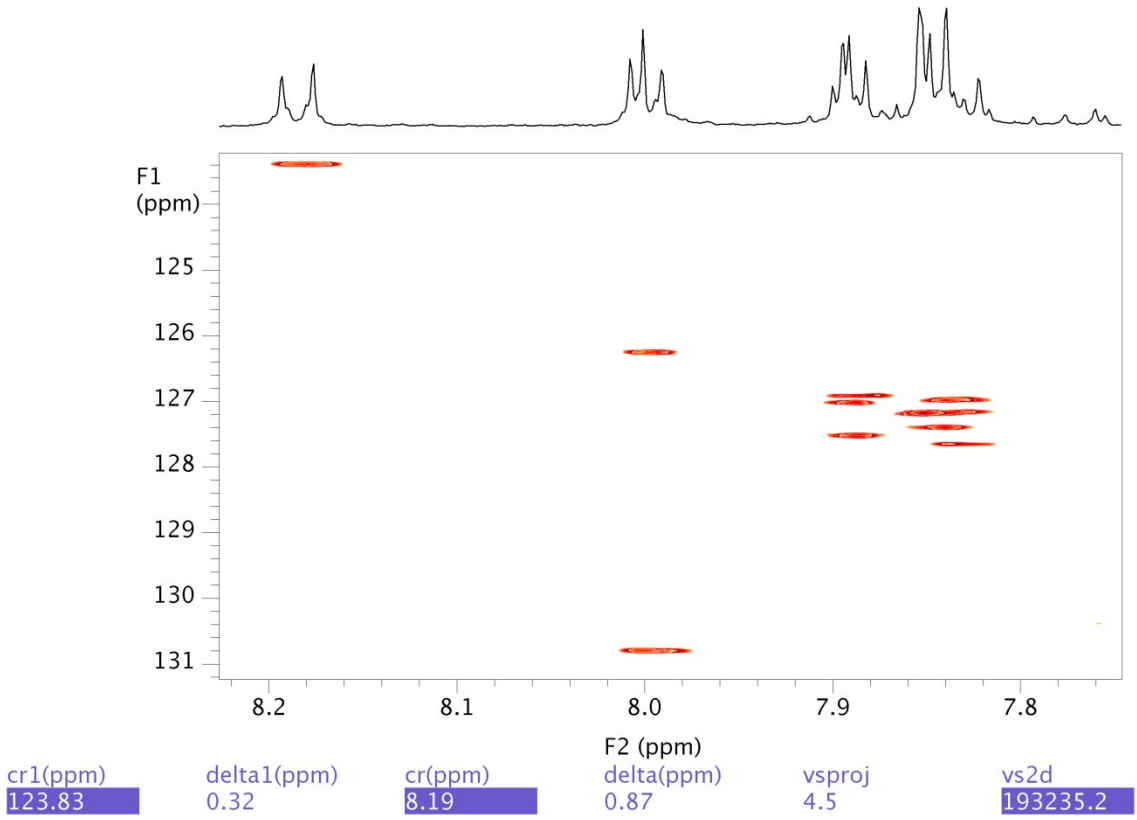

Figure S19: ^{1}H - ^{13}C band selective HSQC ($CDCl_3$) of **6a**.

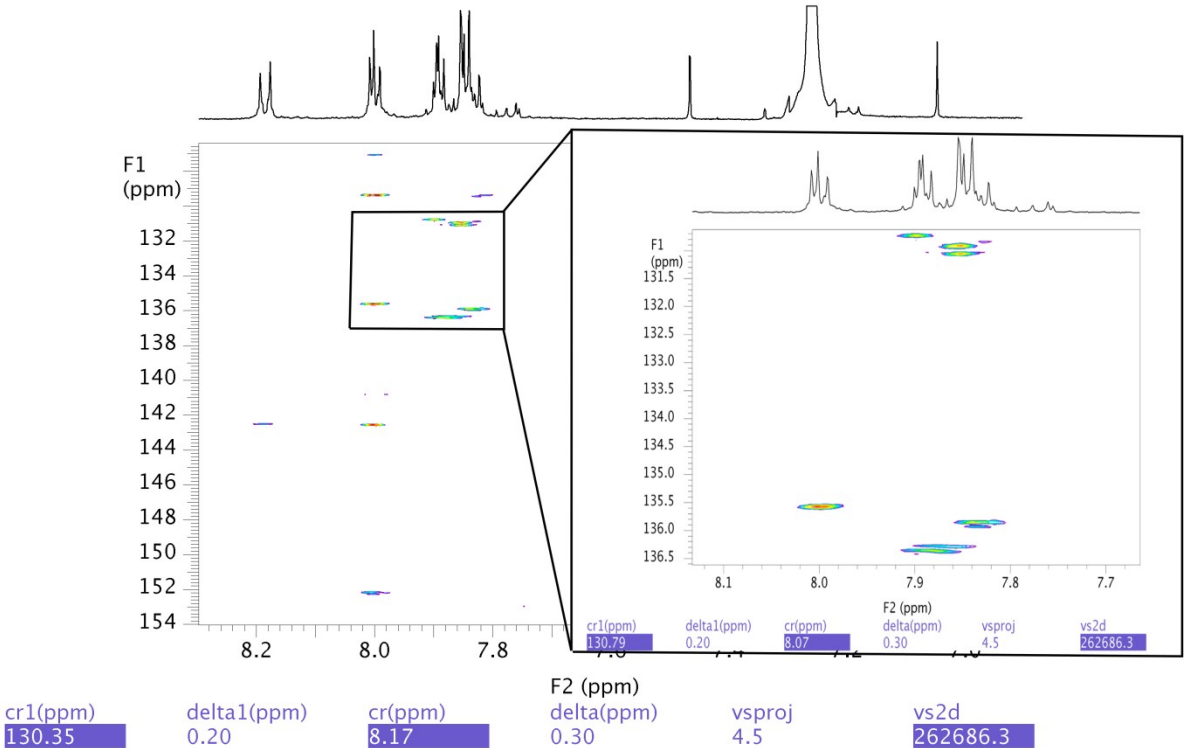

Figure S20: ^{1}H - ^{13}C band selective HMBC ($CDCl_3$) of **6a**.

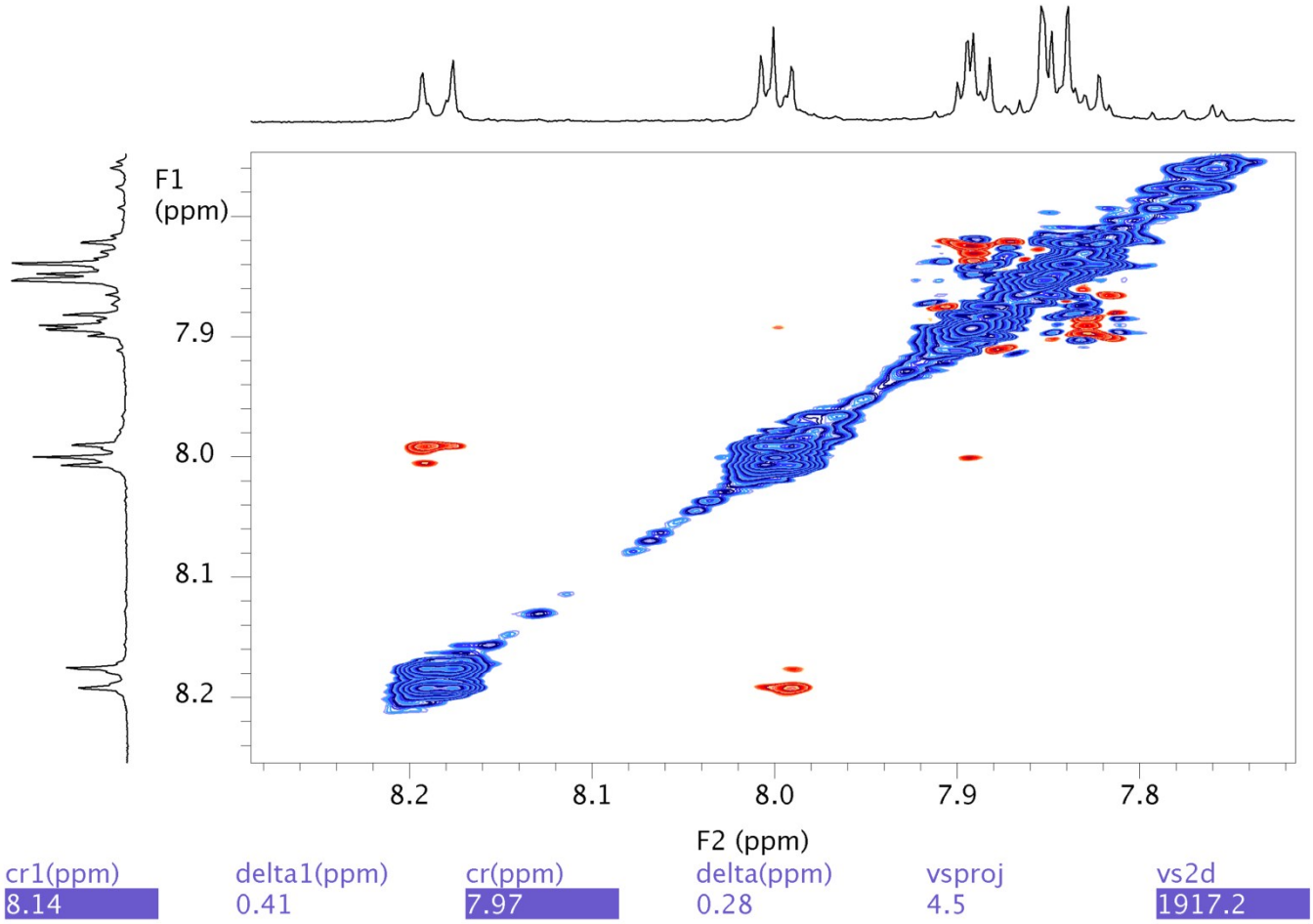

Figure S21: ^{1}H - ^{1}H band selective ROESY ($CDCl_3$) of **6a**.

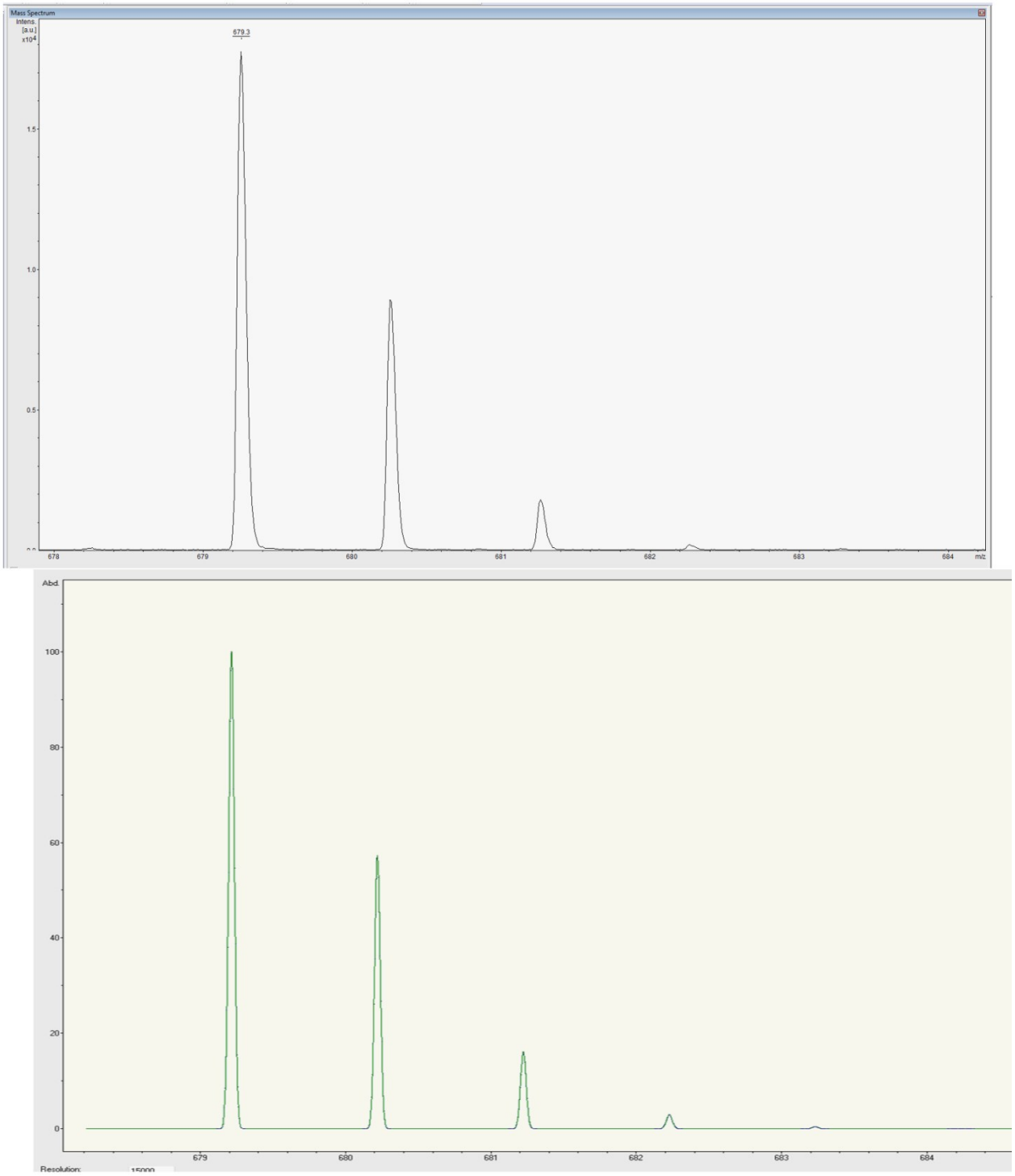

Figure S22: MS (MALDI-TOF) in dithranol of **6a** $[M+H]^+$ (up) and predicted spectrum (bottom).

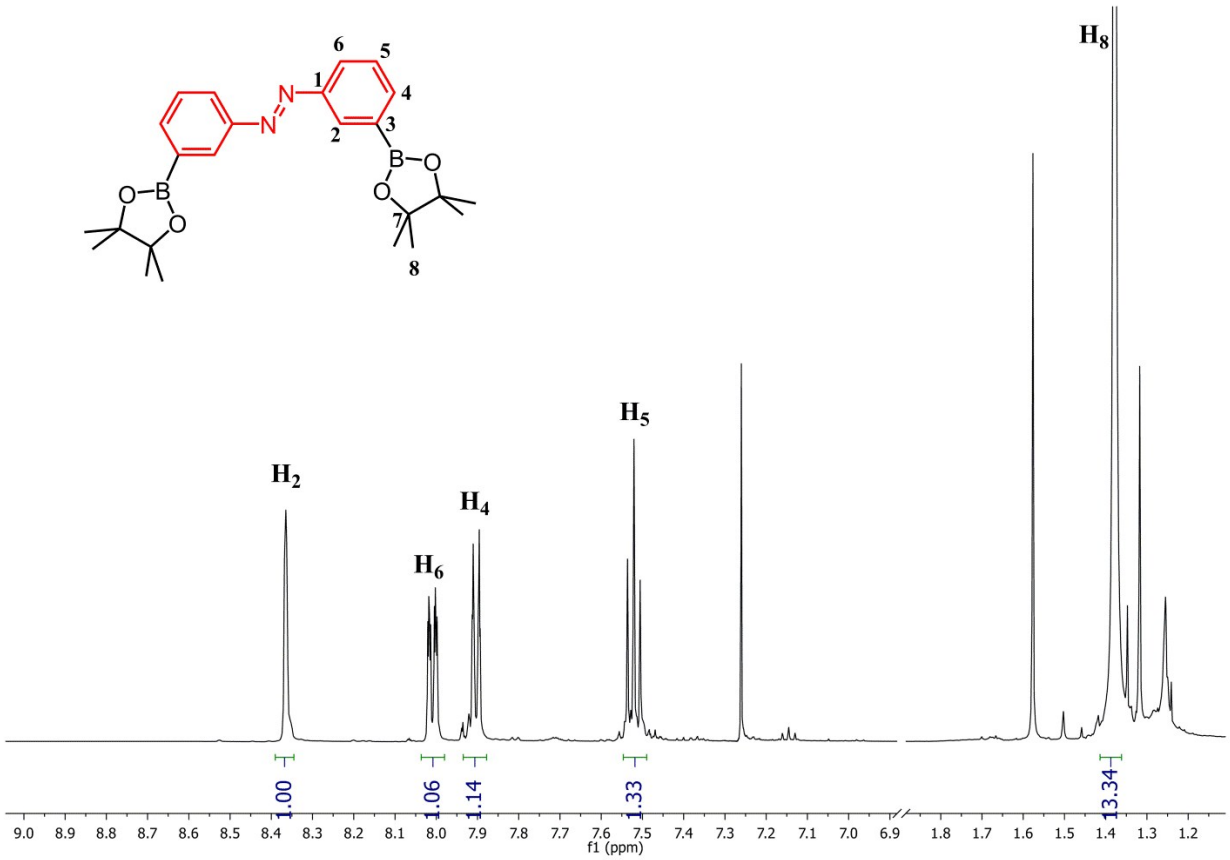

Figure S23: ^{1}H NMR (500MHz, $CDCl_3$) of **3b**.

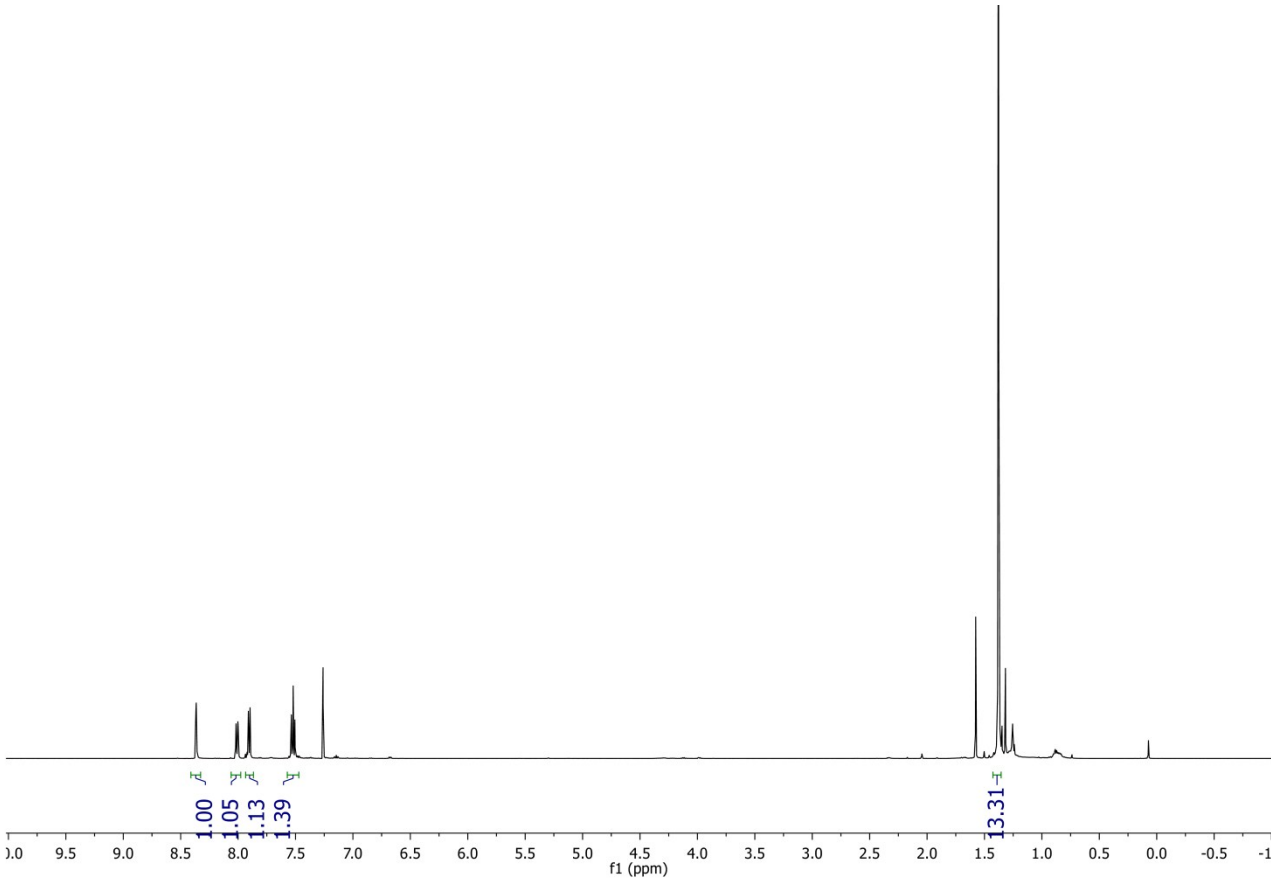

Figure S24: Full ^{1}H NMR (500MHz, $CDCl_3$) of **3b**.

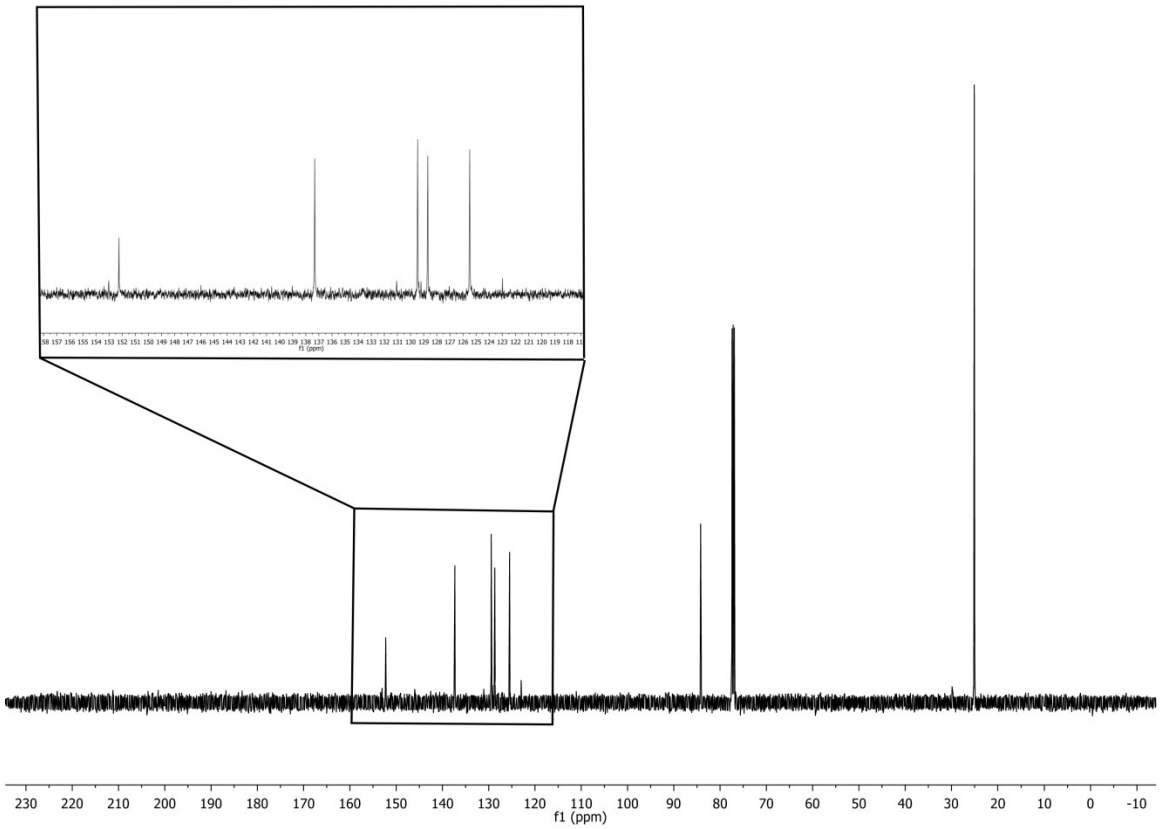

Figure S25: $^{13}C\{^{1}H\}$ NMR (126MHz, $CDCl_3$) of **3b**.

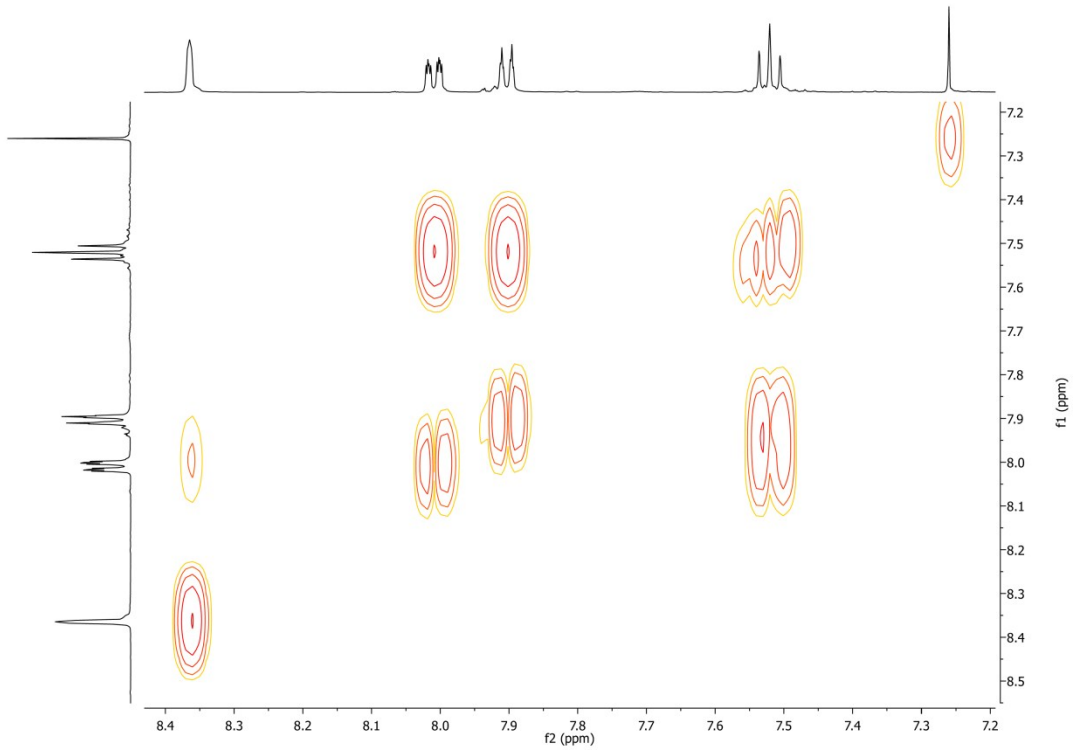

Figure S26: ^{1}H - ^{1}H COSY ($CDCl_3$) of **3b**.

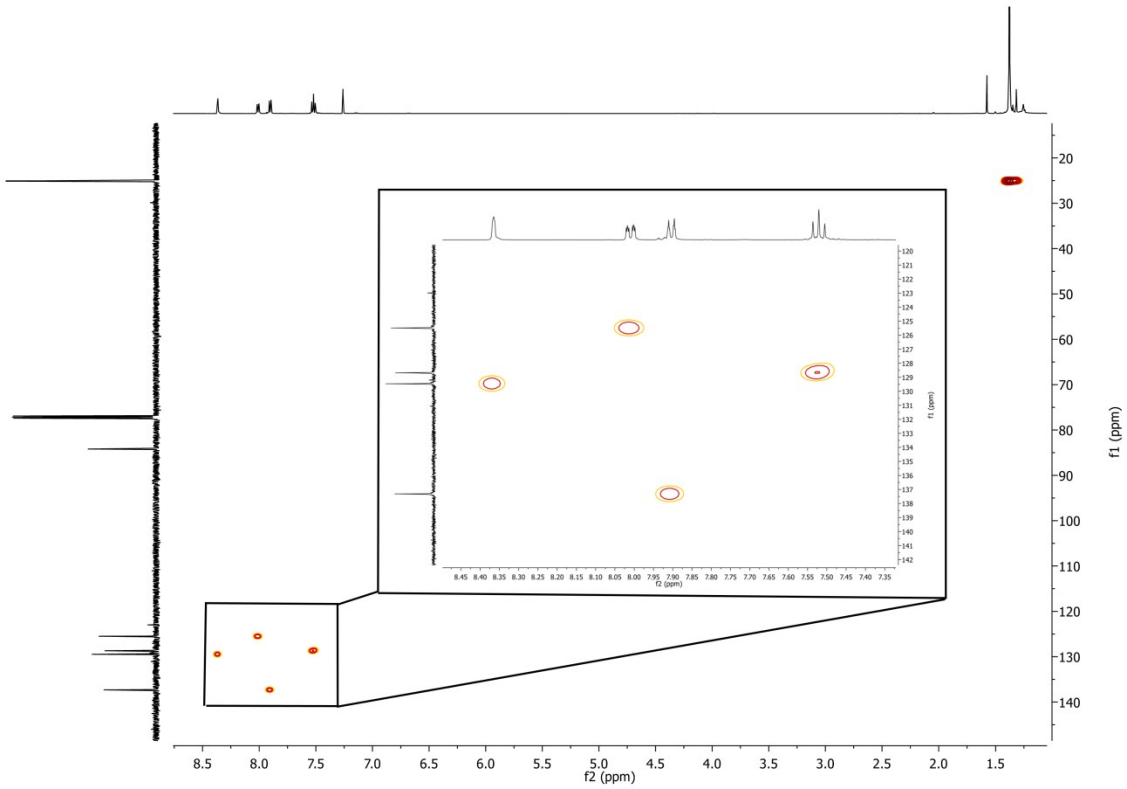

Figure S27: ^{1}H - ^{13}C HSQC ($CDCl_3$) of **3b**.

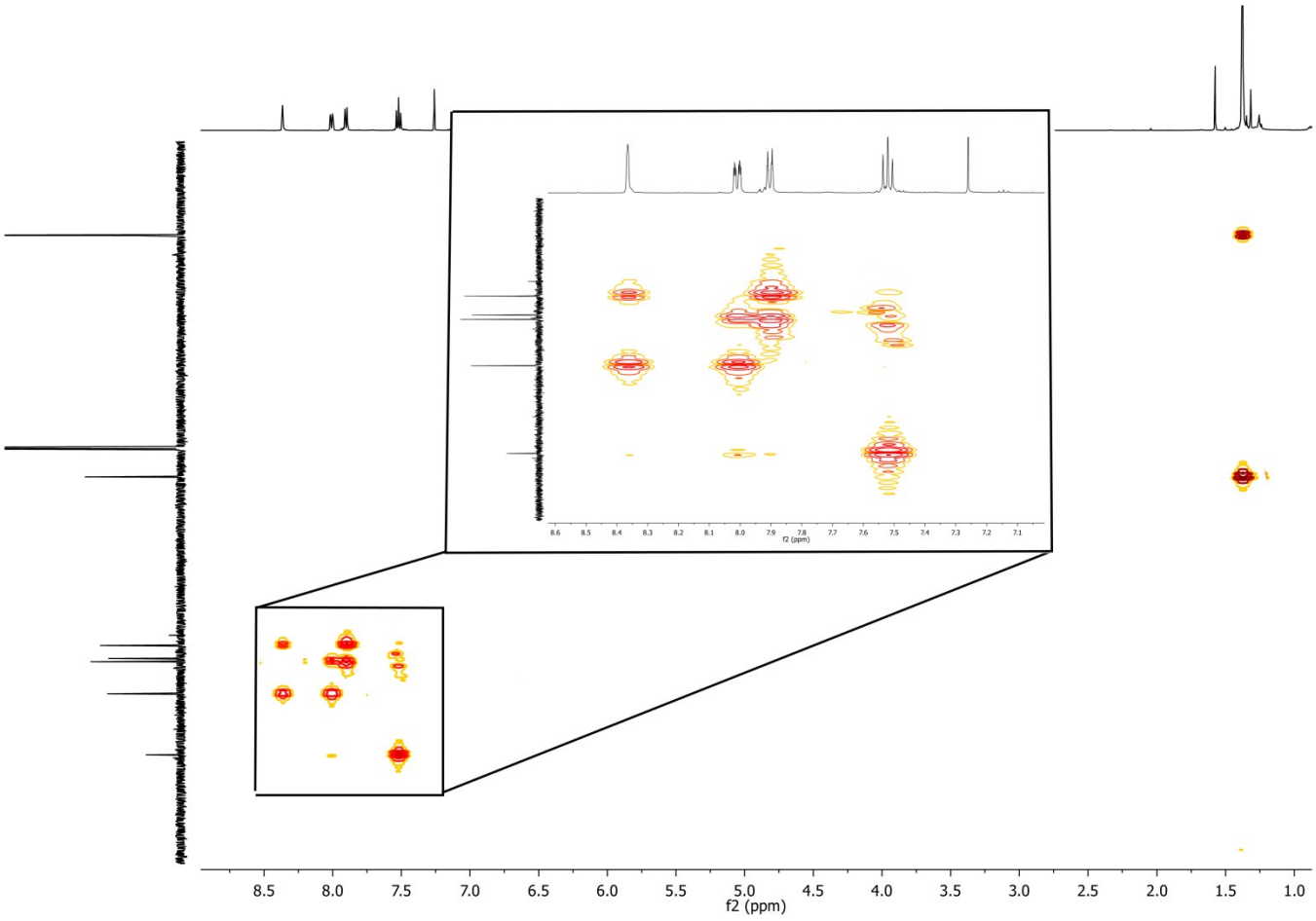

Figure S28: ^{1}H - ^{13}C HMBC ($CDCl_3$) of **3b**.

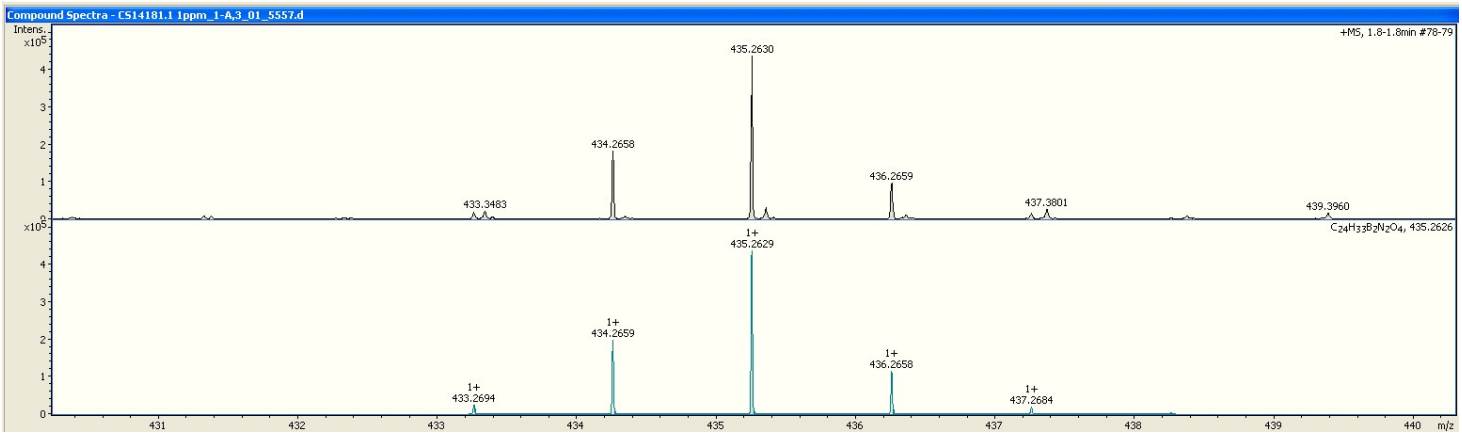

Figure S29: MS (ESI-TOF) **3b** $[M+H]^+$ (up) and predicted spectrum (bottom).

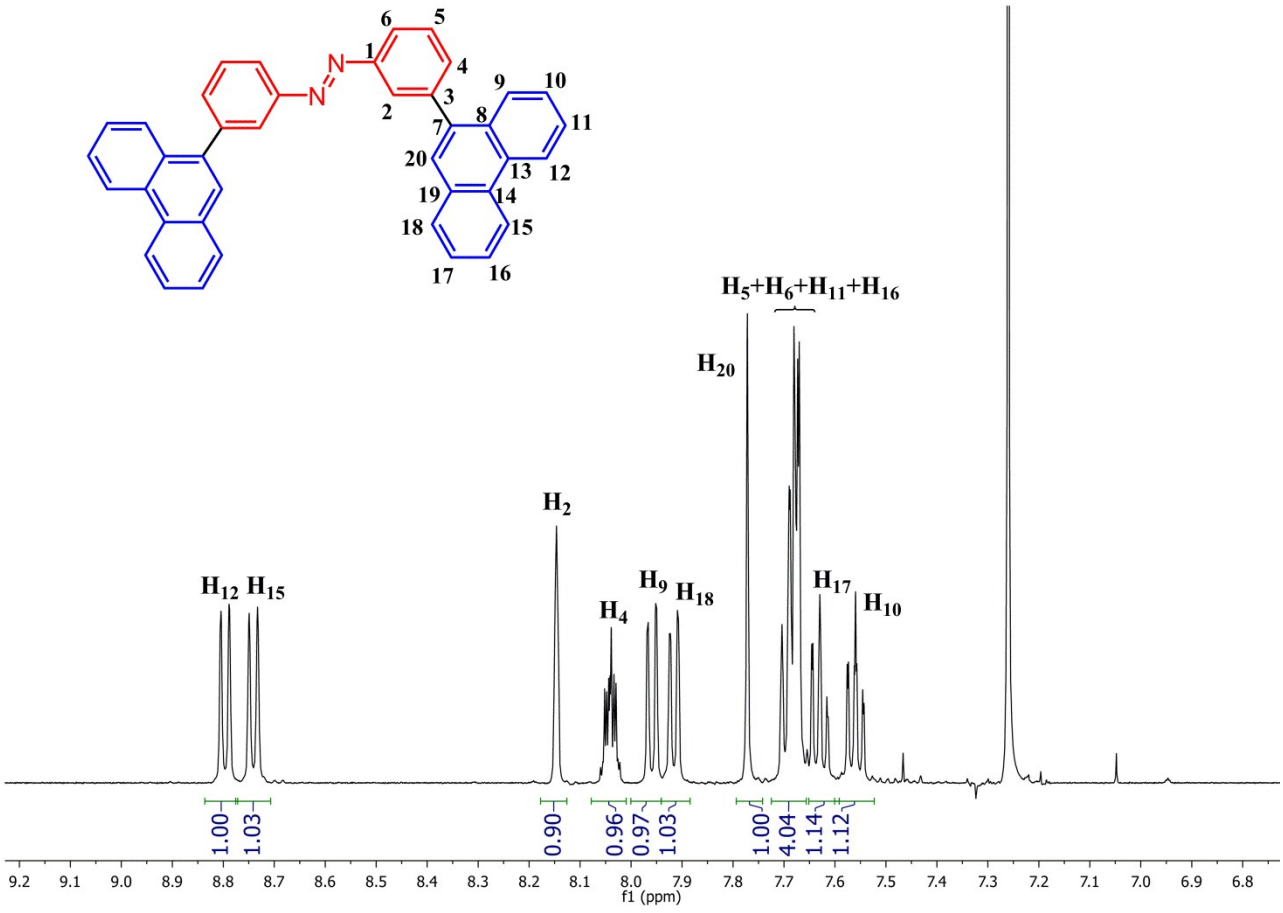

Figure S30: ^1H NMR (500MHz, $CDCl_3$) of **4b**.

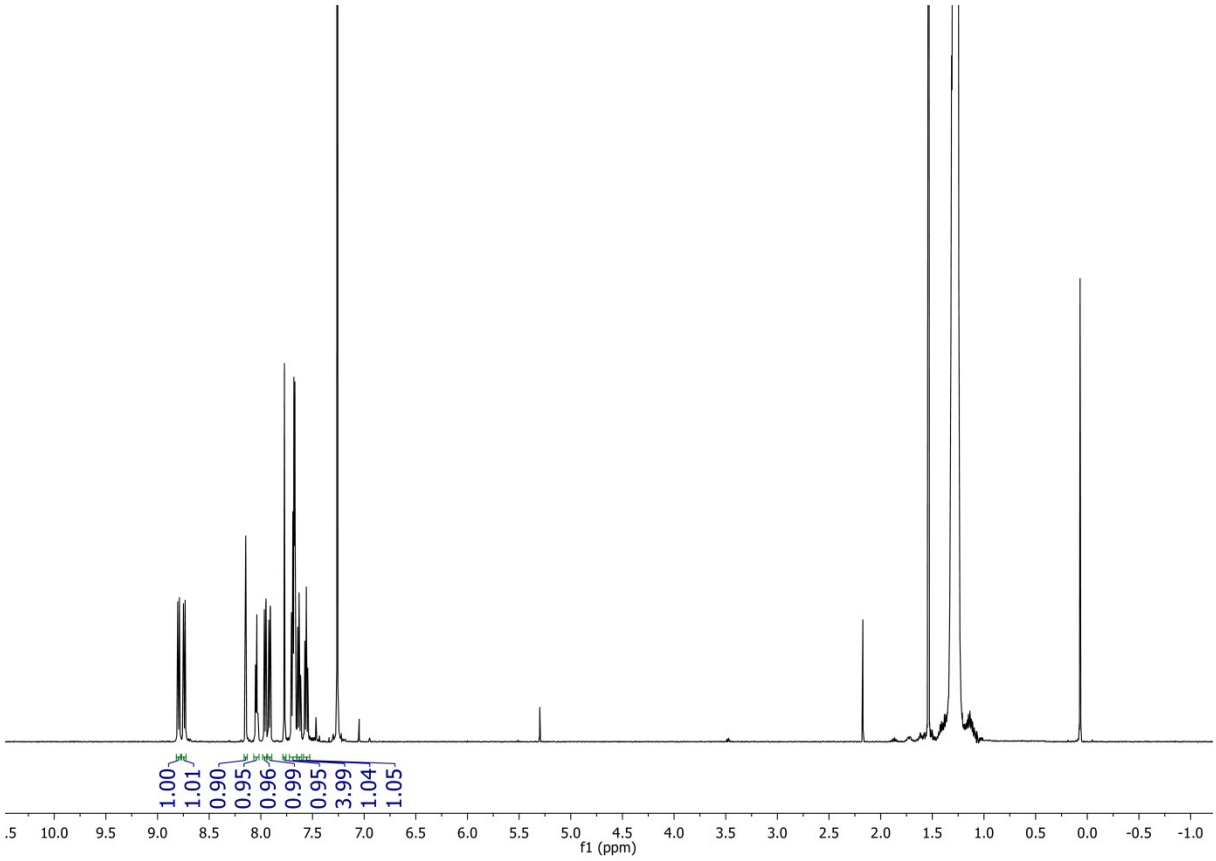

Figure S31: Full ^{1}H NMR (500MHz, $CDCl_3$) of **4b**.

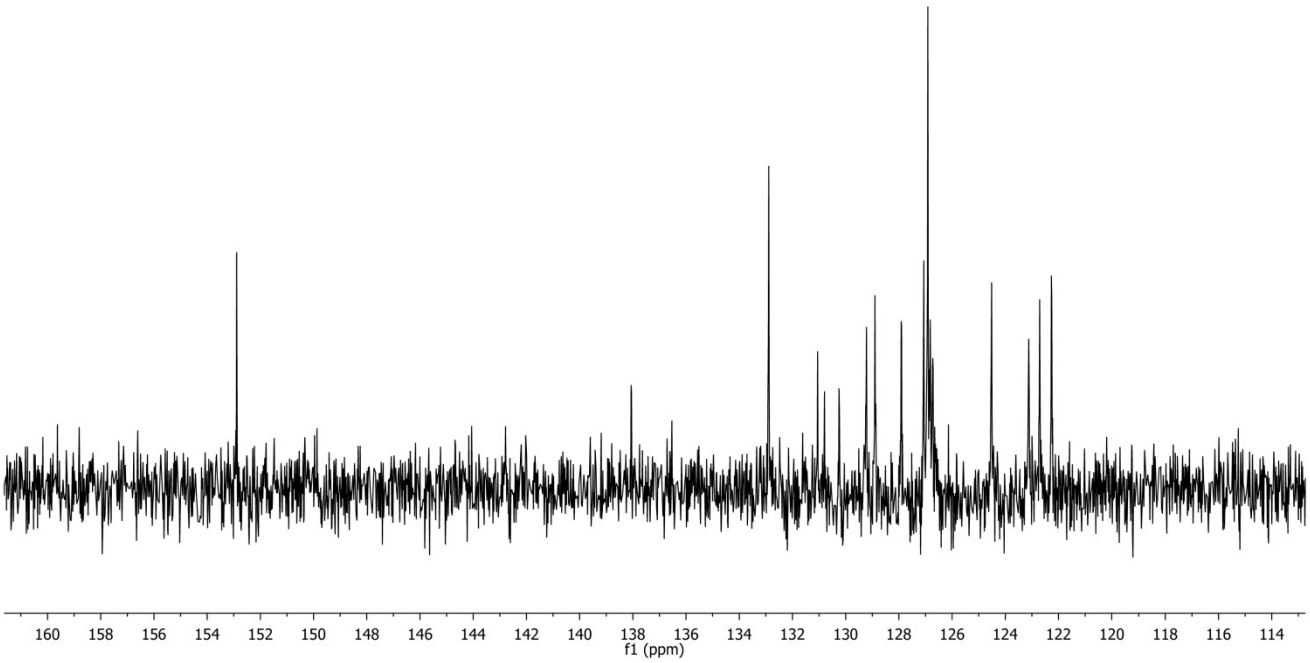

Figure S32: $^{13}C\{^{1}H\}$ NMR (126MHz, $CDCl_3$) of **4b**.

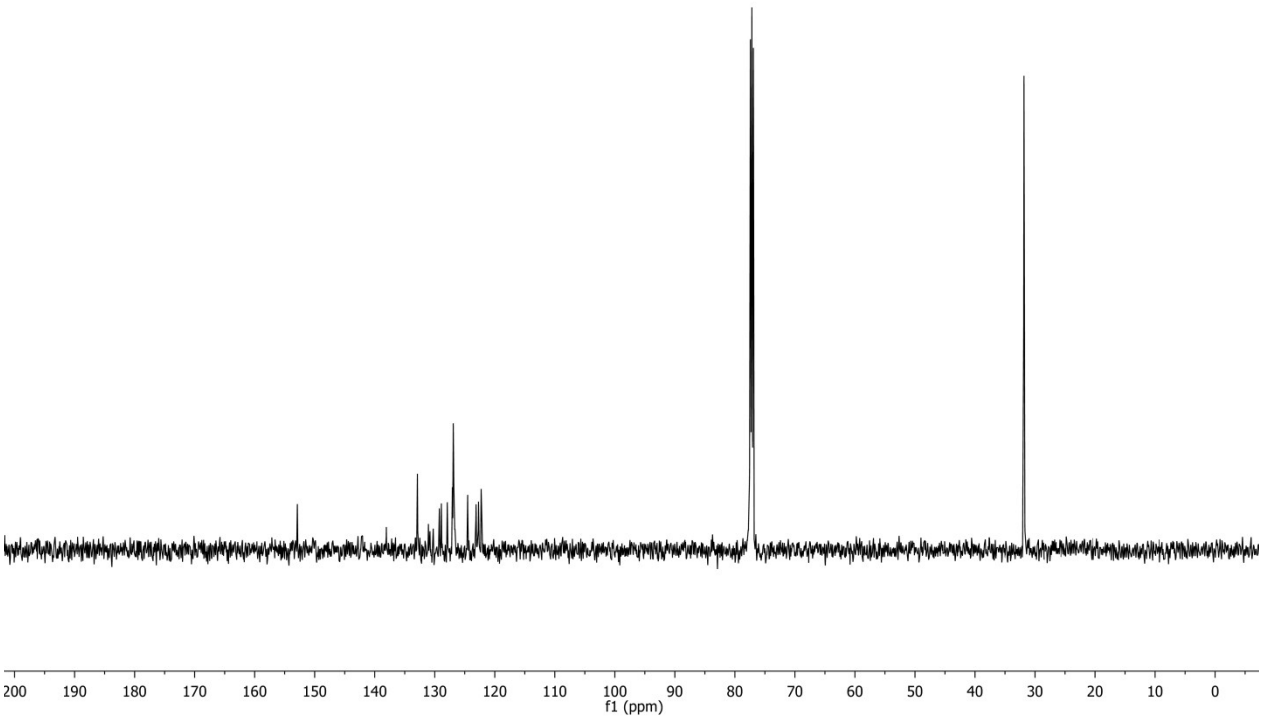

Figure S33: Full $^{13}C\{^{1}H\}$ NMR (126MHz, $CDCl_3$) of **4b**.

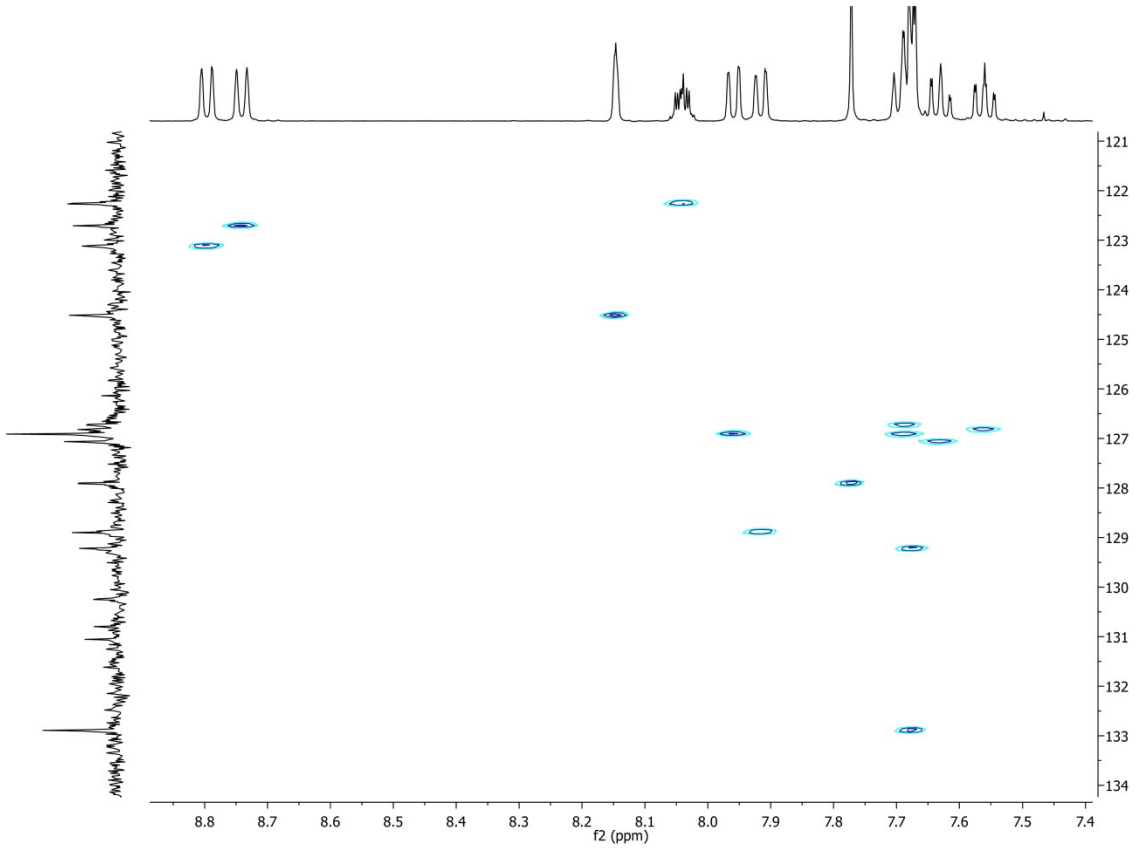

Figure S34: ^{1}H - ^{13}C band selective HSQC ($CDCl_3$) of **4b**.

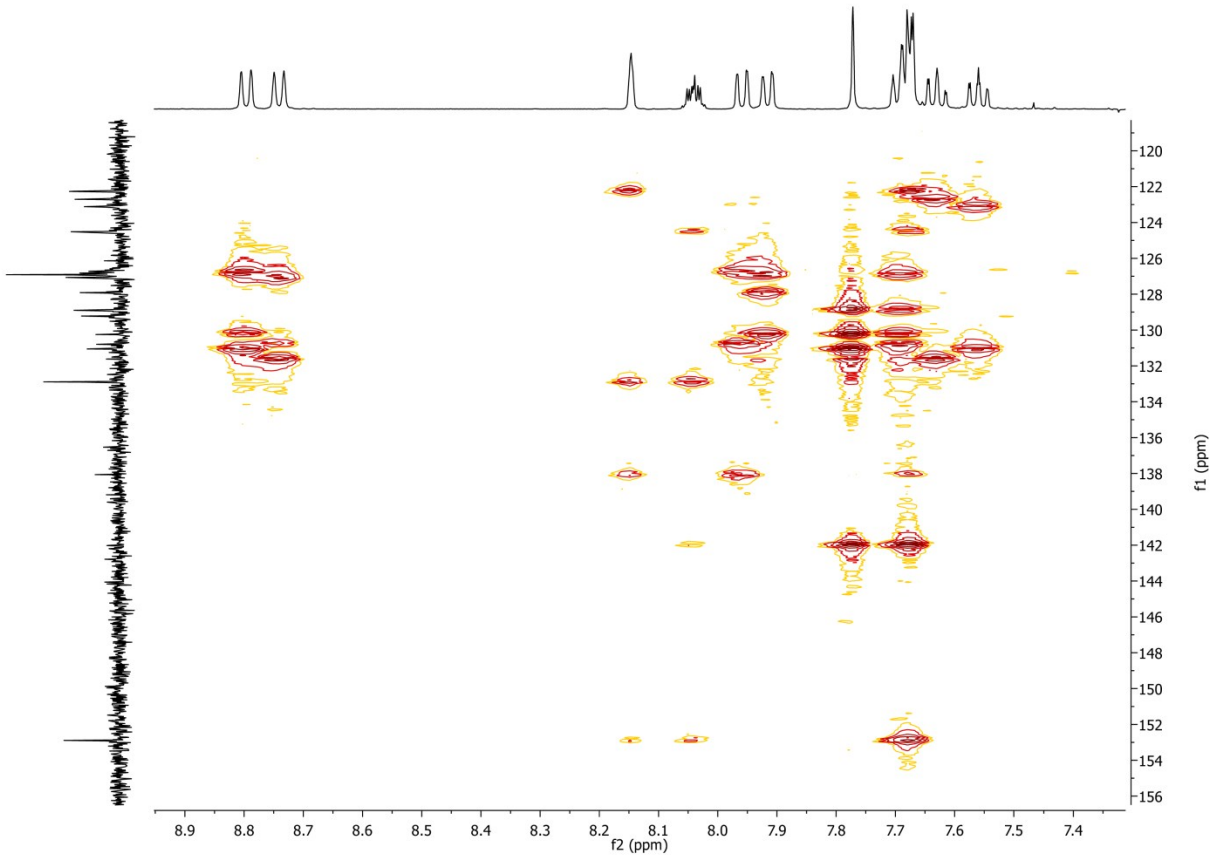

Figure S35: ^{1}H - ^{13}C band selective HMBC ($CDCl_3$) of **4b**.

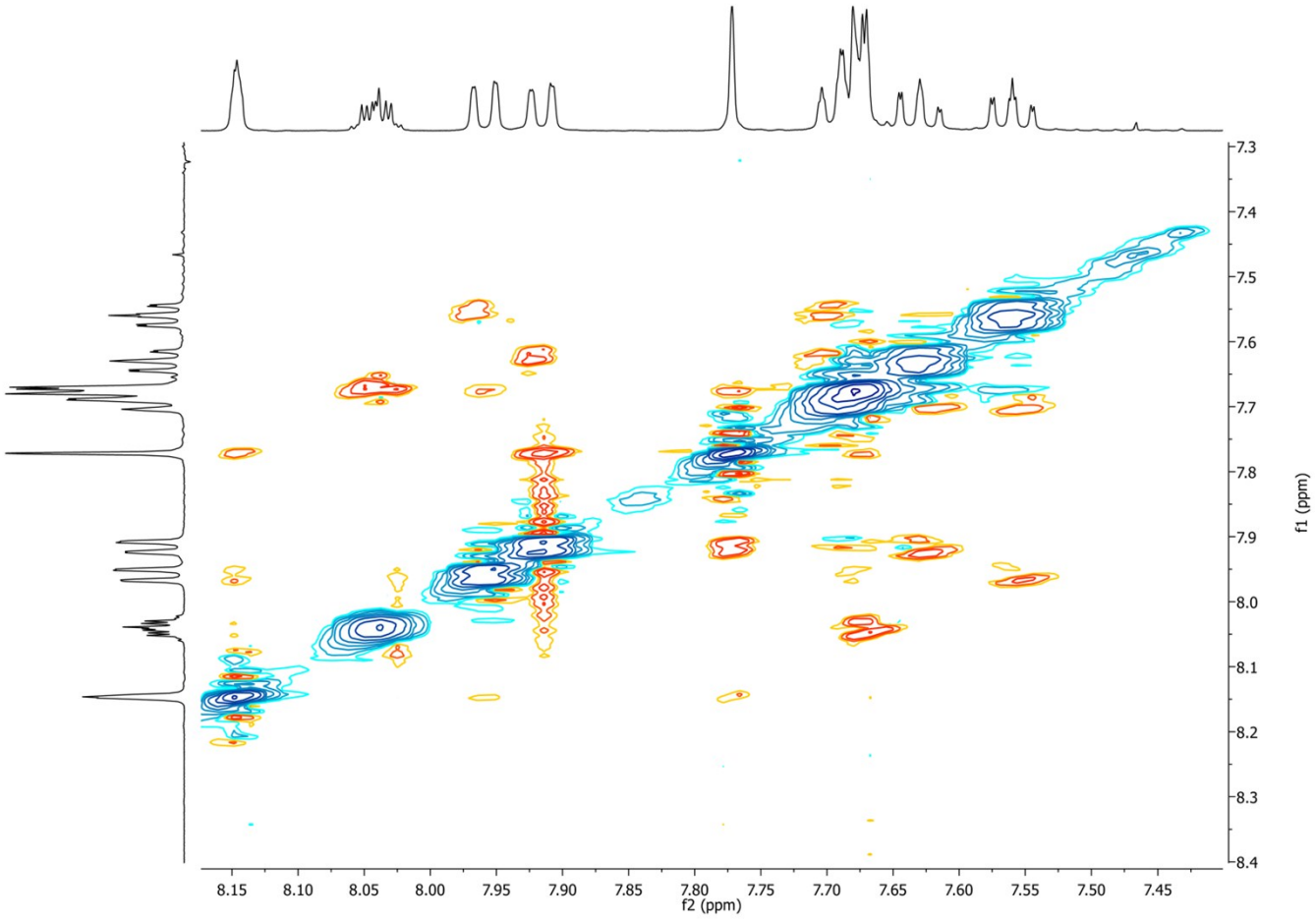

Figure S36: ^{1}H - ^{1}H band selective ROESY ($CDCl_3$) of **4b**.

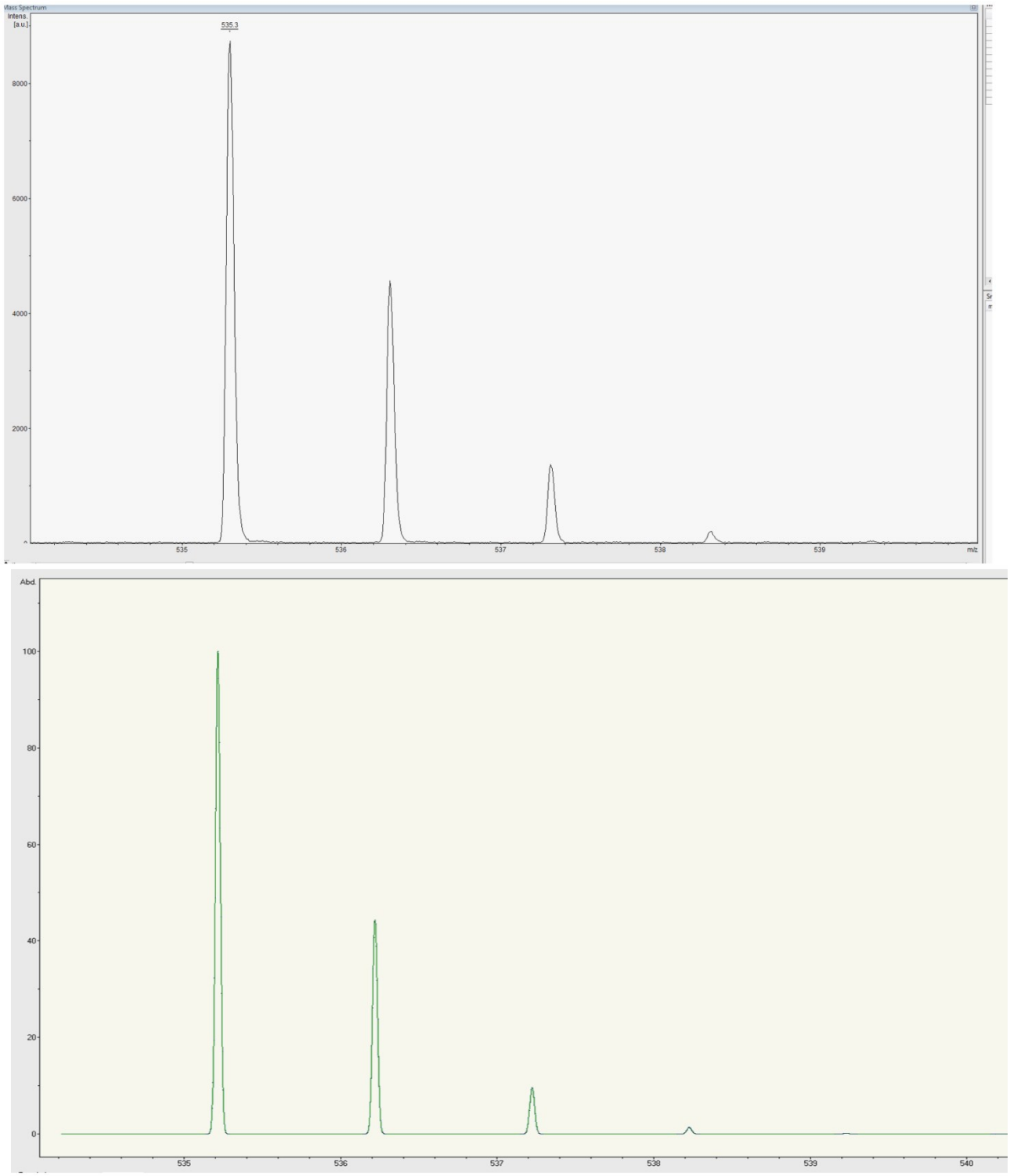

Figure 37: MS (MALDI-TOF) in dithranol of **4b** $[M+H]^+$ (up) and predicted spectrum (bottom).

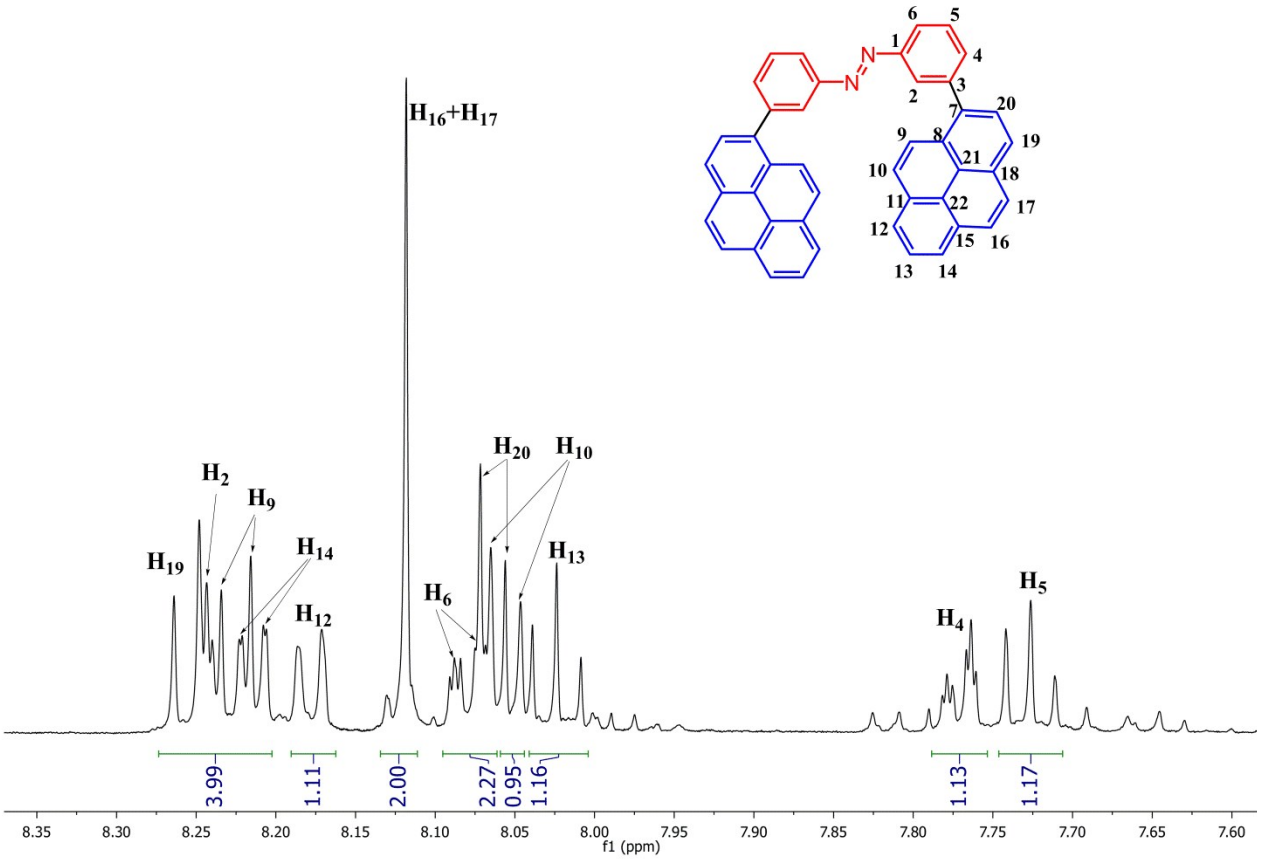

Figure S38: ^{1}H NMR (500MHz, $CDCl_3$) of **5b**.

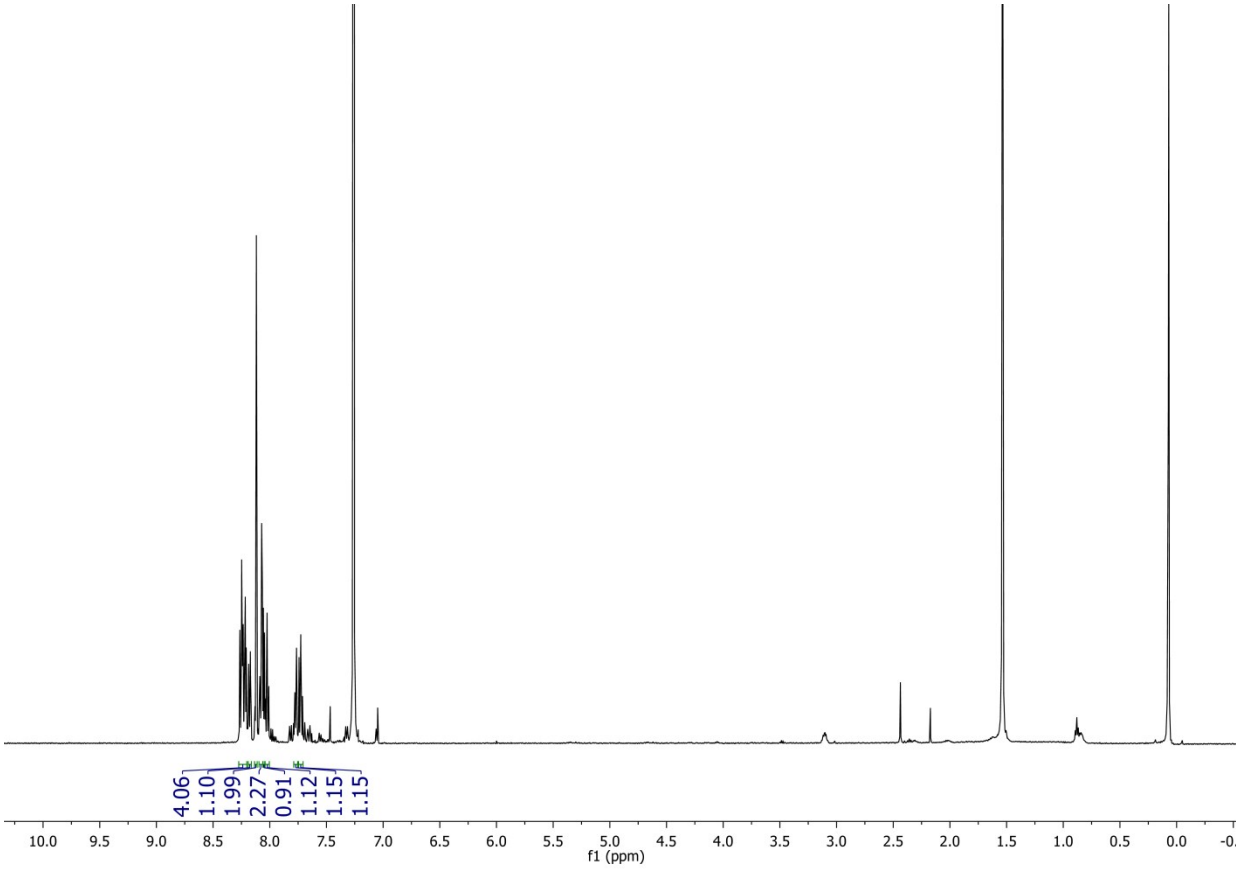

Figure S39: Full ^{1}H NMR (500MHz, $CDCl_3$) of **5b**.

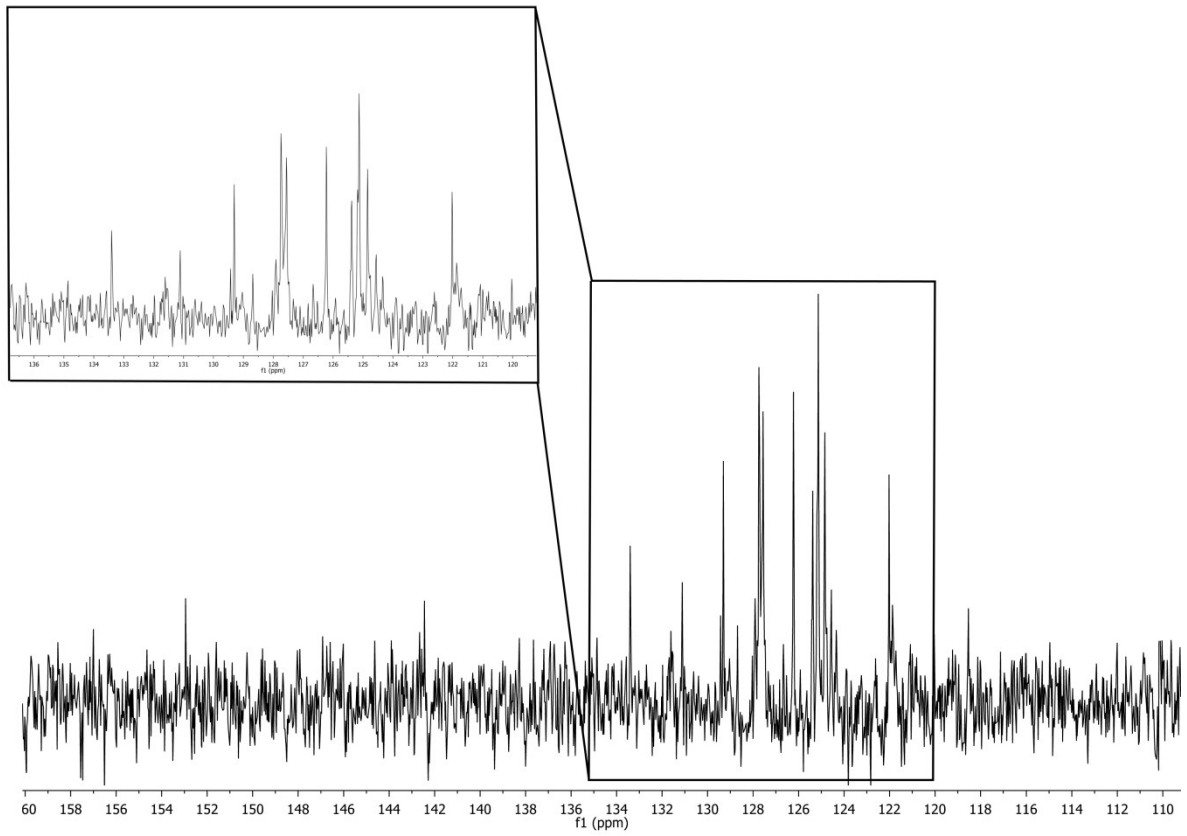

Figure S40: $^{13}C\{^{1}H\}$ NMR (126MHz, $CDCl_3$) of **5b**.

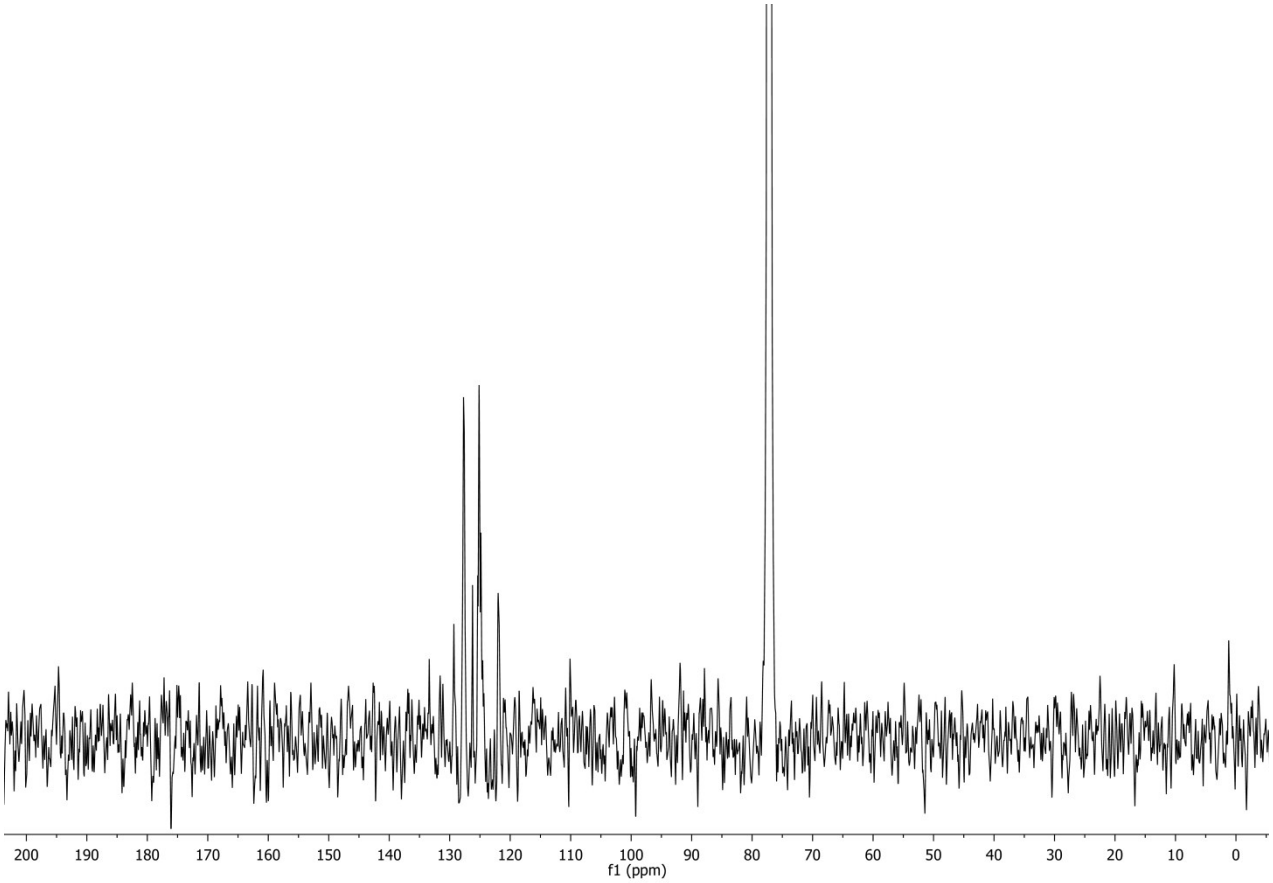

Figure S41: Full $^{13}C\{^{1}H\}$ NMR (126MHz, $CDCl_3$) of **5b**.

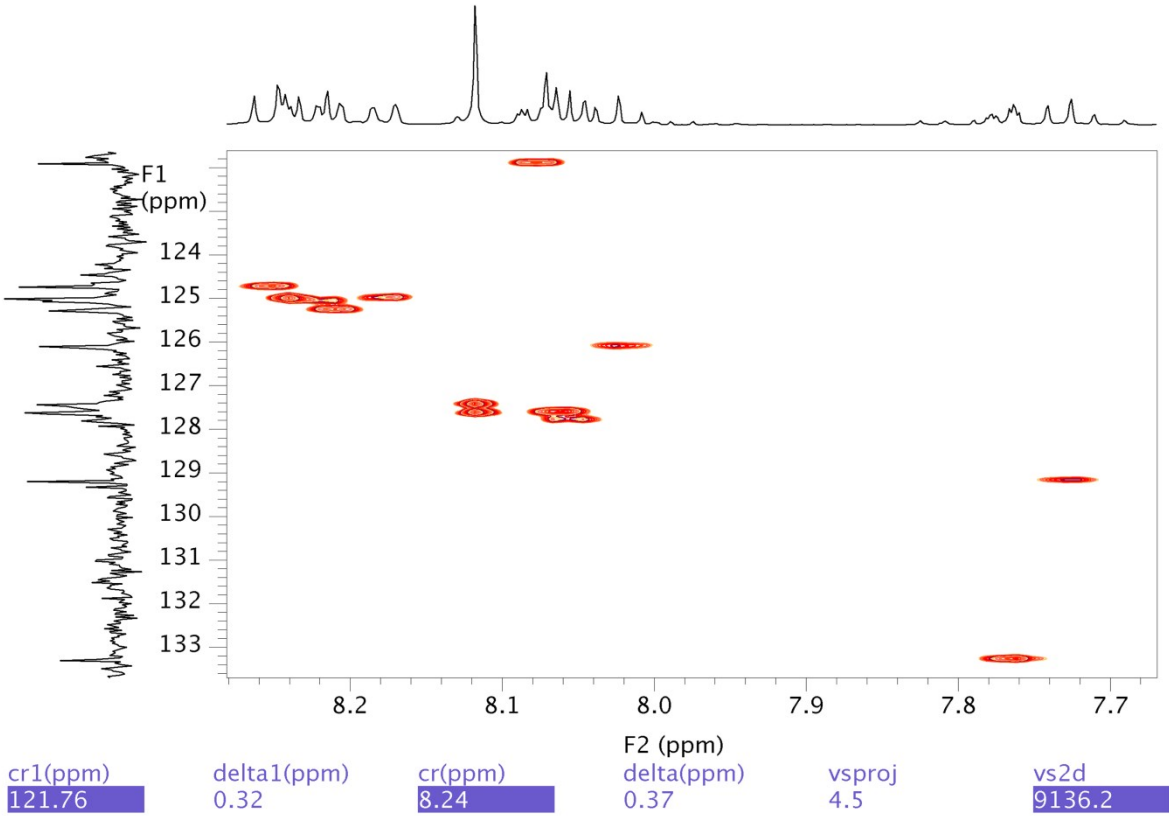

Figure S42: ^{1}H - ^{13}C band selective HSQC ($CDCl_3$) of **5b**.

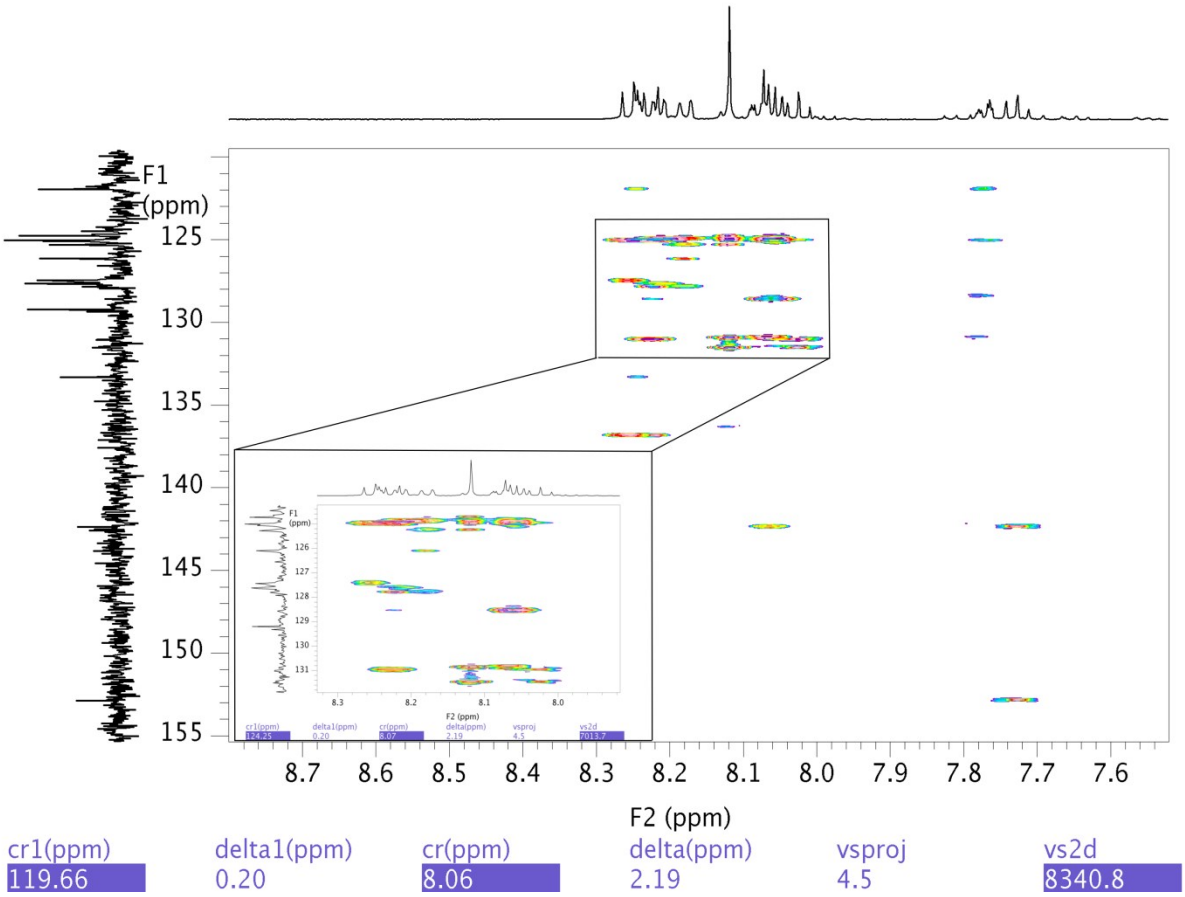

Figure S43: ^{1}H - ^{13}C band selective HMBC ($CDCl_3$) of **5b**.

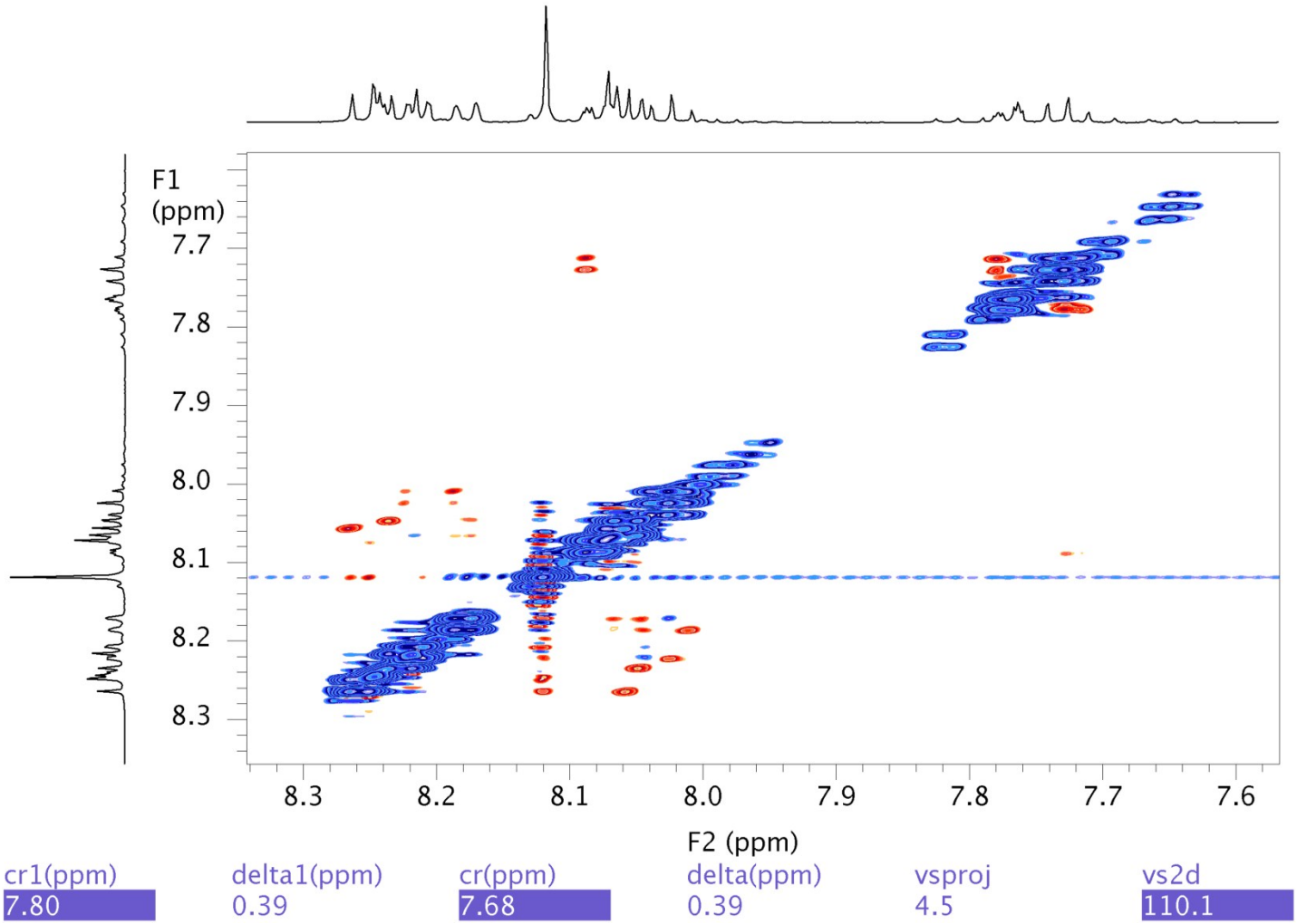

Figure S44: ^{1}H - ^{1}H band selective ROESY ($CDCl_3$) of **5b**.

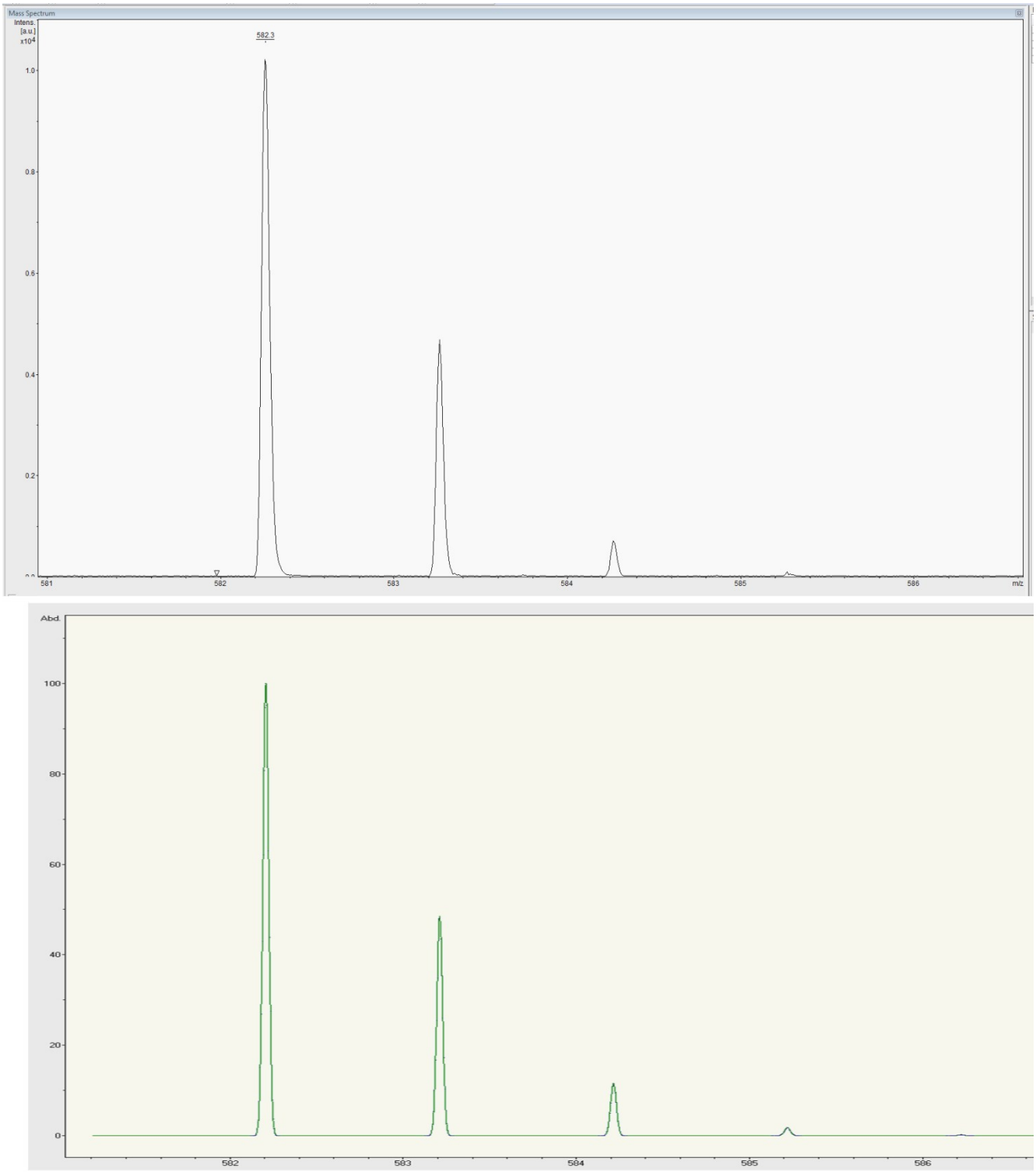

Figure S45: MS (MALDI-TOF) in DCTB of **5b** $[M]^+$ (up) and predicted spectrum (bottom).

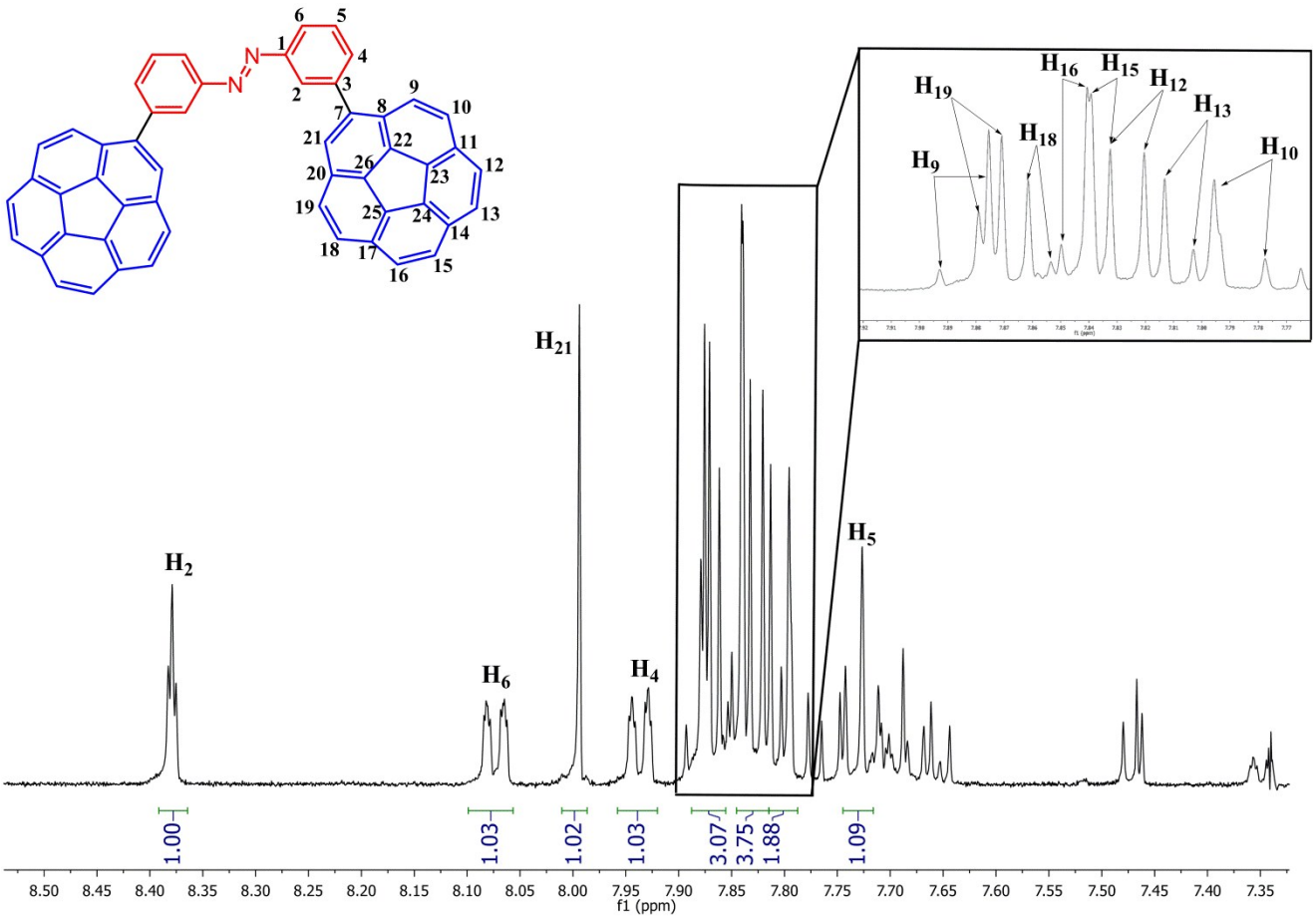

Figure S46: ^{1}H NMR (500MHz, $CDCl_3$) of **6b**.

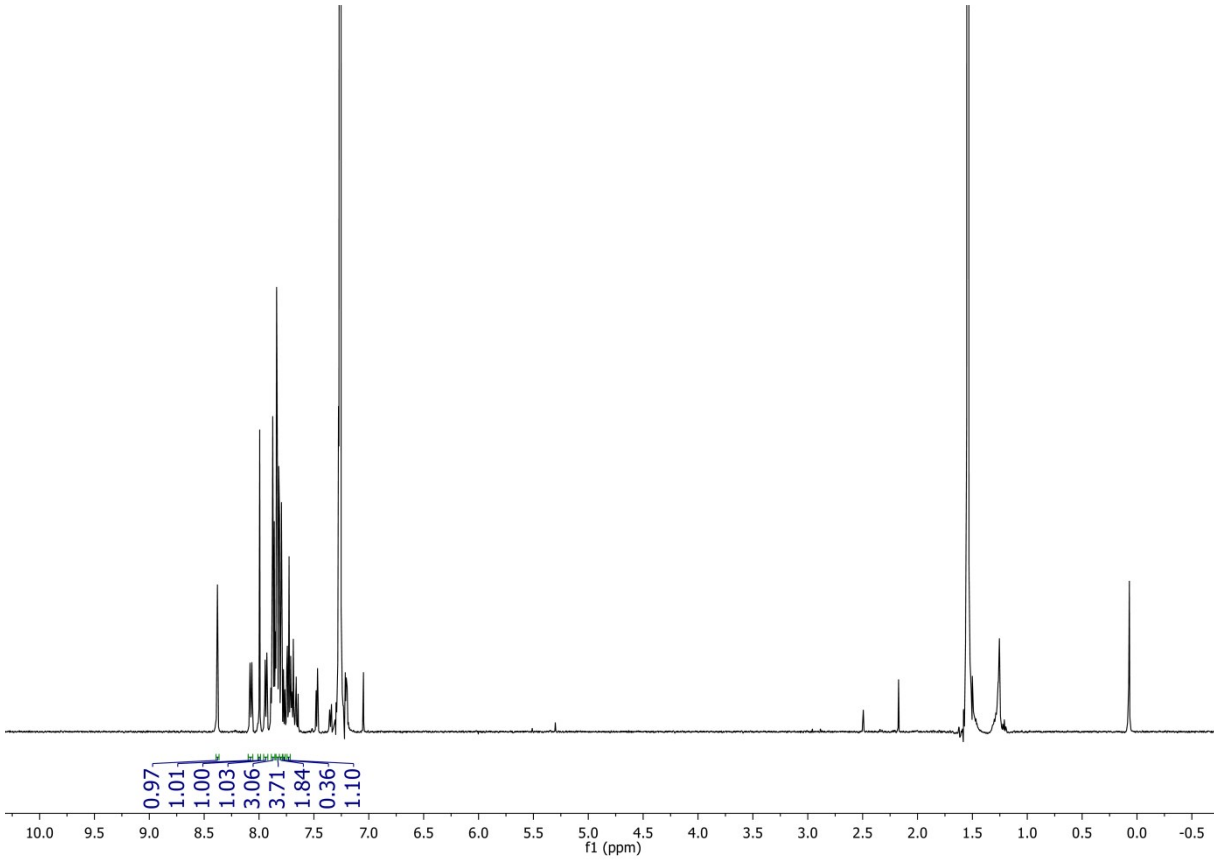

Figure S47: Full ^{1}H NMR (500MHz, $CDCl_3$) of **6b**.

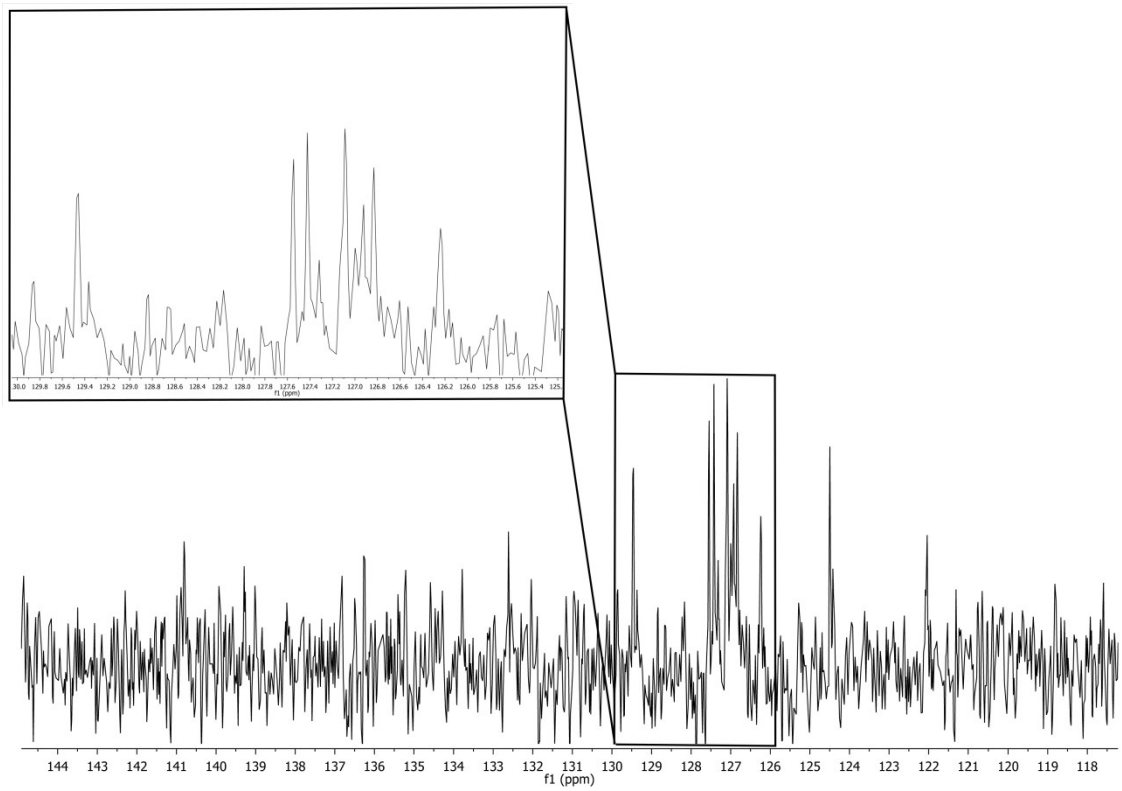

Figure S48: $^{13}C\{^{1}H\}$ NMR (126MHz, $CDCl_3$) of **6b**.

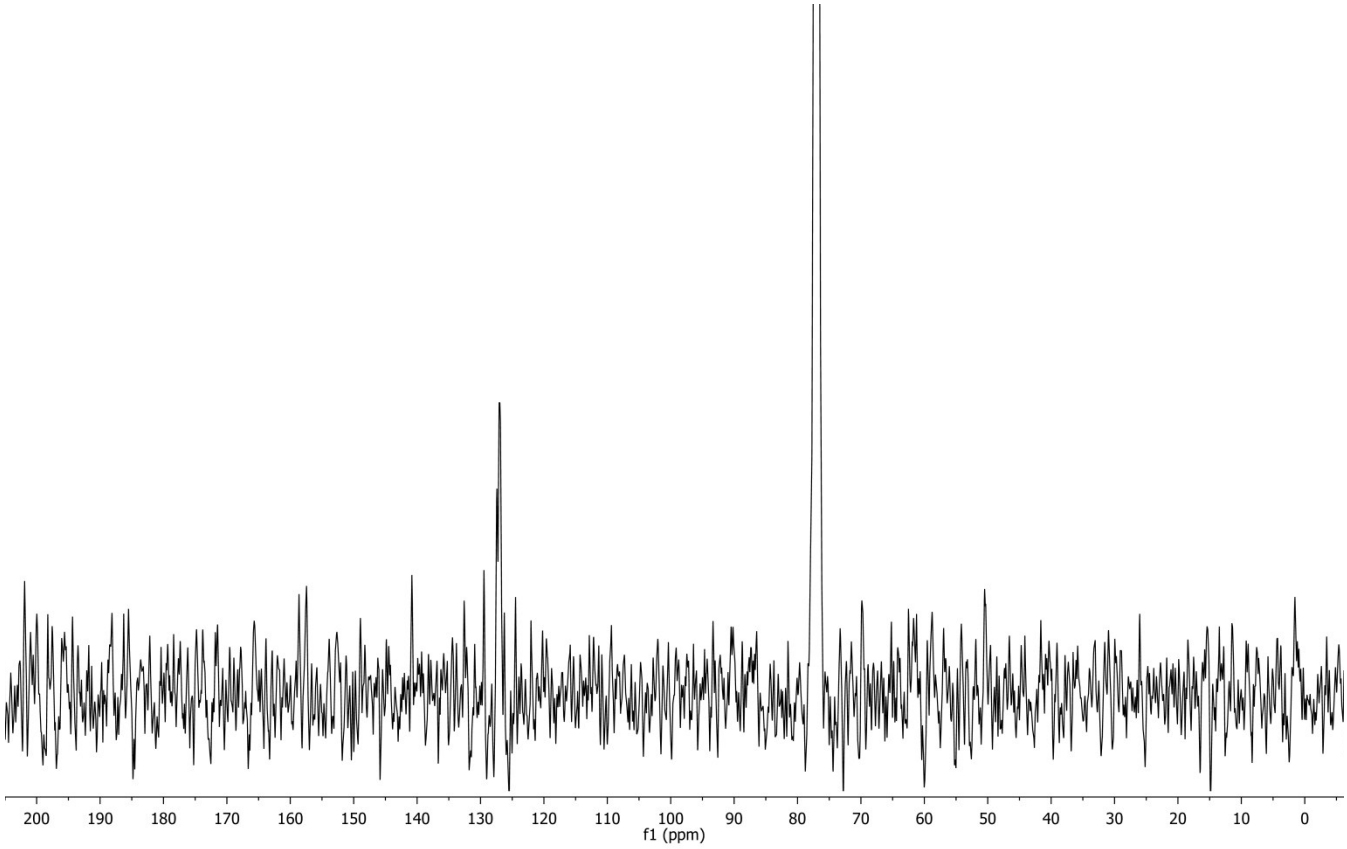

Figure S49: Full $^{13}C\{^{1}H\}$ NMR (126MHz, $CDCl_3$) of **6b**.

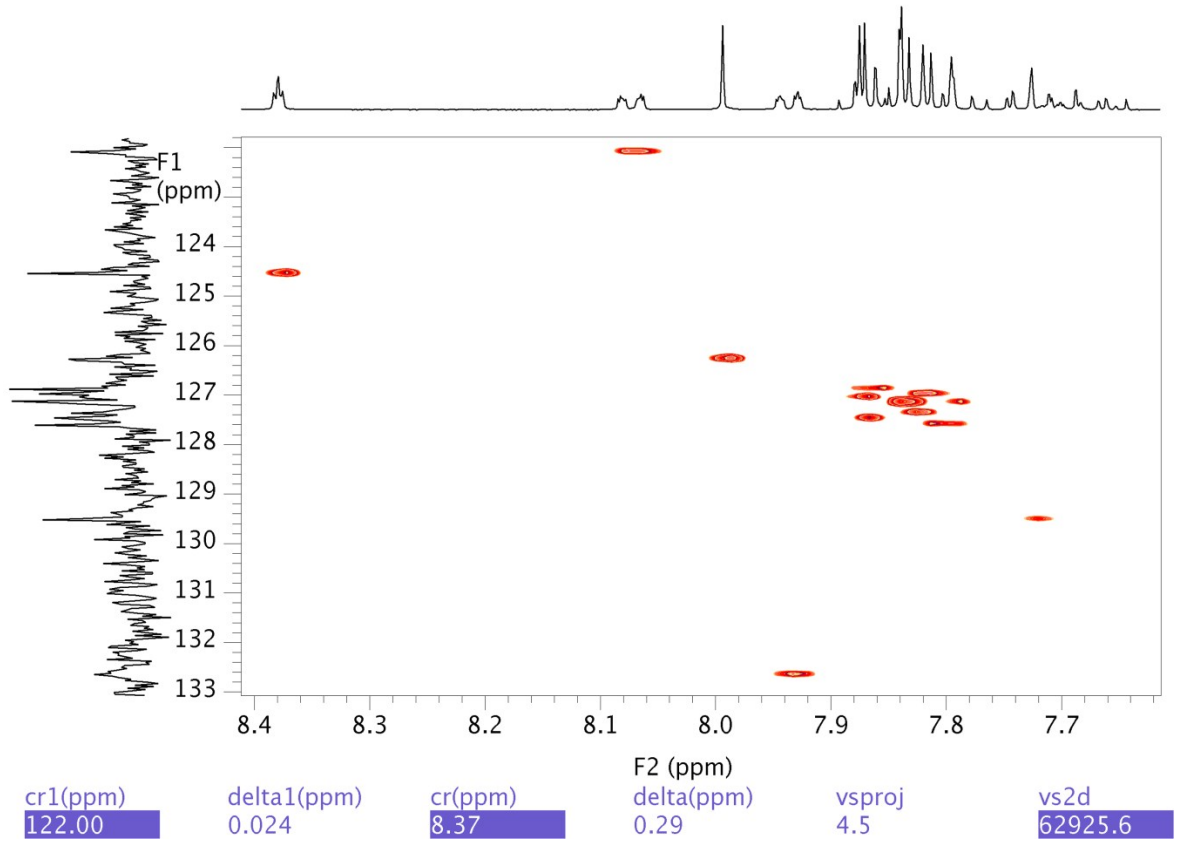

Figure S50: ^{1}H - ^{13}C band selective HSQC ($CDCl_3$) of **6b**.

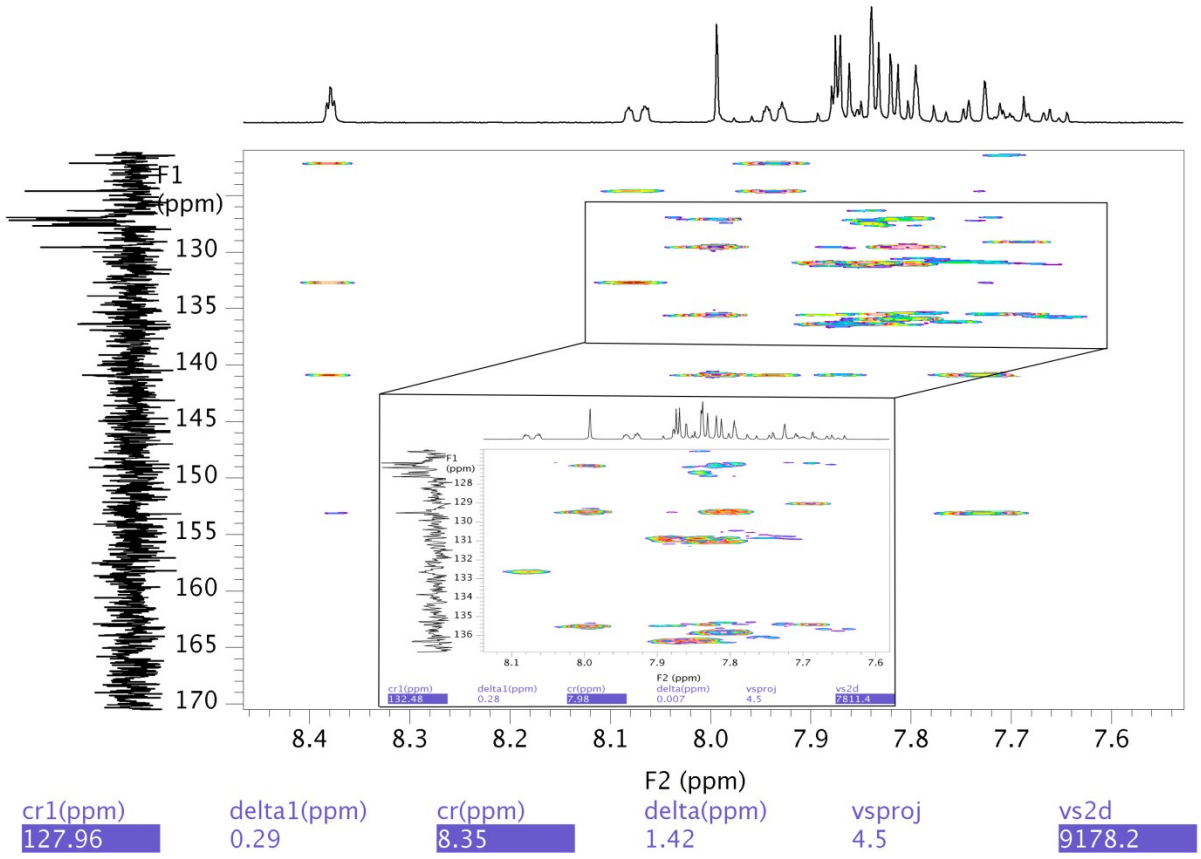

Figure S51: ^{1}H - ^{13}C gradient crisis HMBC ($CDCl_3$) of **6b**.

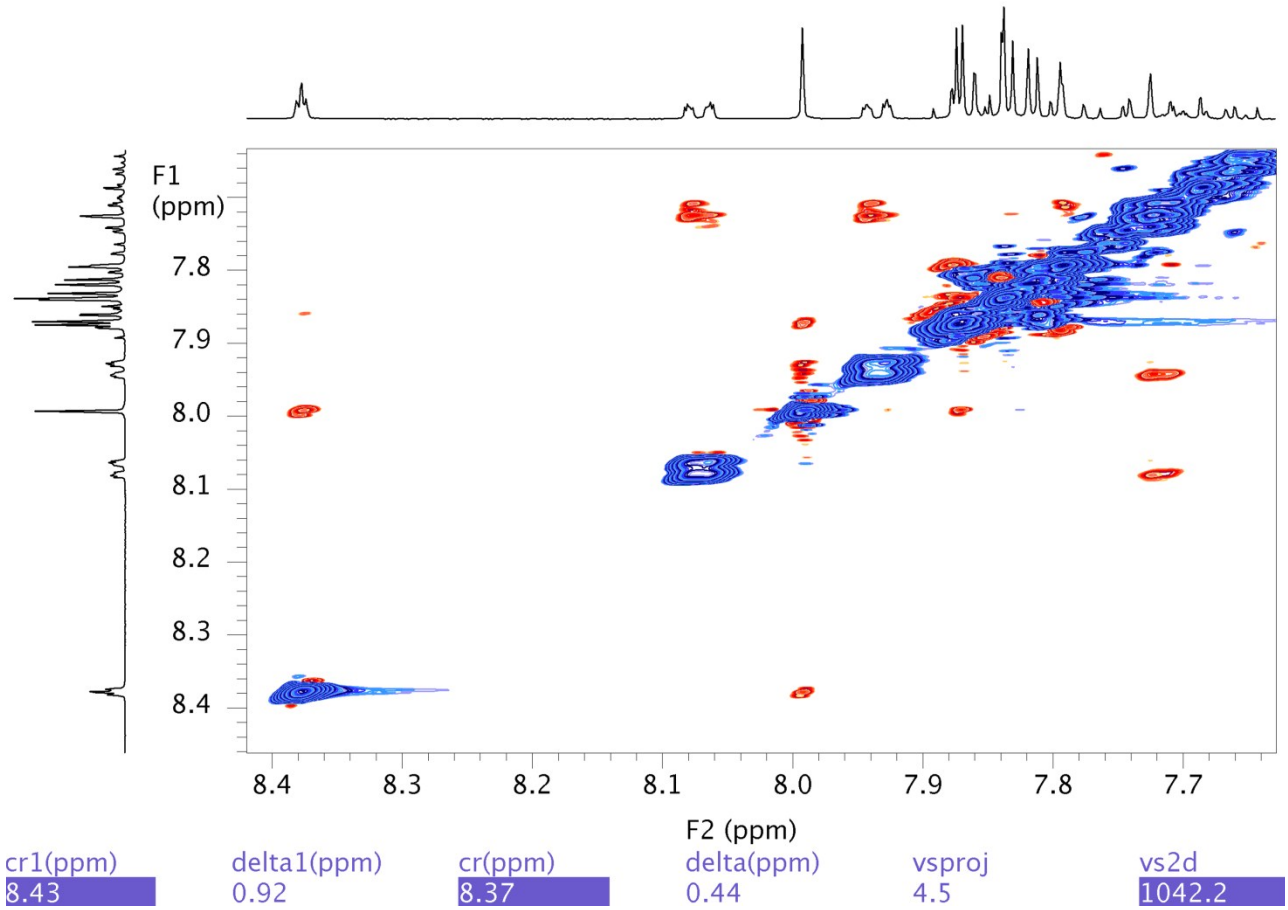

Figure S52: ^{1}H - ^{1}H band selective ROESY ($CDCl_3$) of **6b**.

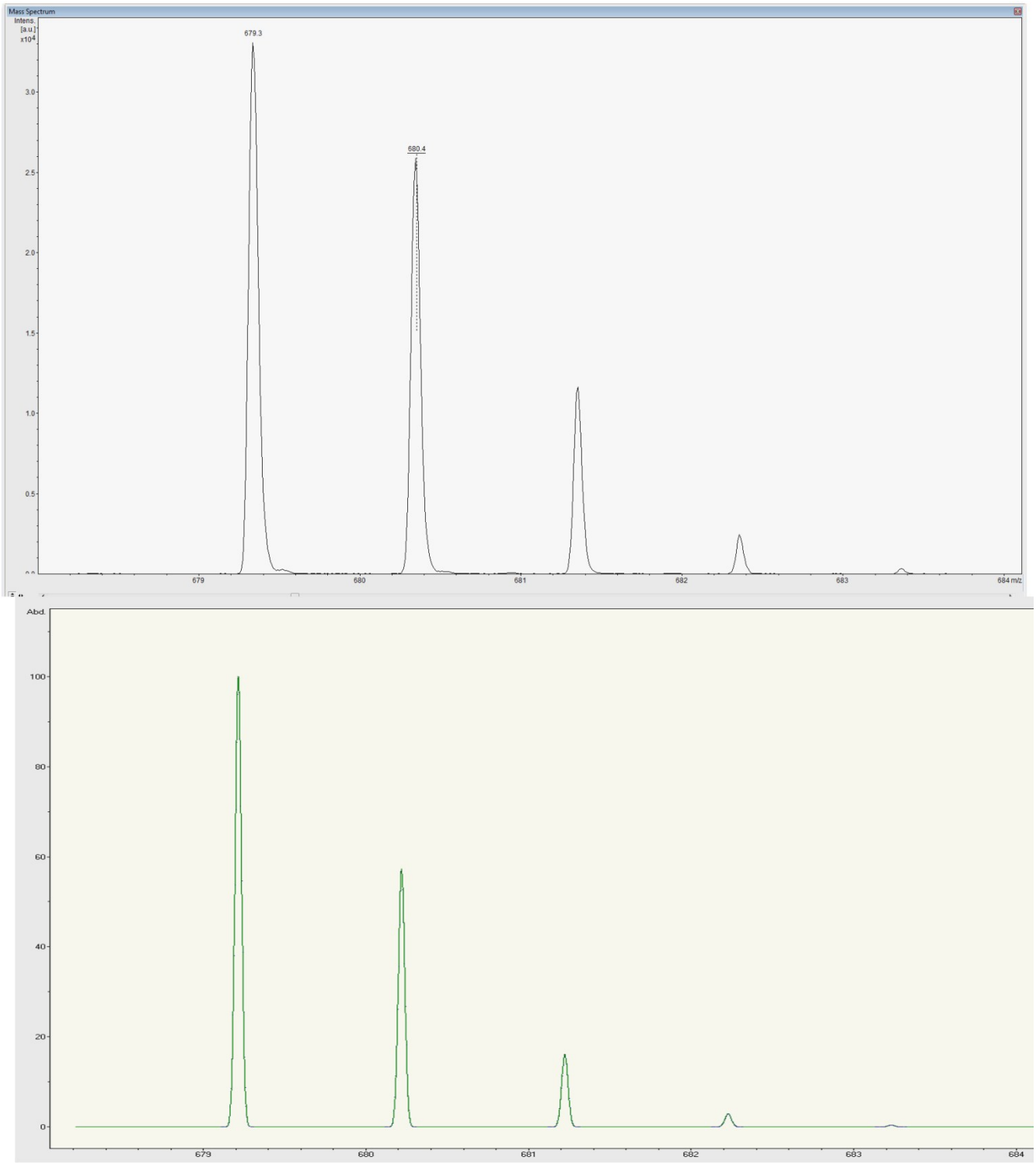

Figure S53: MS (MALDI-TOF) in dithranol of **6b** $[M+H]^+$ (up) and predicted spectrum (bottom).

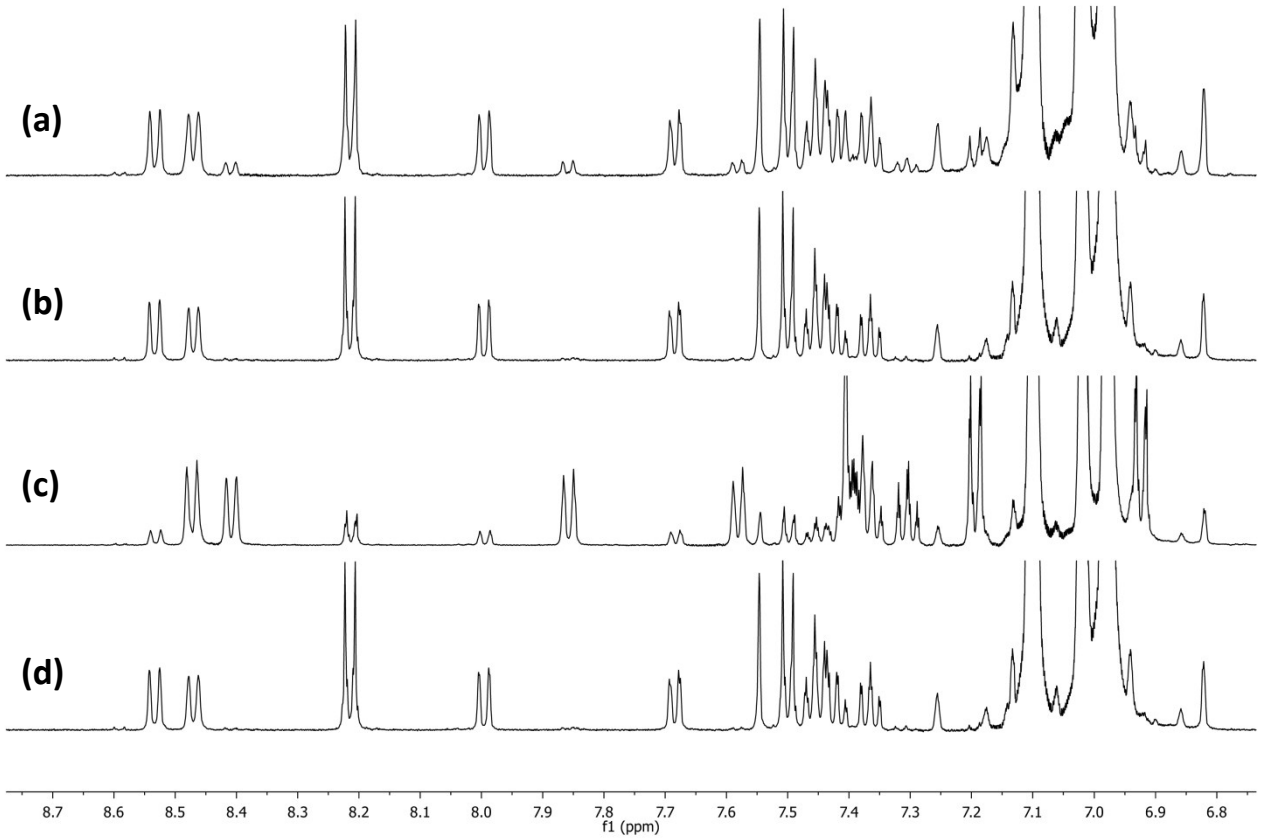

Figure S54: ^{1}H-NMR (500 MHz, tol-d8) of **4a** (a), after heating at 80º for 15 minutes (b), after irradiation at 365nm (c) and after heating at 80º again (d).

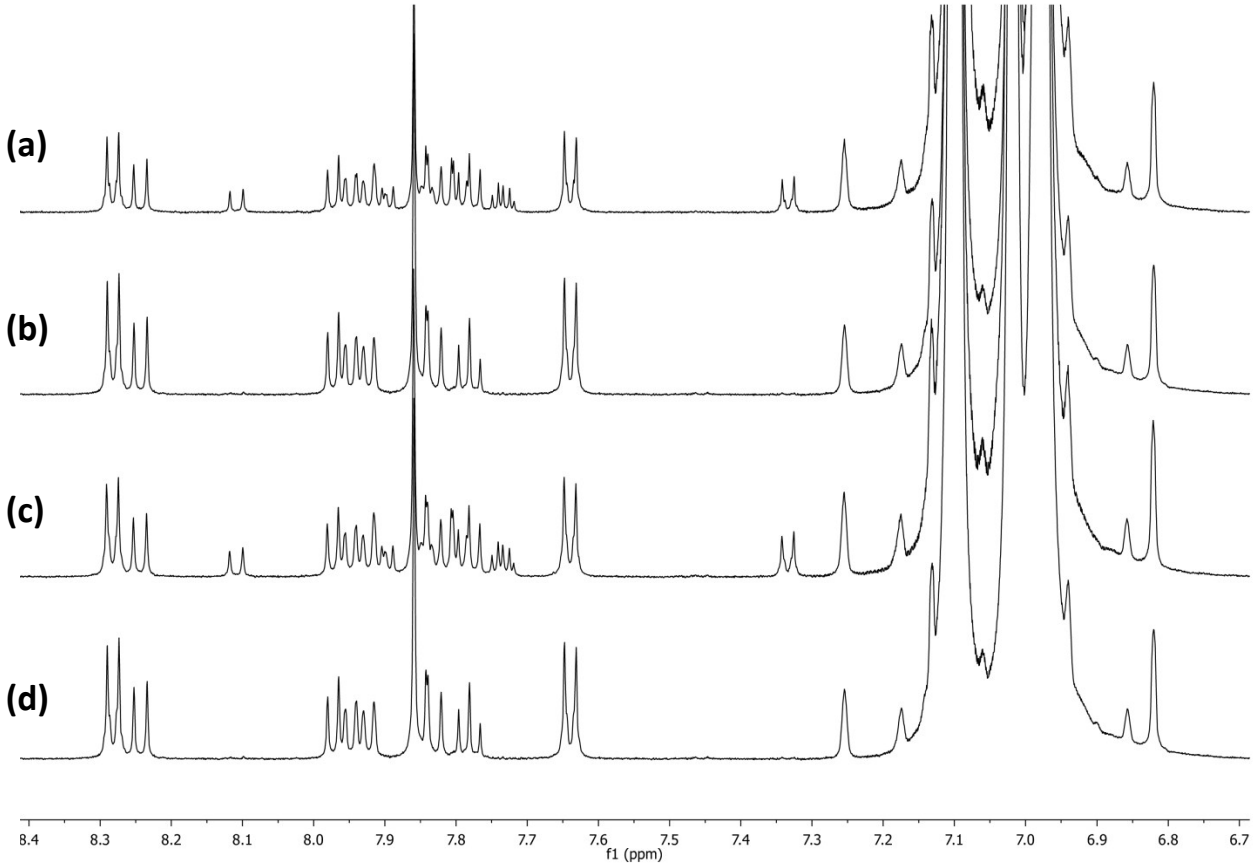

Figure S55: ^{1}H-NMR (500 MHz, tol-d8) of **5a** (a), after heating at 80º for 15 minutes (b), after irradiation at 365nm (c) and after heating at 80º again (d).

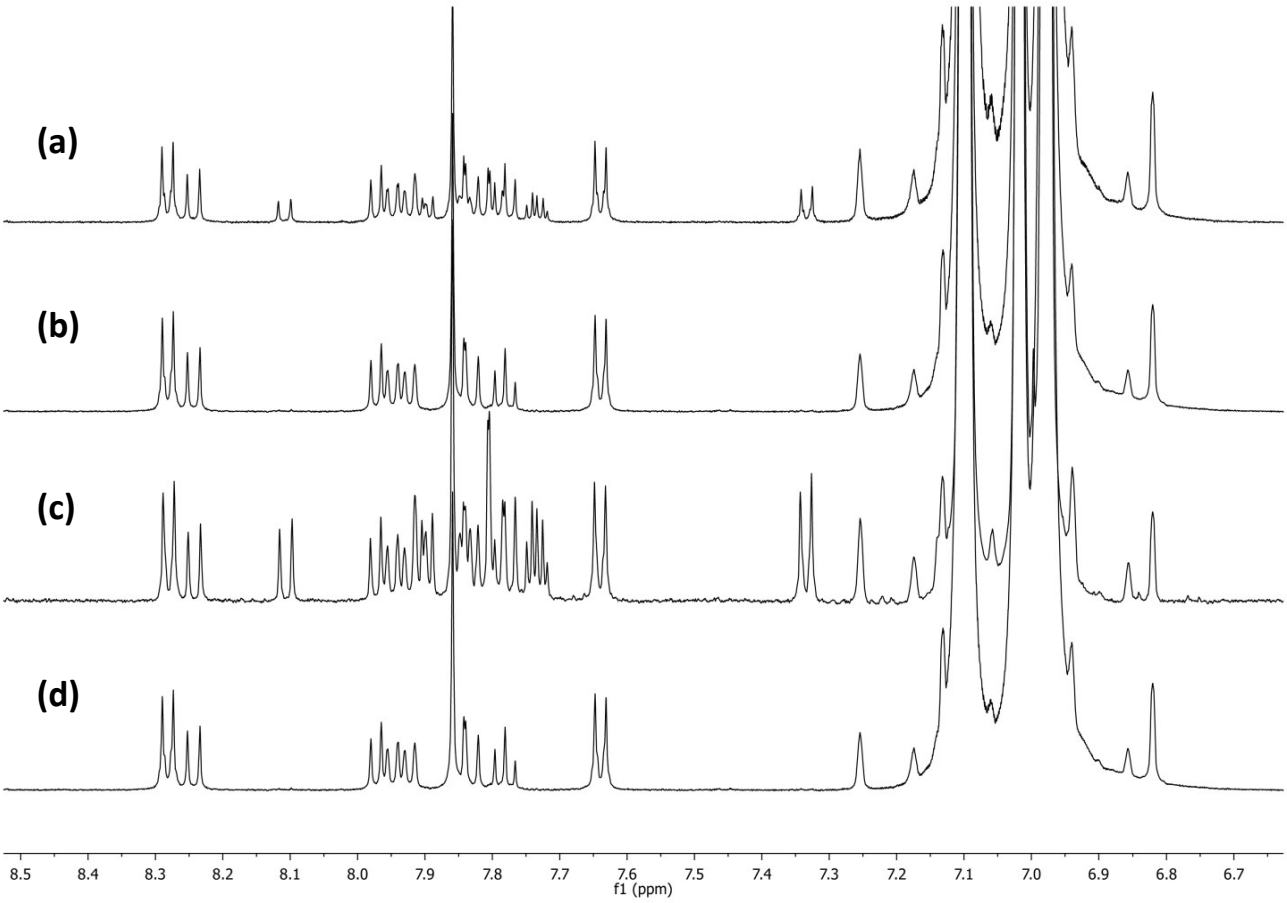

Figure S56: ^{1}H-NMR (500 MHz, tol-d8) of **5a** (a), after heating at 80º for 15 minutes (b), after irradiation at 380nm (c) and after heating at 80º again (d).

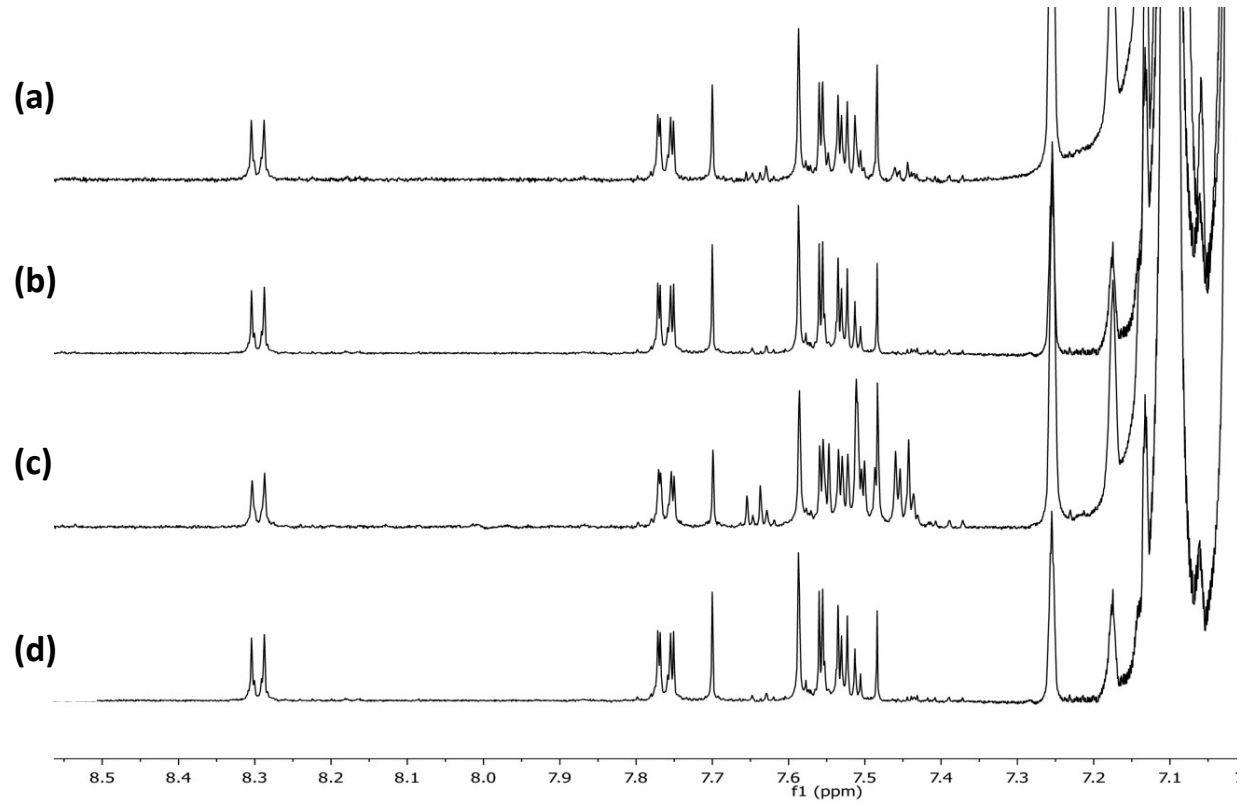

Figure S57: ^{1}H-NMR (500 MHz, tol-d8) of **6a** (a), after heating at 80º for 15 minutes (b), after irradiation at 365nm (c) and after heating at 80º again (d).

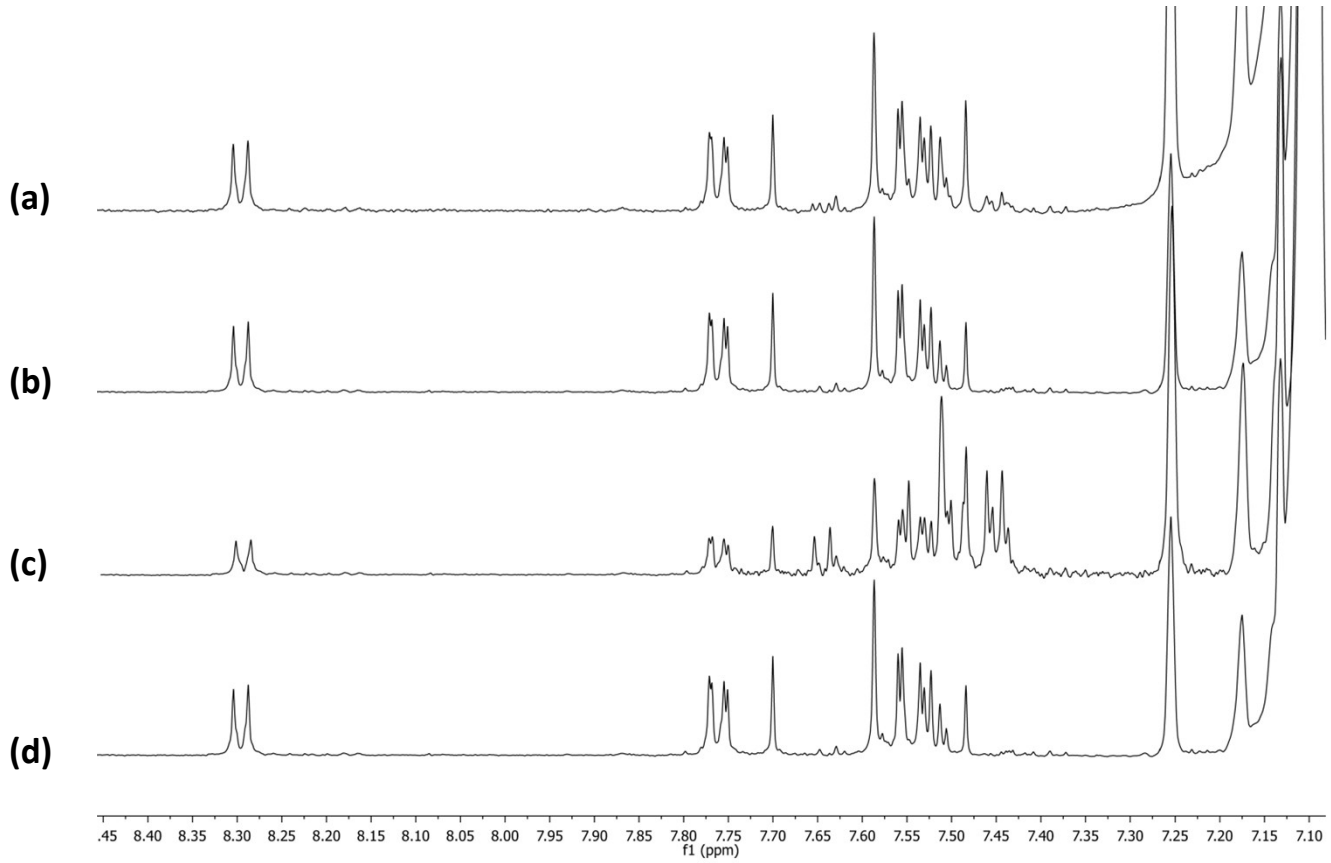

Figure S58: ^{1}H-NMR (500 MHz, tol-d8) of **6a** (a), after heating at 80º for 15 minutes (b), after irradiation at 380nm (c) and after heating at 80º again (d).

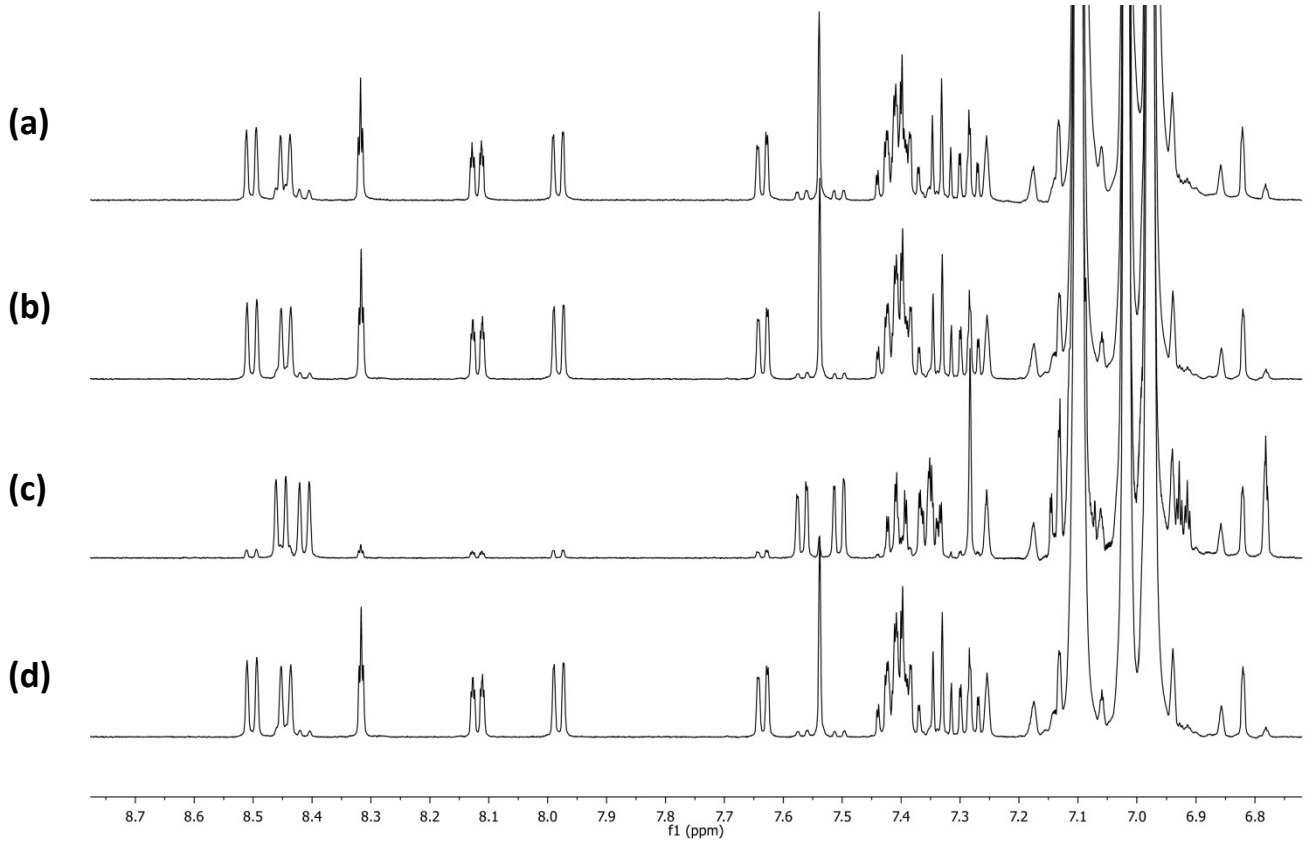

Figure S59: ^{1}H-NMR (500 MHz, tol-d8) of **4b** (a), after heating at 80º for 15 minutes (b), after irradiation at 365nm (c) and after heating at 80º again (d).

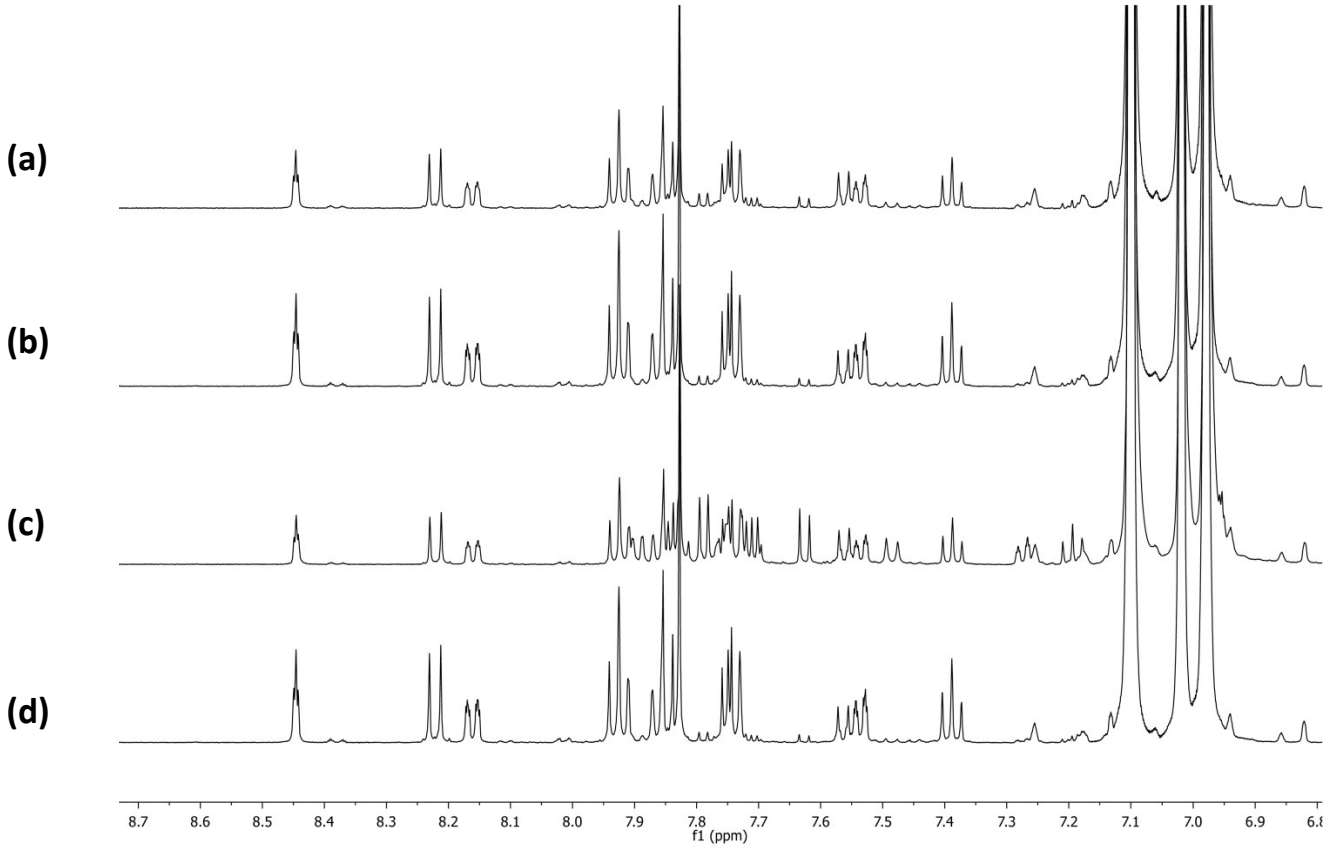

Figure S60: ^{1}H-NMR (500 MHz, tol-d8) of **5b** (a), after heating at 80º for 15 minutes (b), after irradiation at 365nm (c) and after heating at 80º again (d).

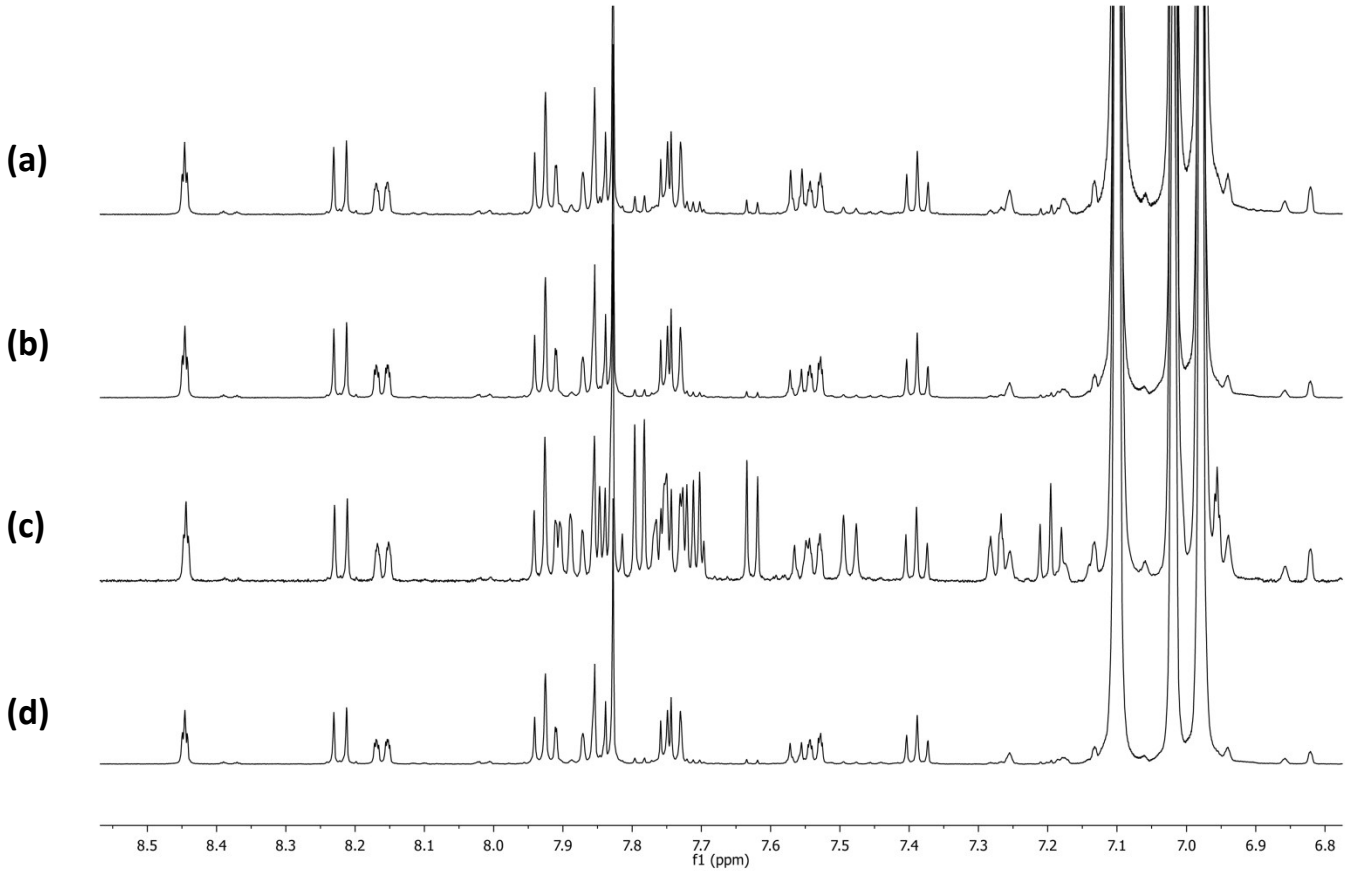

Figure S61: ^{1}H-NMR (500 MHz, tol-d8) of **5b** (a), after heating at 80º for 15 minutes (b), after irradiation at 380nm (c) and after heating at 80º again (d).

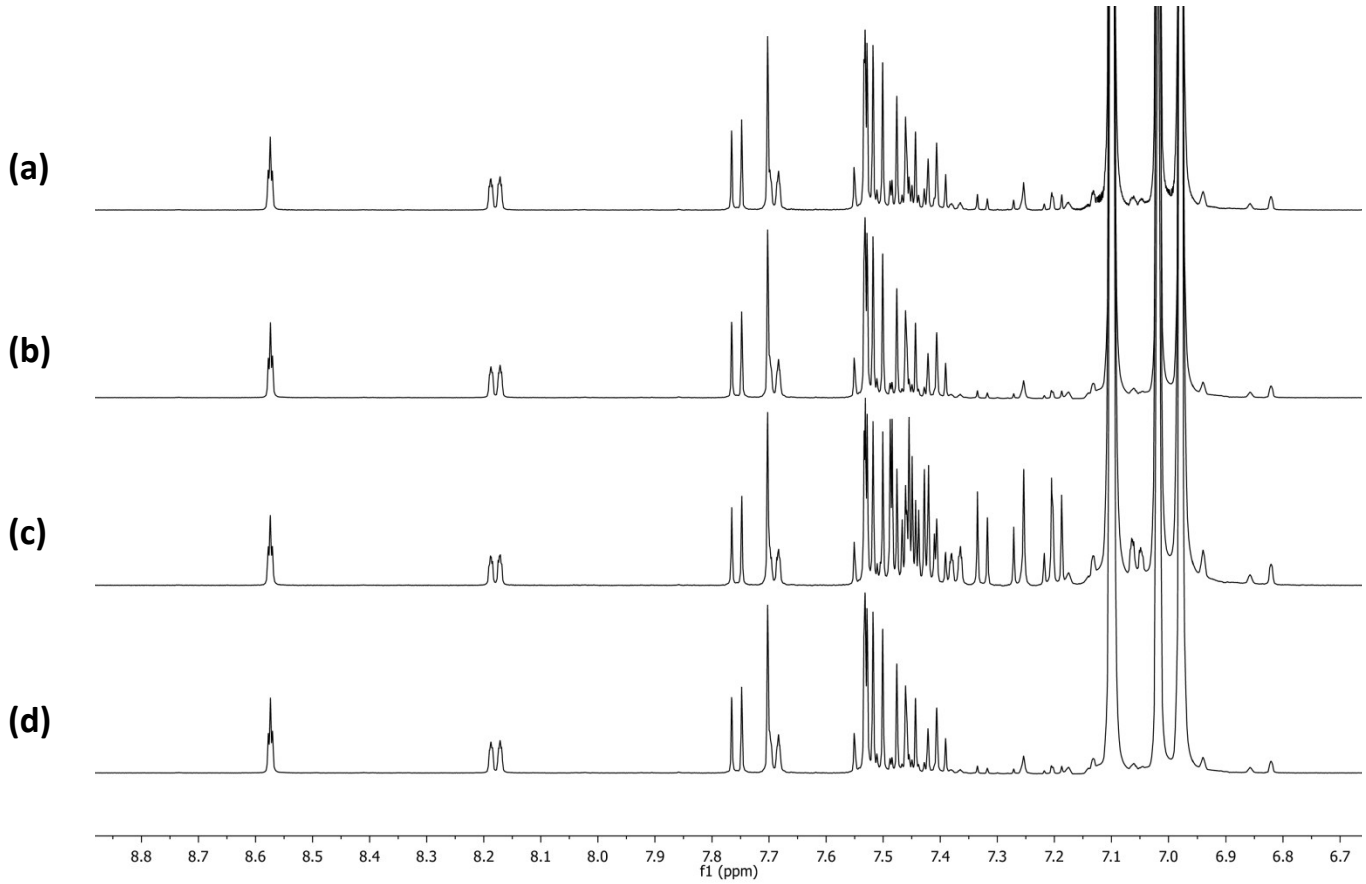

Figure S62: ^{1}H-NMR (500 MHz, tol-d8) of **6b** (a), after heating at 80º for 15 minutes (b), after irradiation at 365nm (c) and after heating at 80º again (d).

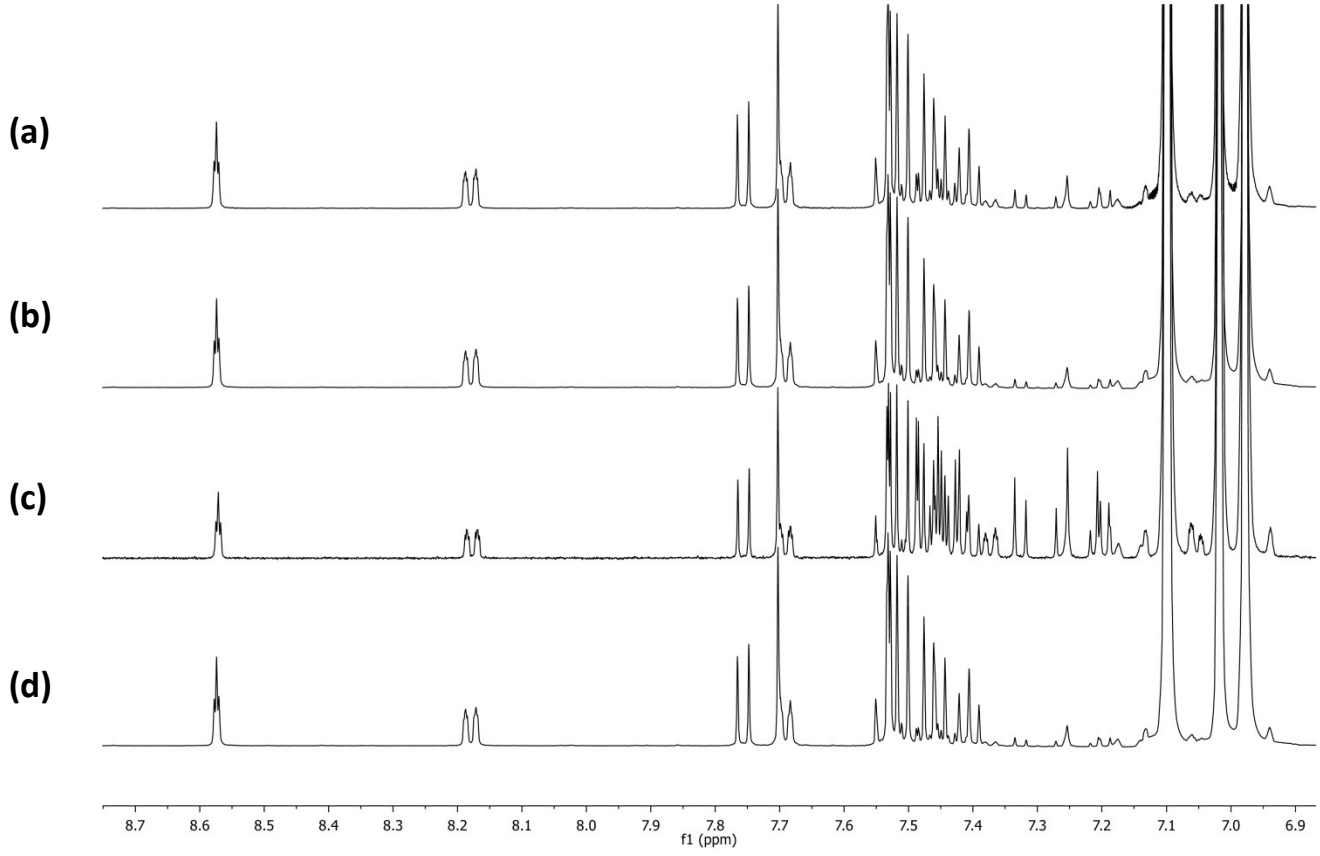

Figure S63: ^{1}H-NMR (500 MHz, tol-d8) of **6b** (a), after heating at 80º for 15 minutes (b), after irradiation at 380nm (c) and after heating at 80º again (d).

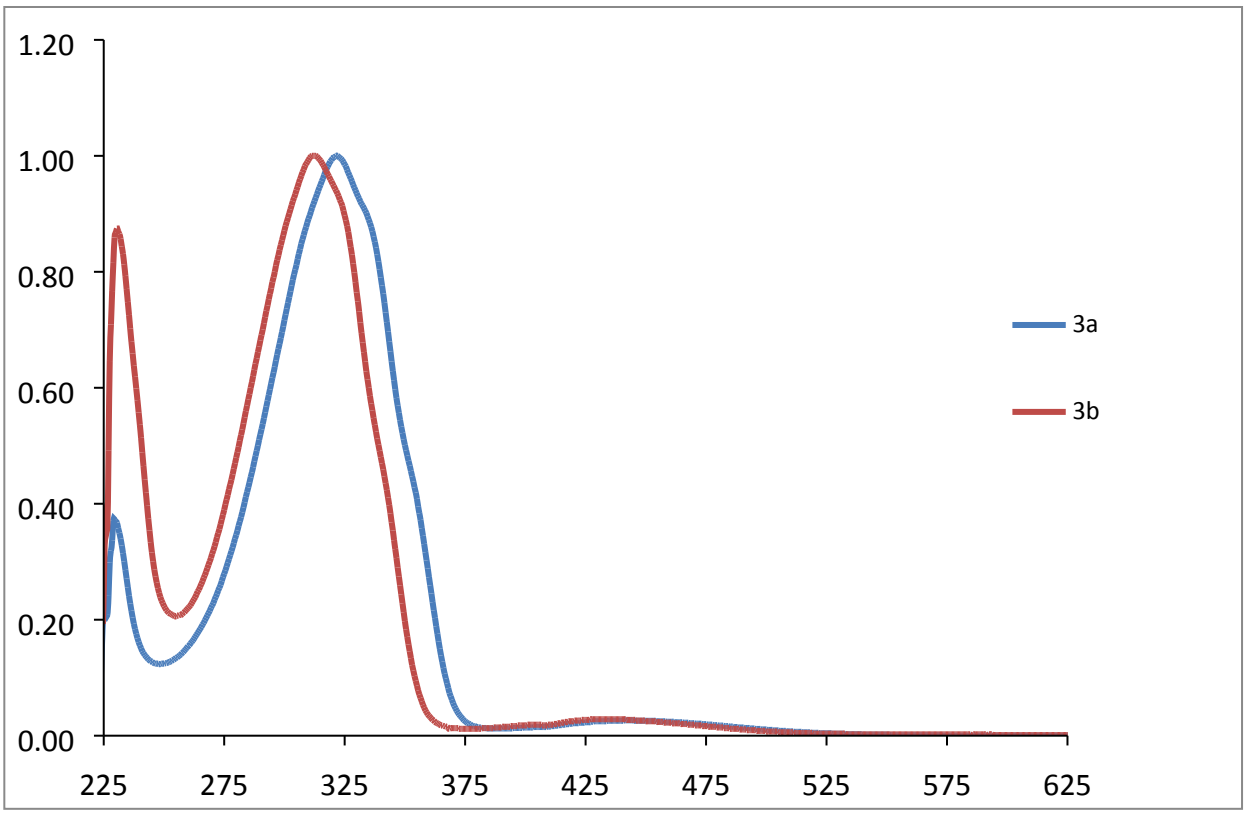

Figure S64: Normalized UV/Vis absorption spectra for **3a** and **3b** in chloroform.

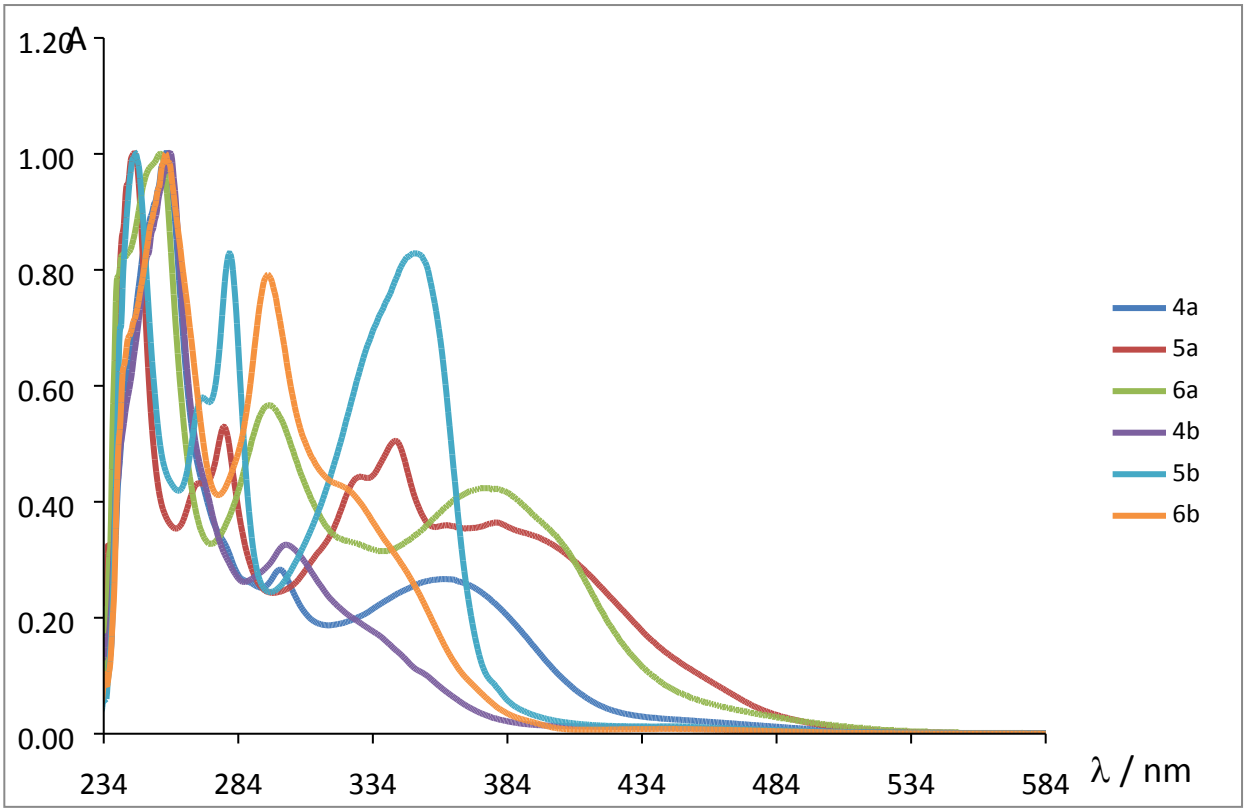

Figure S65: Normalized UV/Vis absorption spectra for azobenzene derivatives **4 - 6** in chloroform.

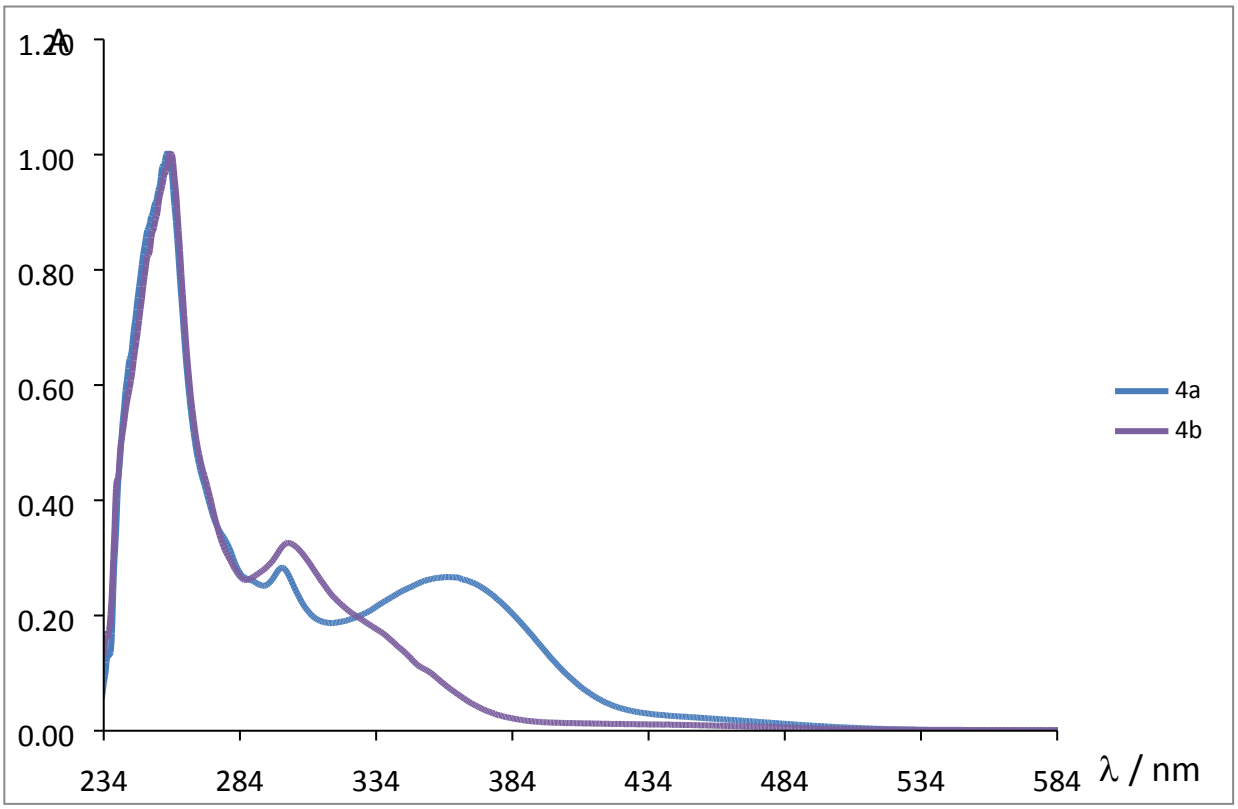

Figure S66: Normalized UV/Vis absorption spectra for the pair **4a** and **4b** in chloroform.

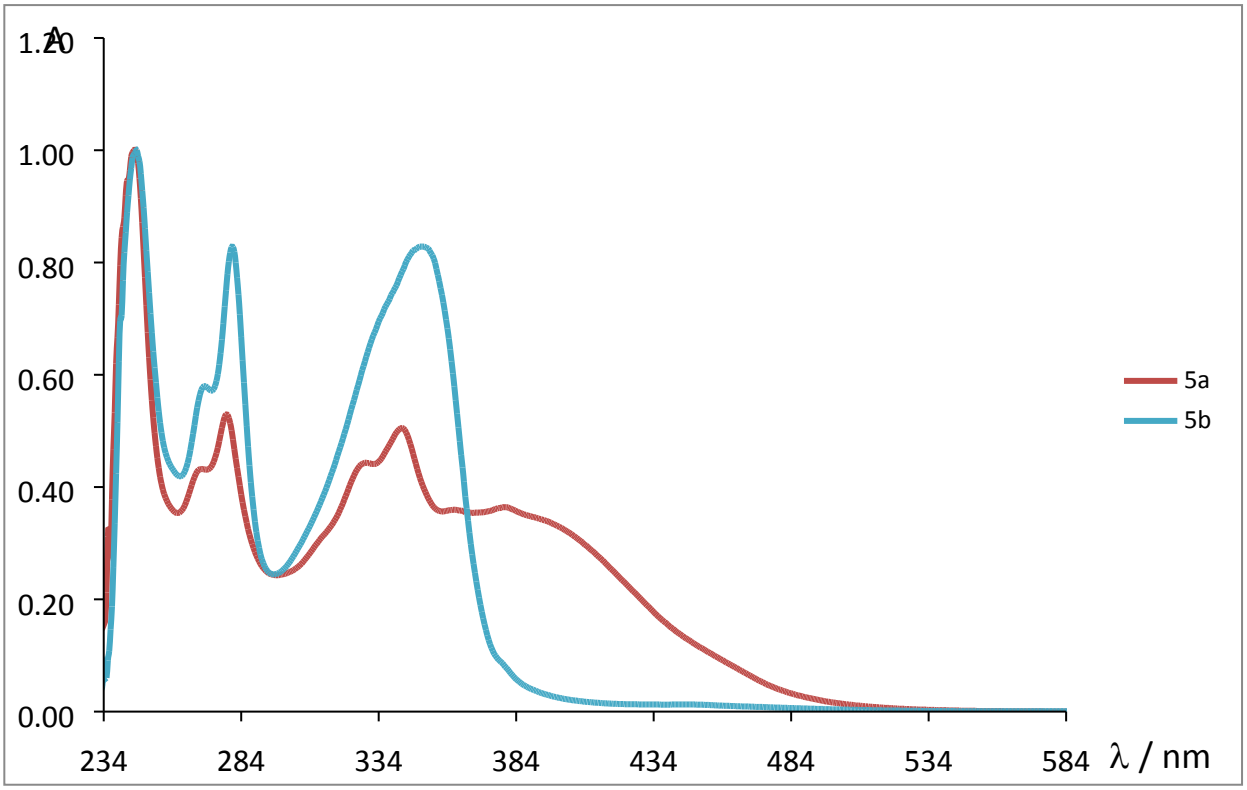

Figure S67: Normalized UV/Vis absorption spectra for the pair **5a** and **5b** in chloroform.

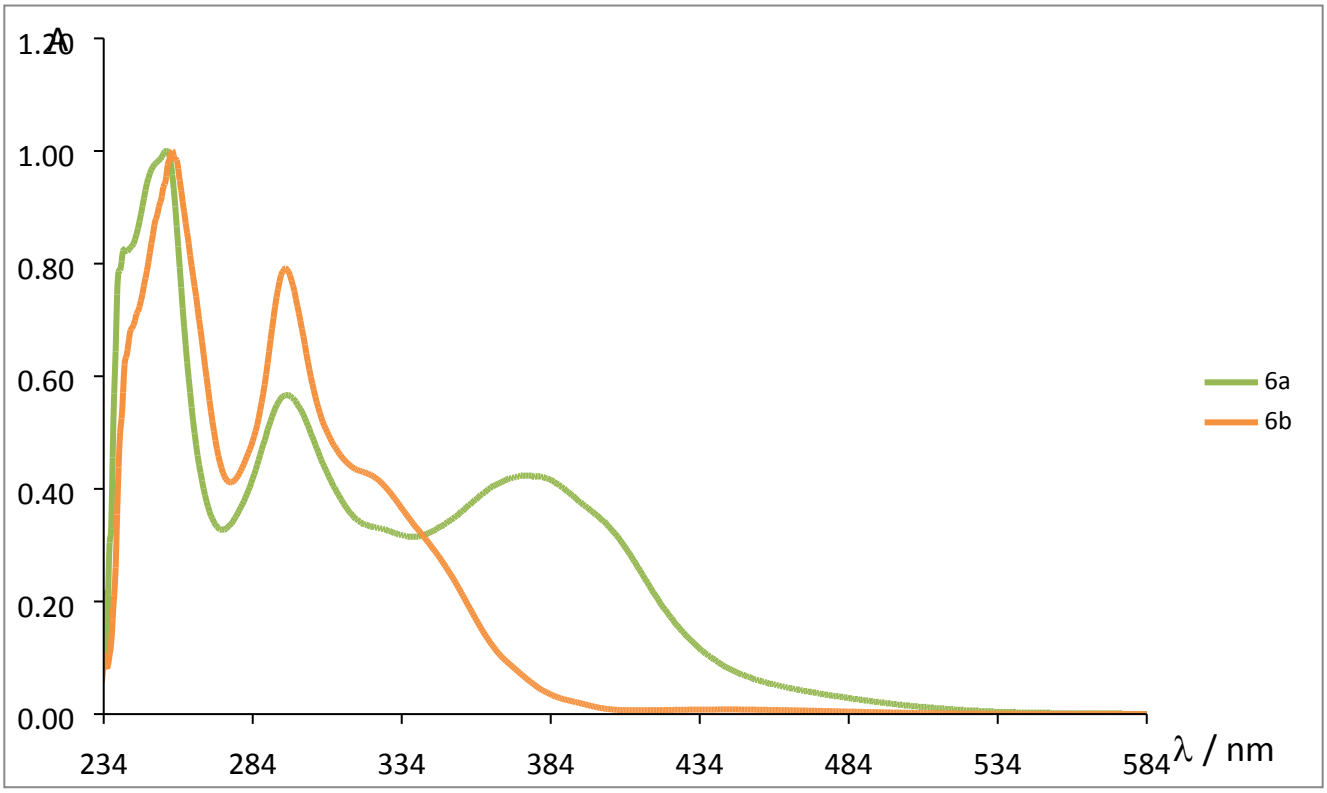

Figure S68: Normalized UV/Vis absorption spectra for the pair **6a** and **6b** in chloroform.

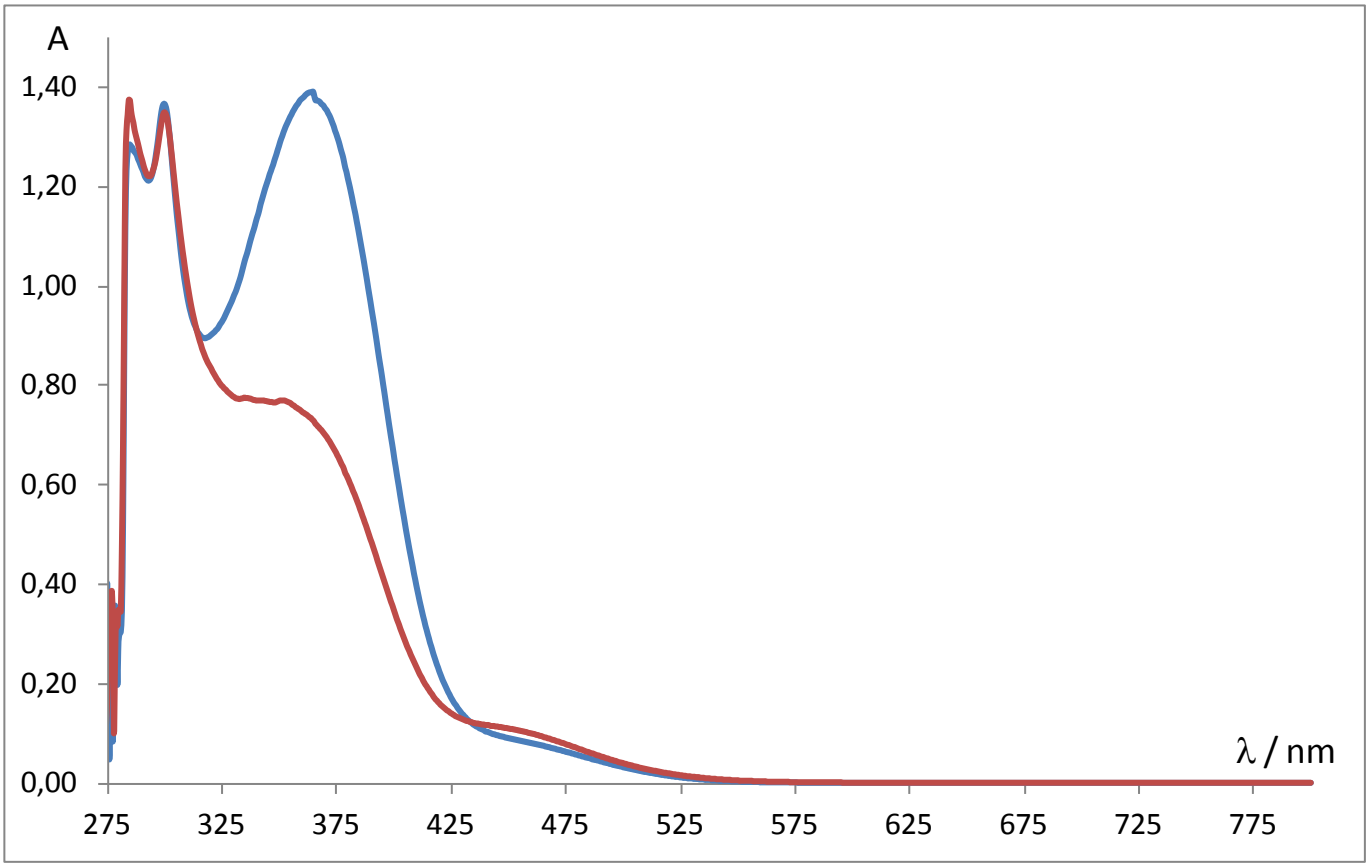

Figure S69: UV/Vis absorption spectra of a 5.35x10^{-5}M solution in toluene of **4a** (blue) and irradiated at 365nm for 15 minutes (red).

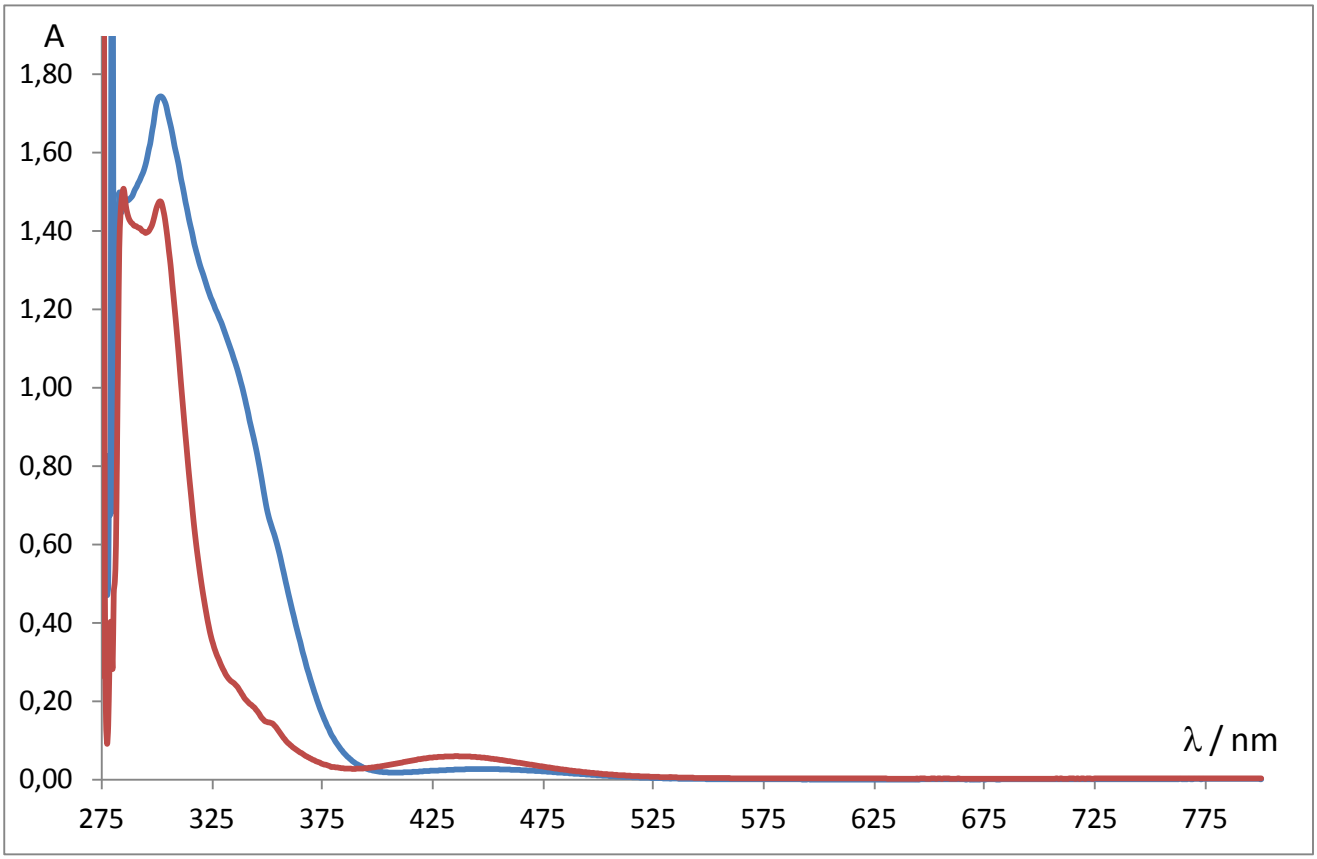

Figure S70: UV/Vis absorption spectra of a 5.24x10^{-5}M solution in toluene of **4b** (blue) and irradiated at 365nm for 15 minutes (red).

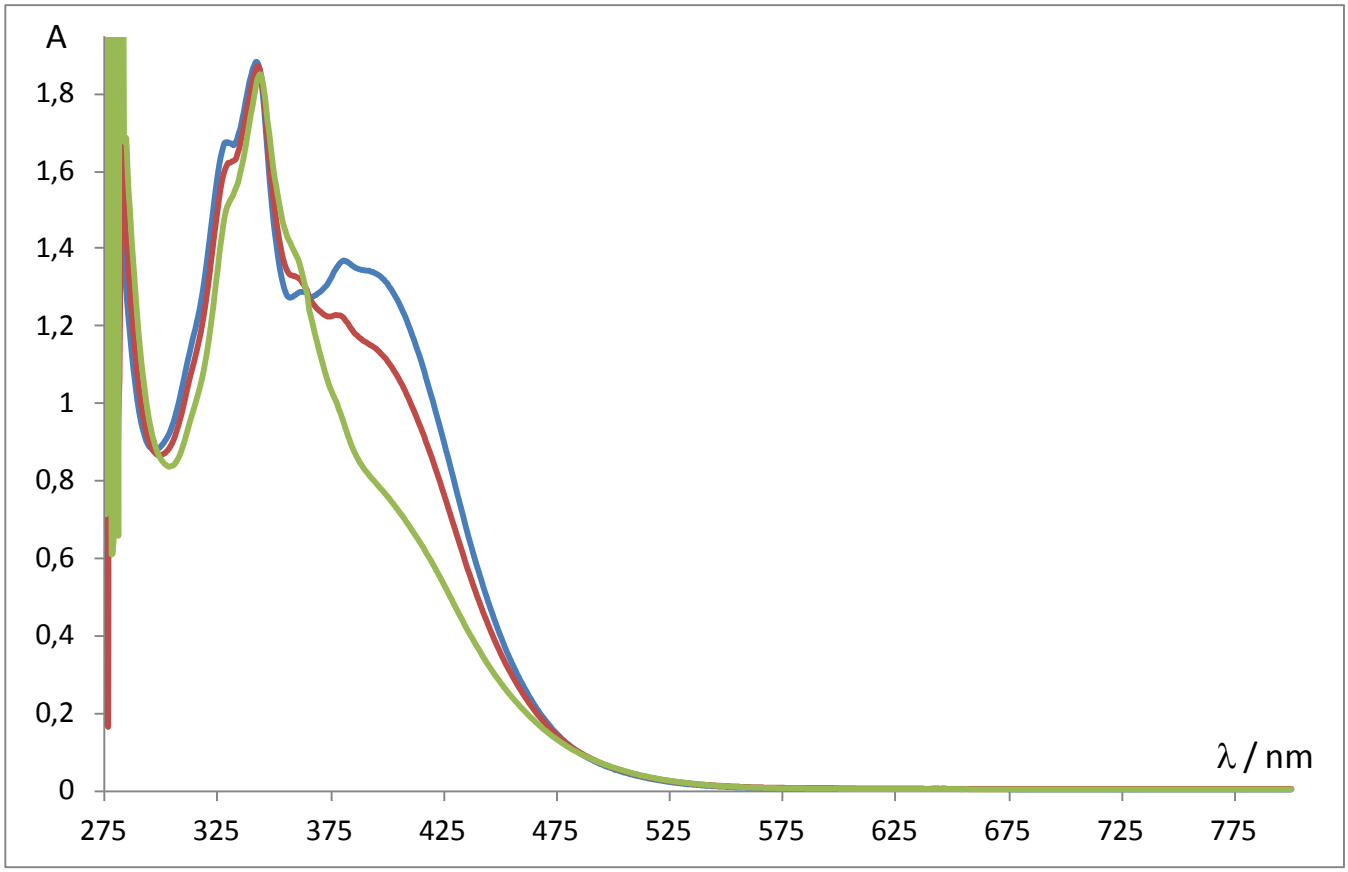

Figure S71: UV/Vis absorption spectra of a 5.03x10^{-5}M solution in toluene of **5a** (blue), irradiated at 365nm for 15 minutes (red) and another aliquot from the same solution irradiated at 380nm for 15 minutes (green).

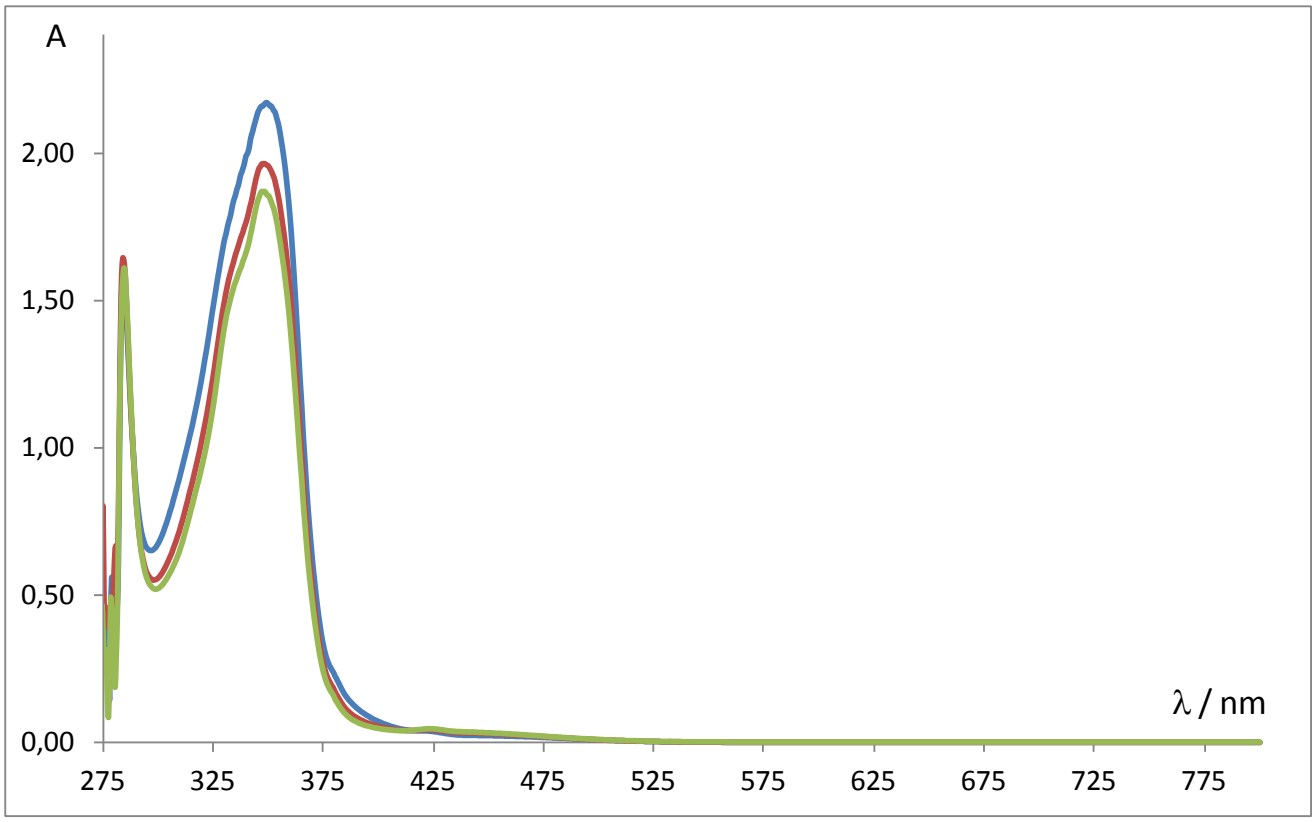

Figure S72: UV/Vis absorption spectra of a 5.17x10^{-5}M solution in toluene of **5b** (blue), irradiated at 365nm for 15 minutes (red) and another aliquot from the same solution irradiated at 380nm for 15 minutes (green).

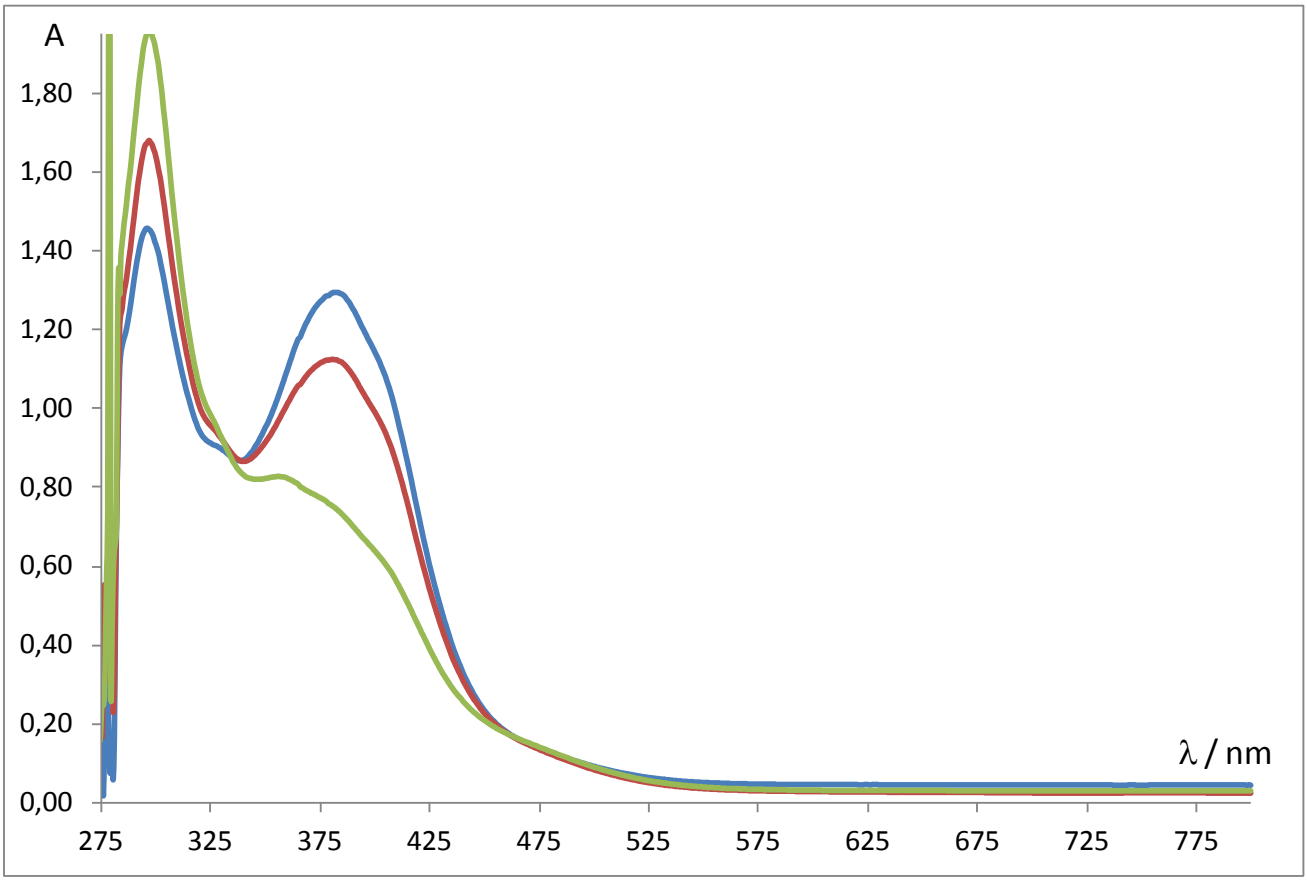

Figure S73: UV/Vis absorption spectra of a 5.17x10^{-5}M solution in toluene of **6a** (blue), irradiated at 365nm for 15 minutes (red) and another aliquot from the same solution irradiated at 380nm for 15 minutes (green).

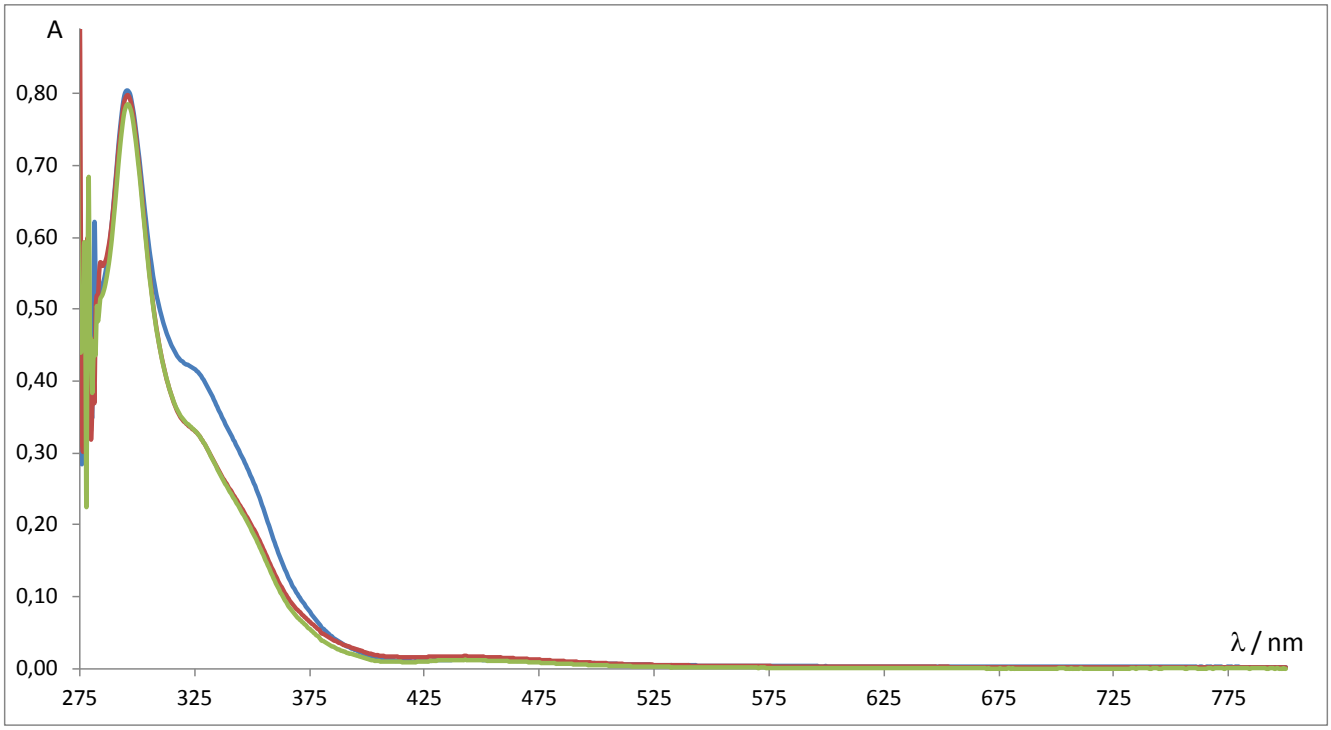

Figure S74: UV/Vis absorption spectra of a 4.96x10^{-5}M solution in toluene of **6b** (blue), irradiated at 365nm for 15 minutes (red) and another aliquot from the same solution irradiated at 380nm for 15 minutes (green).

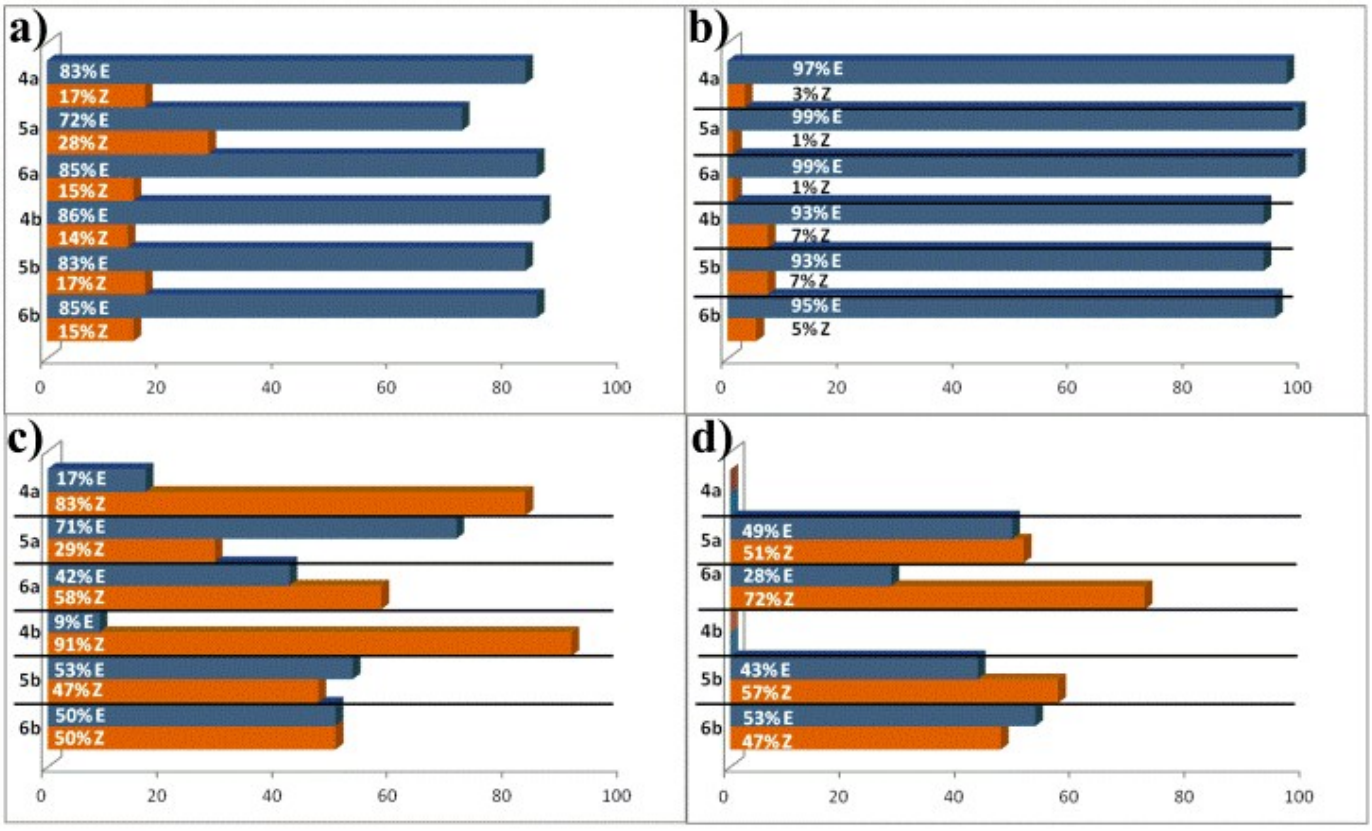

Figure S75: Photostationary states and E/Z ratio of compounds **4**, **5** and **6** in initial state (a), after heating at 80ºC and cooling down to rt (b), after irradiation at 365nm for 30 minutes (c) and after irradiation at 380nm for 30 minutes (d). Determined by ^{1}H-NMR integrals.

Complexation measurementes

In order to estimate association constants (K_a) for compounds **Z6a**, **E6b** and **Z6b** with fullerenes, the dilution method was applied. A 10^{-4} M solution of each compound[6] in deuterated toluene was prepared and a known volume was transferred to a quartz NMR tube (500 μL). It was titrated by adding known portions of a stock solution of C_{60} or C_{70} (10^{-3} M) in deuterated toluene covering a wide range of equivalents. A ^{1}H NMR spectrum was recorded at room temperature after each addition. Compound **E6b** was heated at 70º for 30 minutes before titration experiment and **Z6a** and **Z6b** were obtained after irradiation at 380nm or 365nm, respectively. Once obtained all data, changes in chemical shifts (Δδ) for selected protons (H_2, H_3 and H_7 in **6a** and H_2, H_4 and H_9 in the case of **6b**) were plotted as a function of guest molar fraction and the resulting curve was fitted by a nonlinear method according to the equation:

$$\Delta\delta = \Delta\delta_{max}\left(\frac{[HG]}{[H_0]}\right) \qquad \text{eq. 1}\ [7]$$

where:

$$[HG] = \frac{1}{2}\left\{[G_0] + [H_0] + \frac{1}{K_a}\right\} - \sqrt{\left\{[G_0] + [H_0] + \frac{1}{K_a}\right\}^2 + 4[G_0][H_0]} \qquad \text{eq. 2}$$

$[G_0]$ is the total concentration of Guest

$[H_0]$ is the total concentration of Host[8]

$\Delta\delta_{max}$ is $\Delta\delta$ at maximum complexation (100% supramolecular complex formation)

$\Delta\delta_{max}$ and K_a were optimized as parameters in the non-linear curve fitting by using Statgraphics Centurion XVI package (Version 16.2.04). All binding isotherms were adjusted considering 1:1 stoichiometry.

Continuous variation method (Job Plot)[9] was carried out as well as the sum of their normalized values according to Bühlmann method[10] in order to confirm 1:1 stoichiometry.

Table S1. Estimated K_a values calculated from selected protons in each compound.

Compounds	Estimated K_a / M^{-1}	Average K_a / M^{-1}
C_{60}@Z6a	2337, 2360, 2640	$(2.4\pm0.2)\cdot10^3$
C_{70}@Z6a	2633, 2274	$(2.5\pm0.3)\cdot10^3$
C_{60}@E6b	491, 496, 516	$(5.0\pm0.1)\cdot10^2$
C_{70}@E6b	839, 829, 798	$(8.2\pm0.2)\cdot10^2$
C_{60}@Z6b	655, 669, 696	$(6.7\pm0.2)\cdot10^2$
C_{70}@Z6b	262, 266, 213	$(2.5\pm0.3)\cdot10^2$

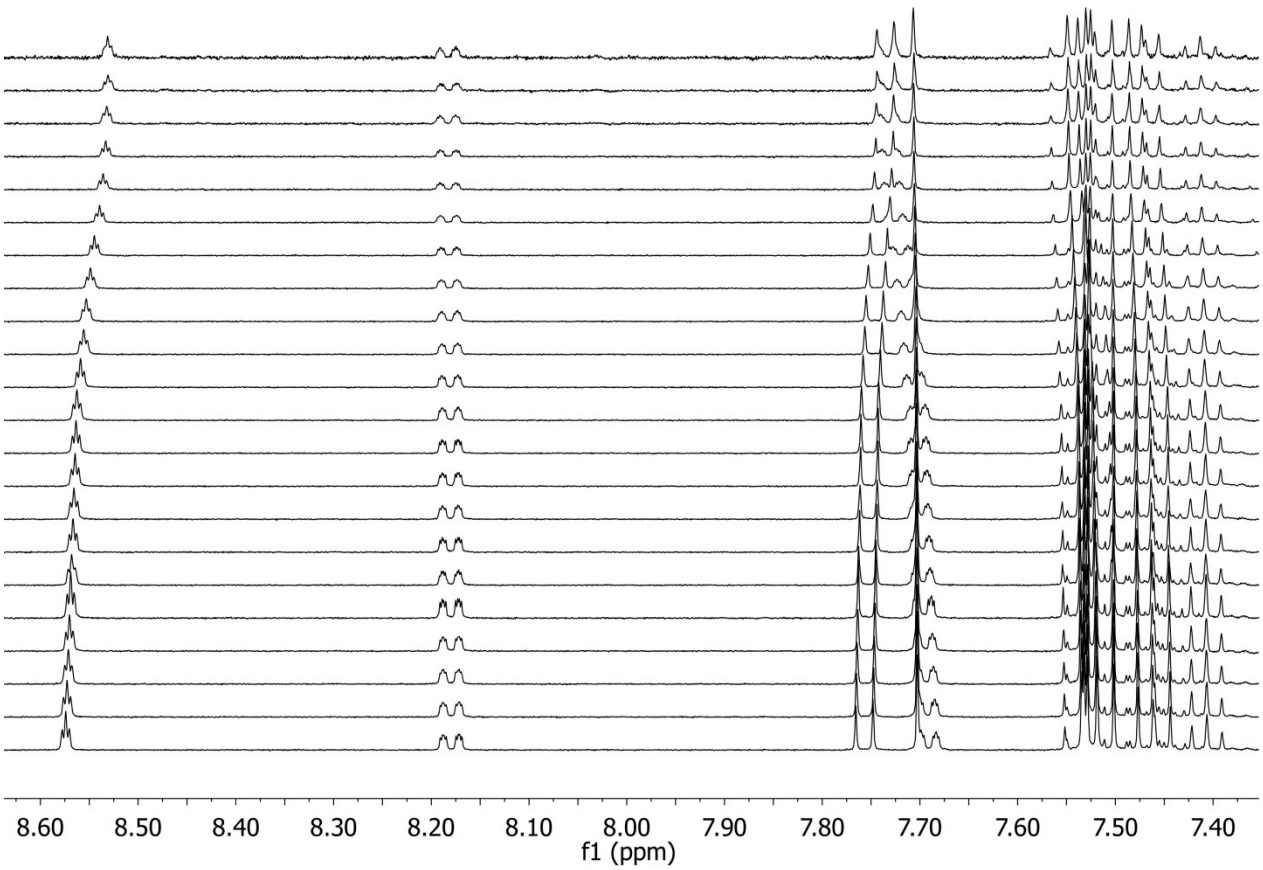

Figure S76: ^{1}H-NMR spectra of **E6b** with variable concentration of C_{60}.

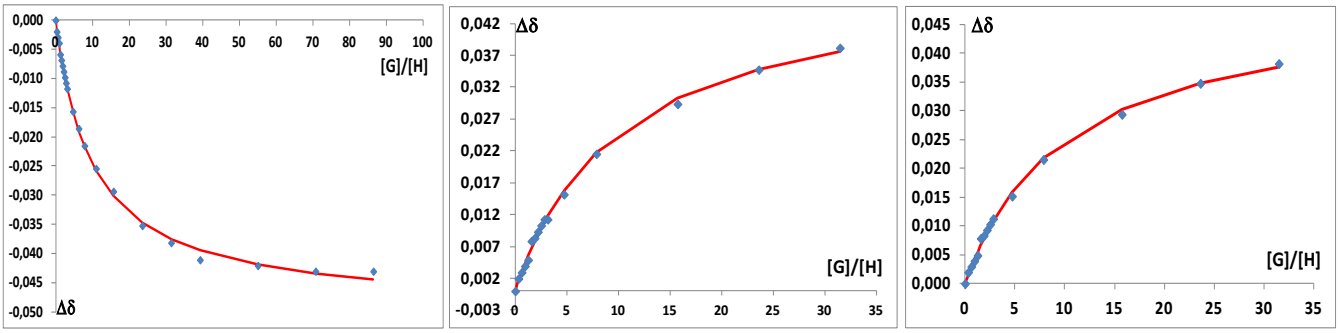

Figure S77: Nonlinear curve regressions for the results of the titration of **E6b** with C_{60} for selected protons.

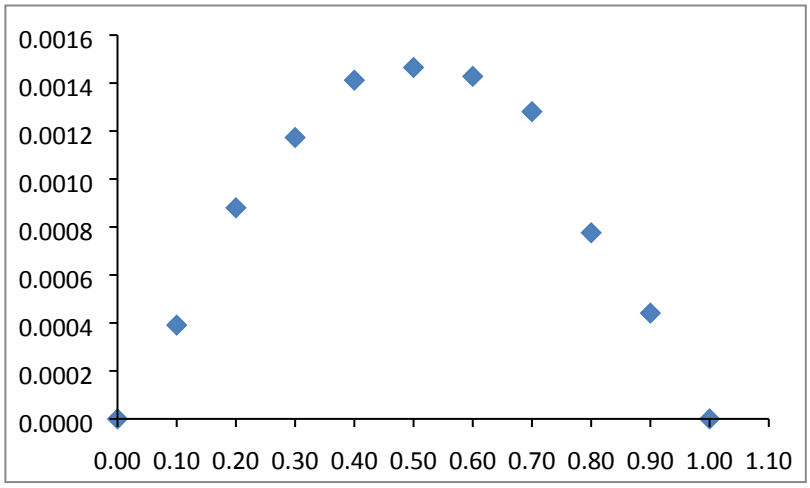

Figure S78: Job plot of **C_{60}@ E6b**. The maximum is observed at $\chi = 0.5$ and $^{\Sigma c}/_{c_{MAX}} = 6.32$ both confirming 1:1 adduct.

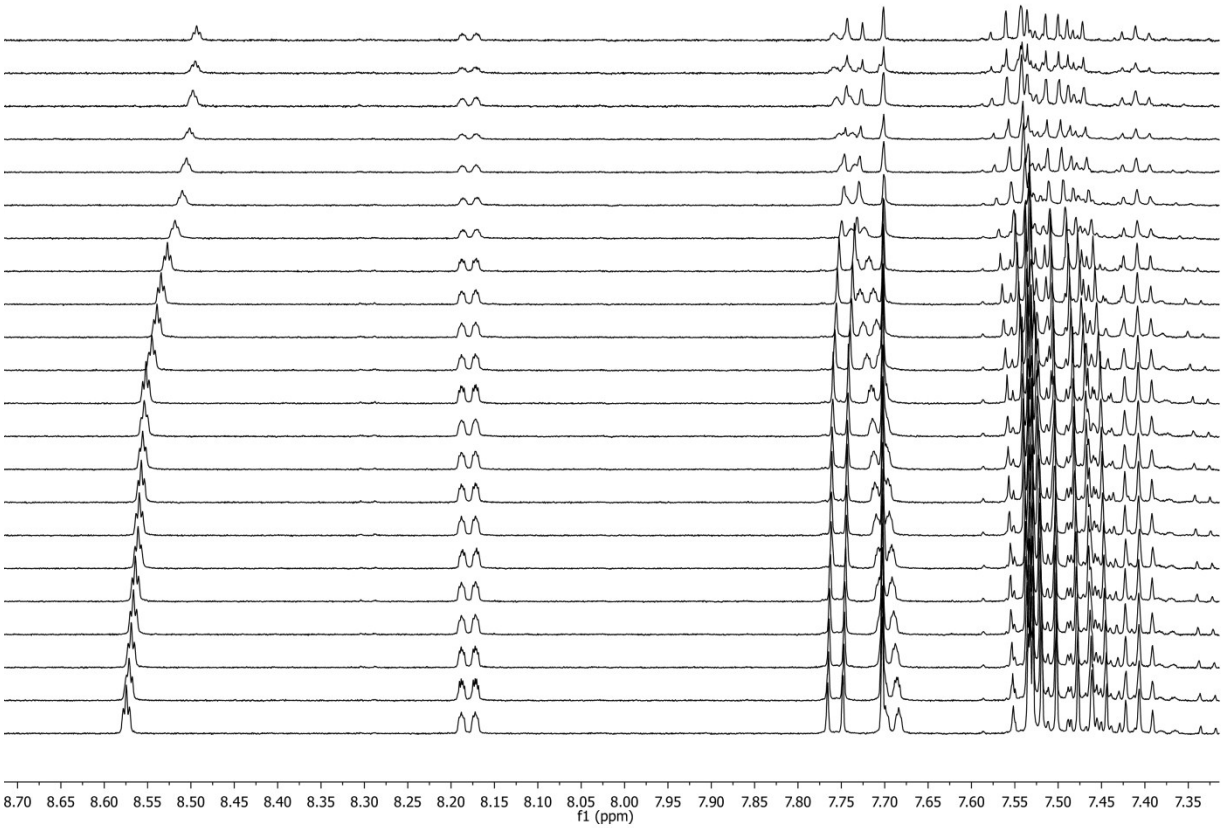

Figure S79: ^{1}H-NMR spectra of **E6b** with variable concentration of C_{70}.

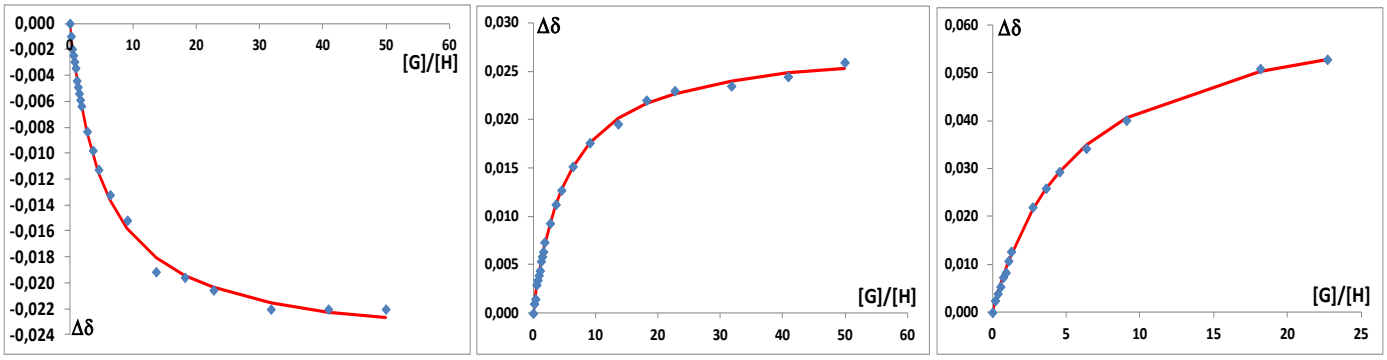

Figure S80: Nonlinear curve regressions for the results of the titration of **E6b** with C_{70} for selected protons.

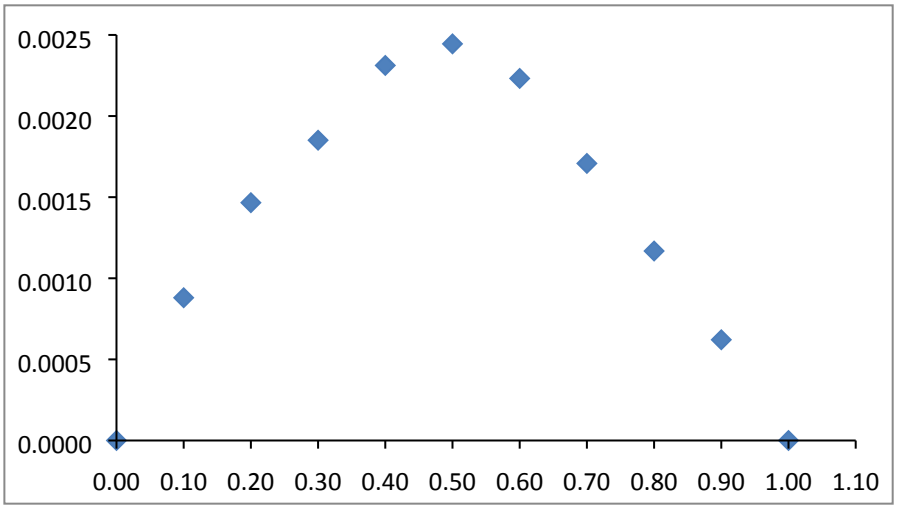

Figure S81: Job plot of C_{70}@ **E6b**. The maximum is observed at $\chi = 0.5$ and $\Sigma c / c_{MAX} = 6.01$ both confirming 1:1 adduct.

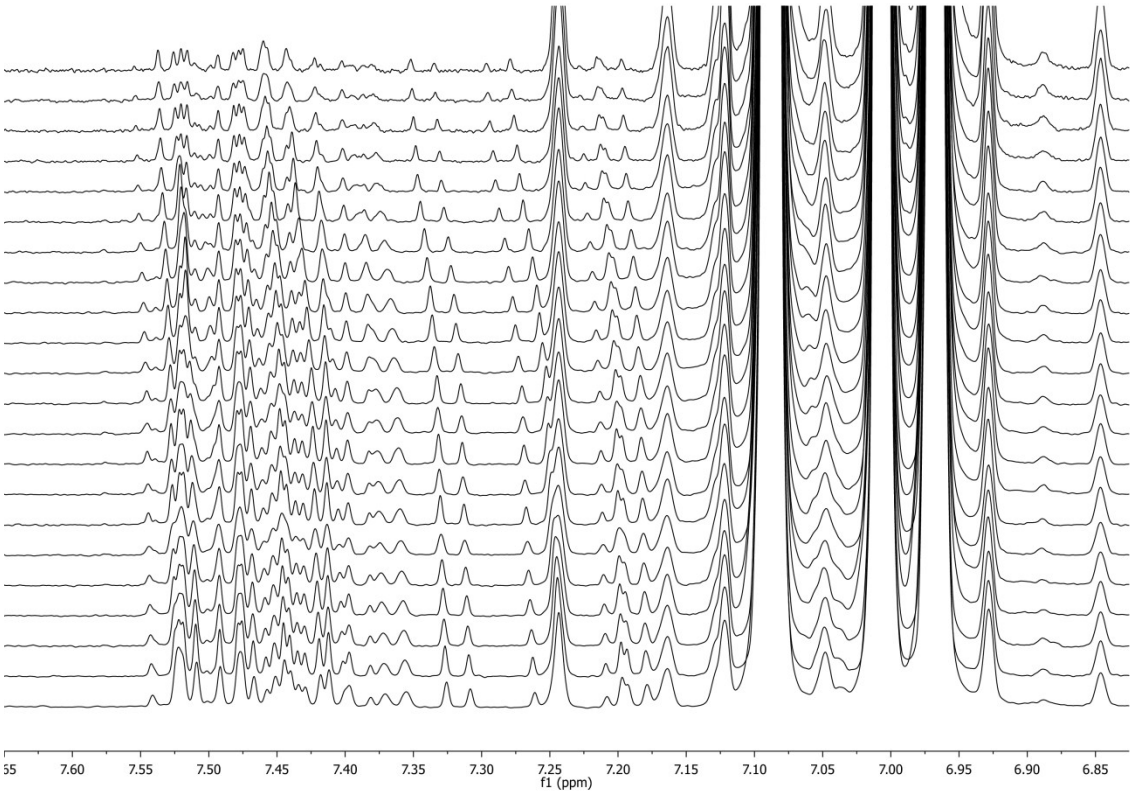

Figure S82: ^{1}H-NMR spectra of **Z6b** with variable concentration of C_{60}.

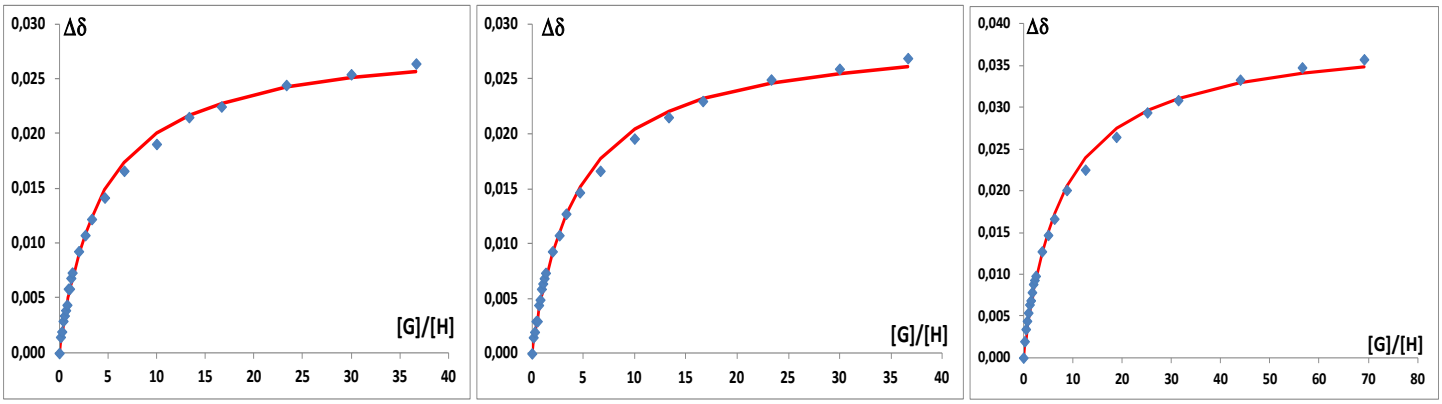

Figure S83: Nonlinear curve regressions for the results of the titration of **Z6b** with C_{60} for selected protons.

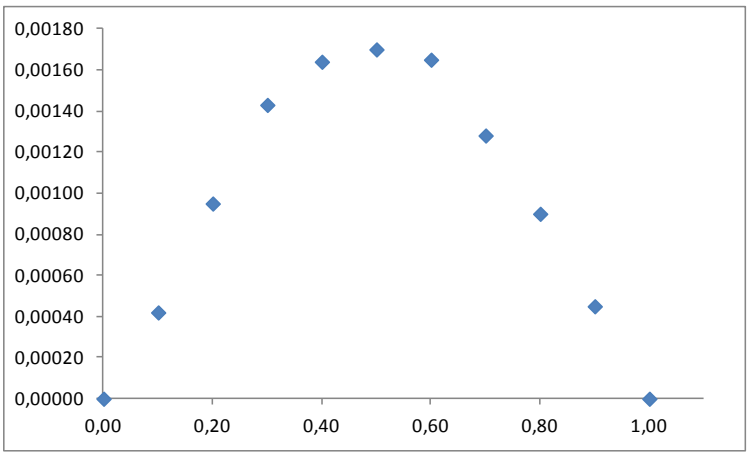

Figure S84: Job plot of C_{60}@ **Z6b**. The maximum is observed at $\chi = 0.5$ and $\Sigma c / c_{MAX} = 6.13$ both confirming 1:1 adduct.

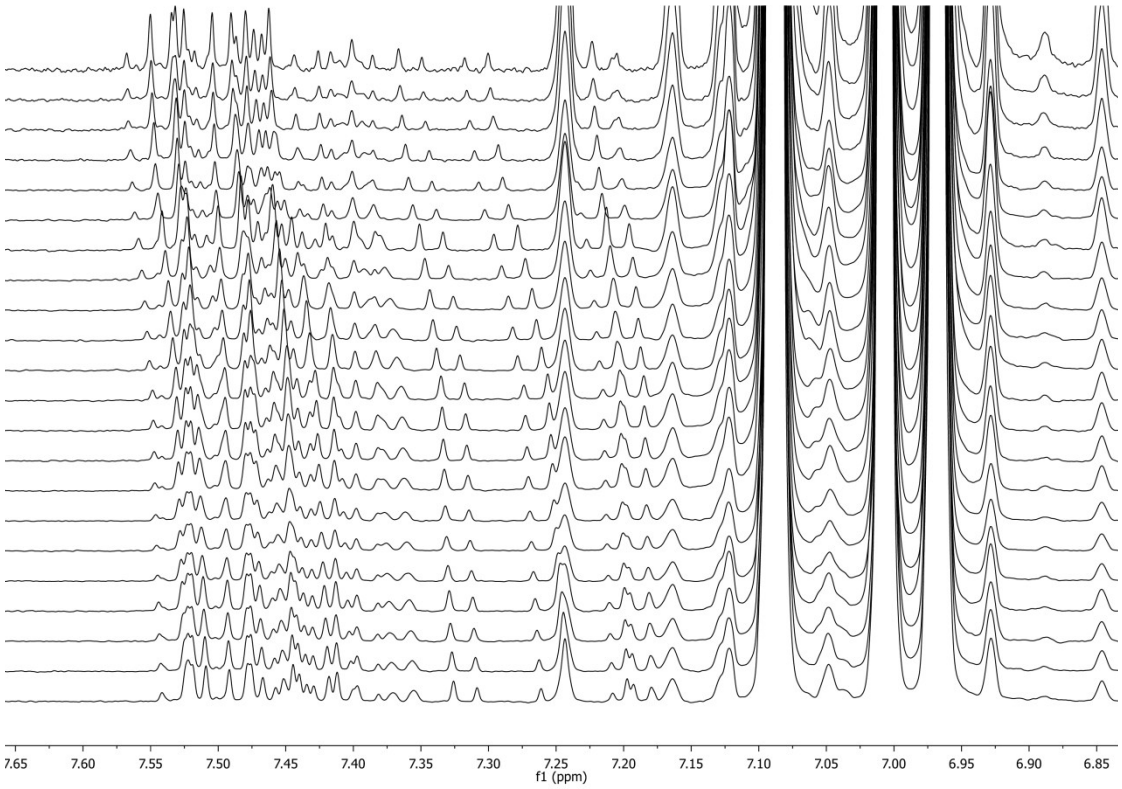

Figure S85: ^{1}H-NMR spectra of **Z6b** with variable concentration of C_{70}.

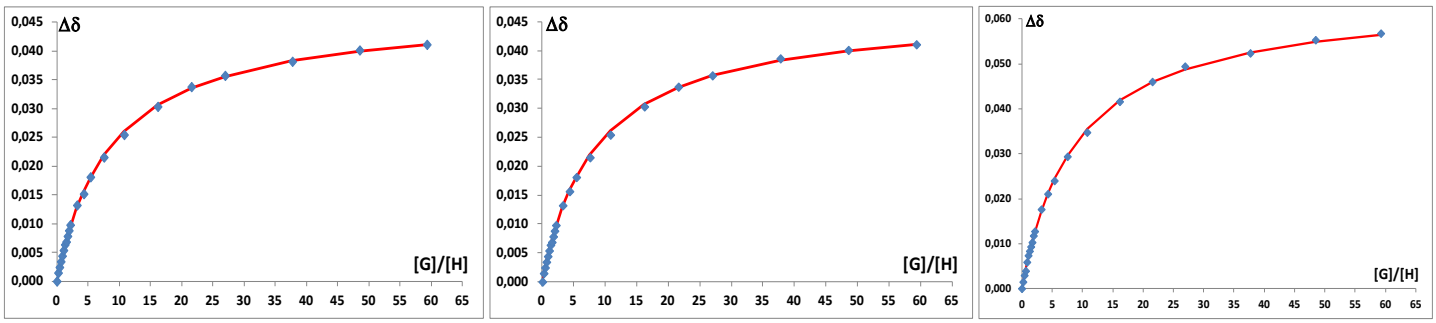

Figure S86: Nonlinear curve regressions for the results of the titration of **Z6b** with C_{70} for selected protons.

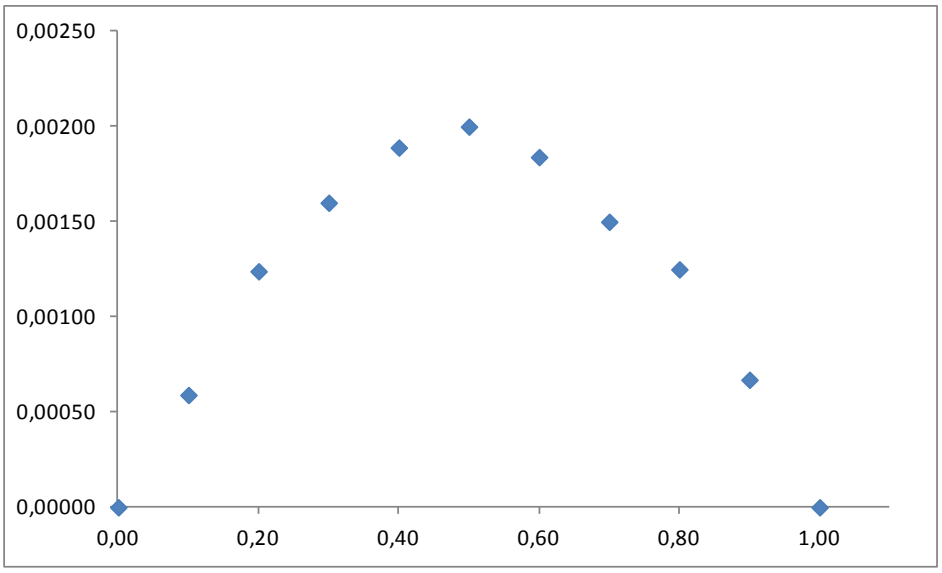

Figure S87: Job plot of C_{70}@ **Z6b**. The maximum is observed at $\chi = 0.5$ and $\Sigma c / c_{MAX} = 6.29$ both confirming 1:1 adduct.

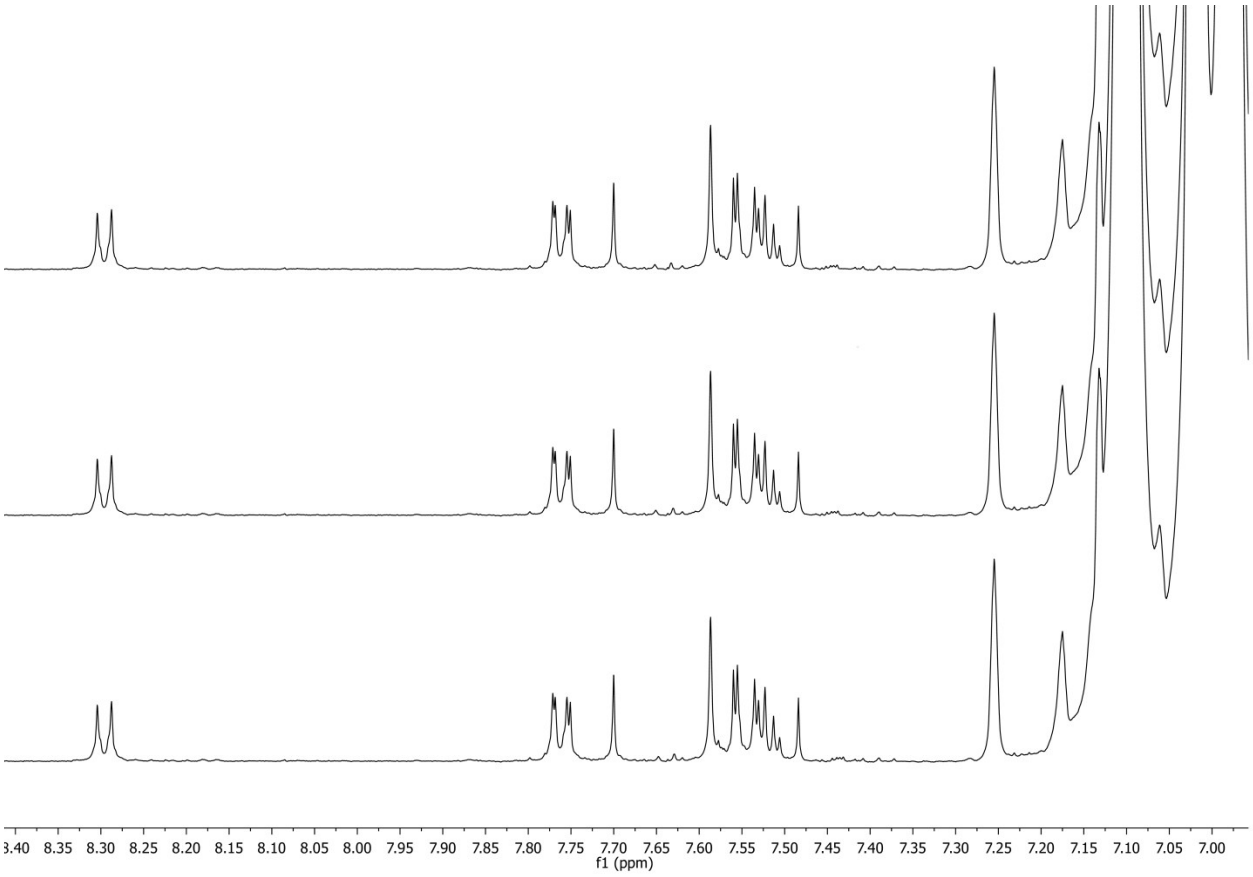

Figure S88: ^{1}H-NMR spectra of **E6a** with variable concentration of C_{60} demonstrating the inexistence of association.

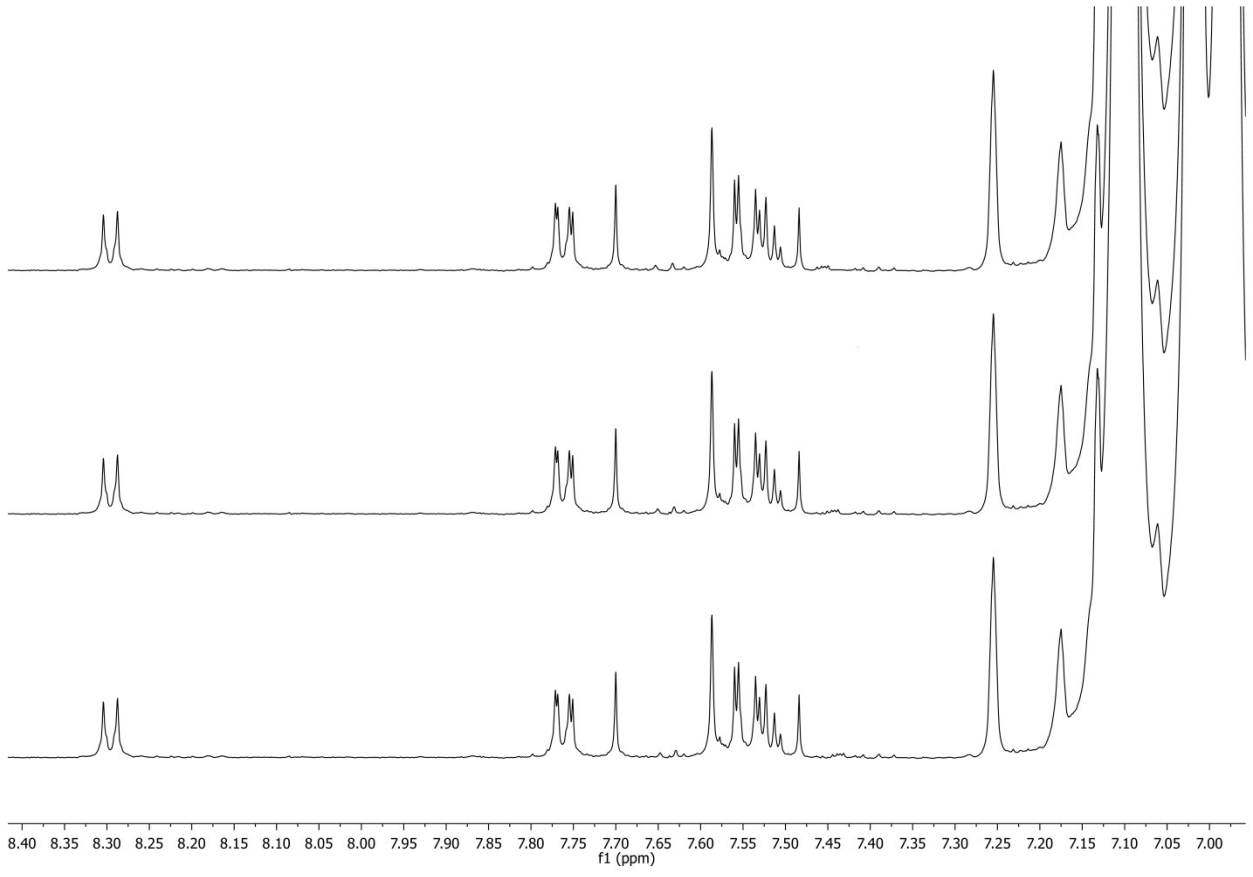

Figure S89: ^{1}H-NMR spectra of **E6a** with variable concentration of C_{70} demonstrating the inexistence of association.

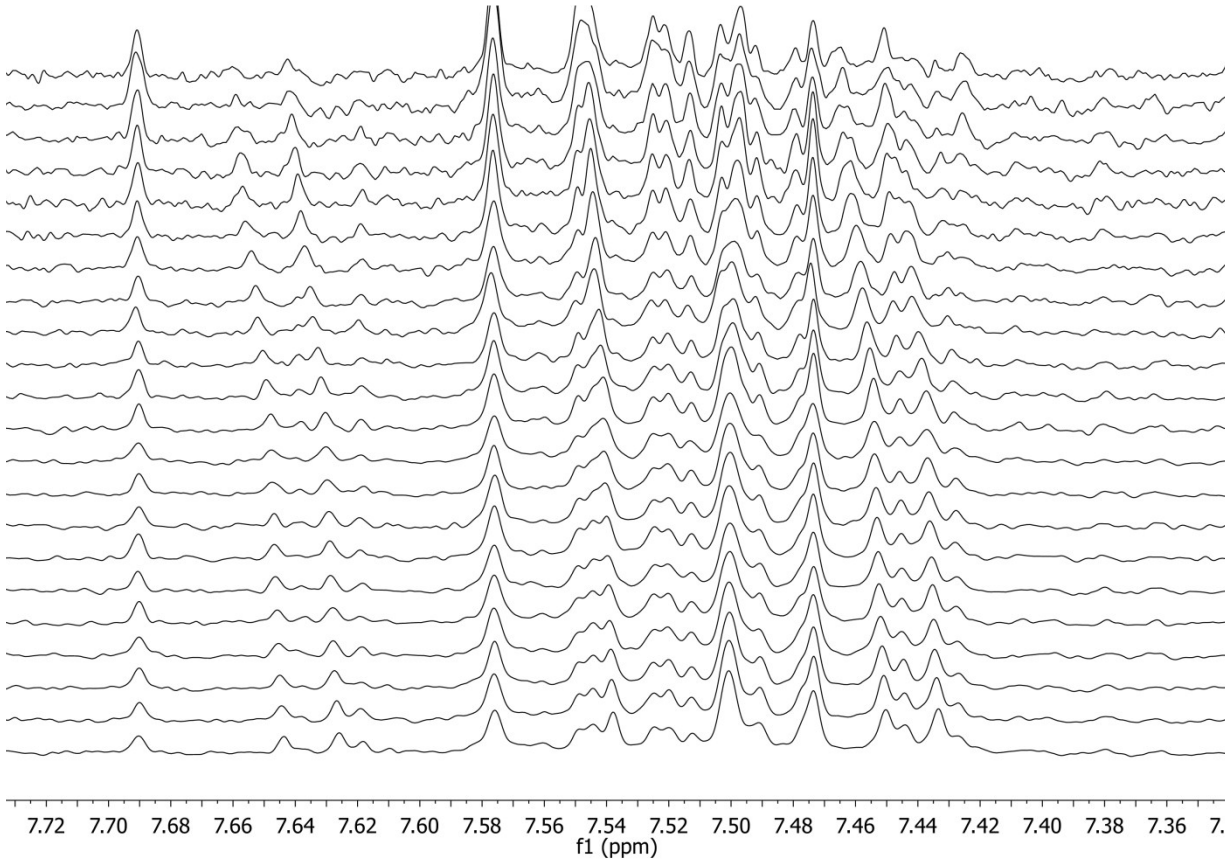

Figure S90: ^{1}H-NMR spectra of **Z6a** with variable concentration of C_{60}.

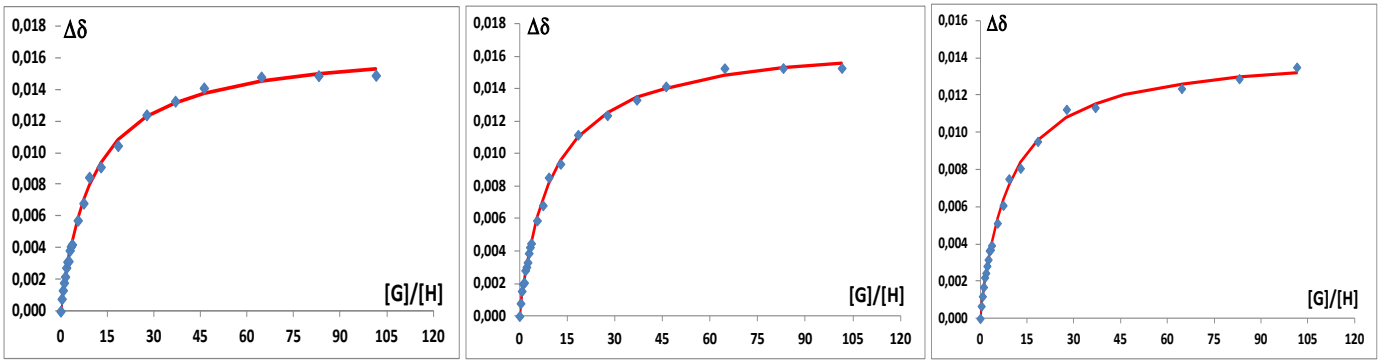

Figure S91: Nonlinear curve regressions for the results of the titration of **Z6a** with C_{60} for selected protons.

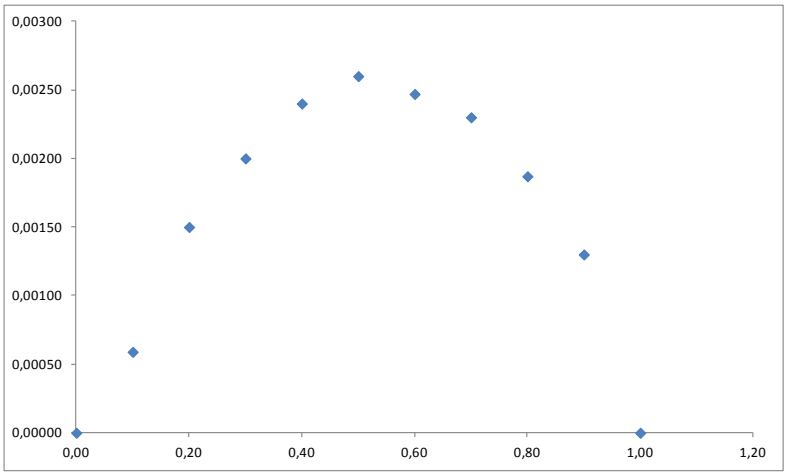

Figure S92: Job plot of C_{60}@ **Z6a**. The maximum is observed at $\chi = 0.5$ and $\Sigma c / c_{MAX} = 6.55$ both confirming 1:1 adduct.

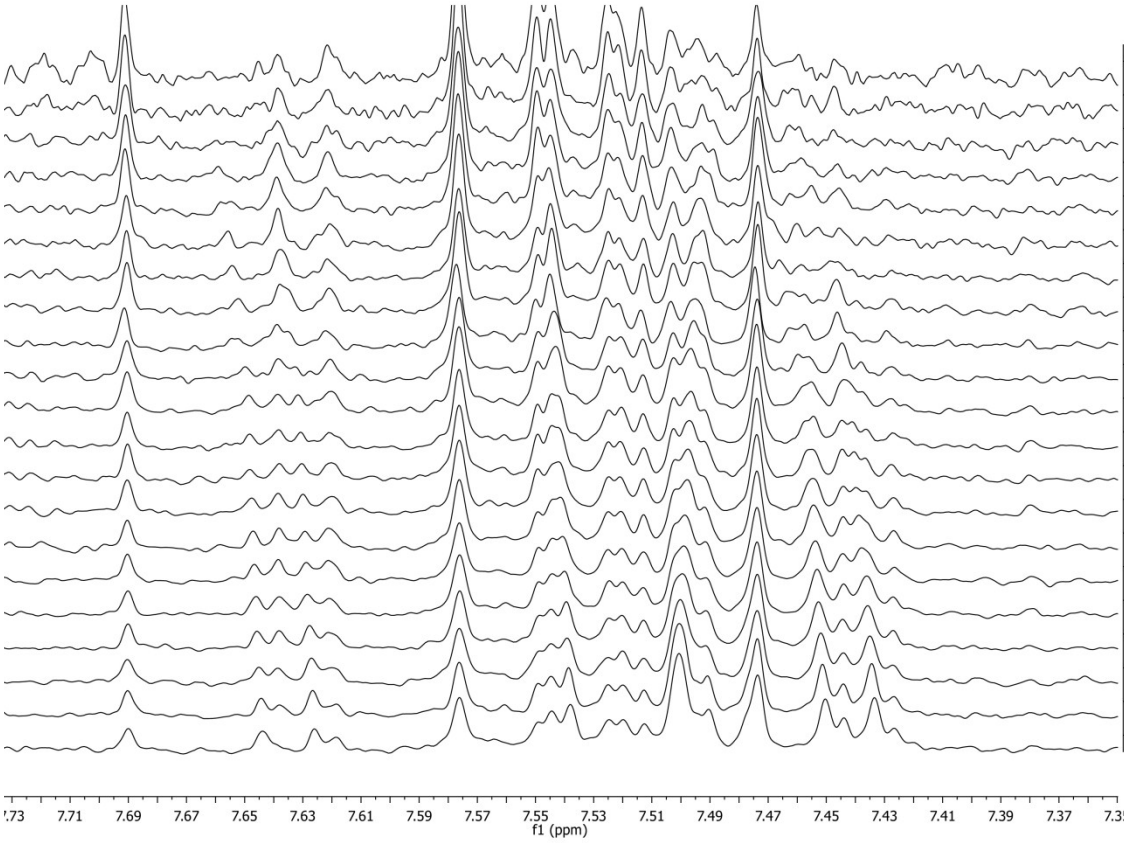

Figure S93: ^{1}H-NMR spectra of **Z6a** with variable concentration of C_{70}.

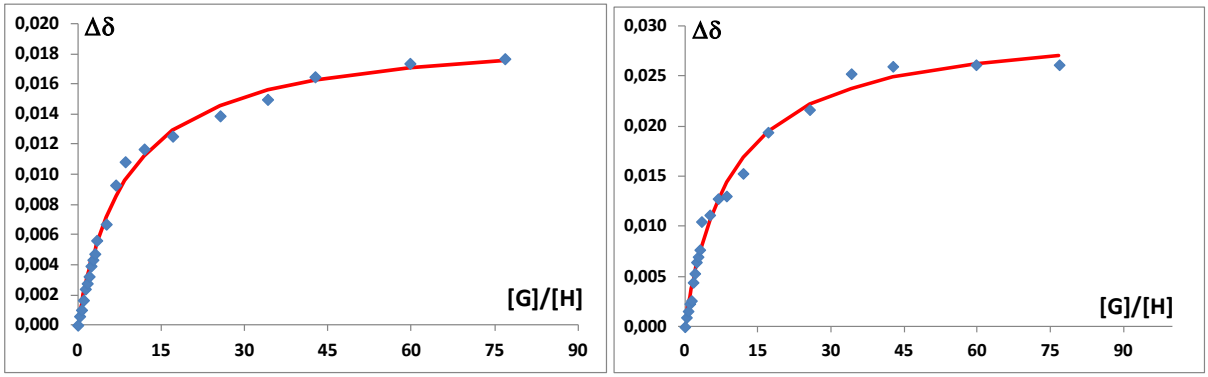

Figure S94: Nonlinear curve regressions for the results of the titration of **Z6a** with C_{70} for selected protons.

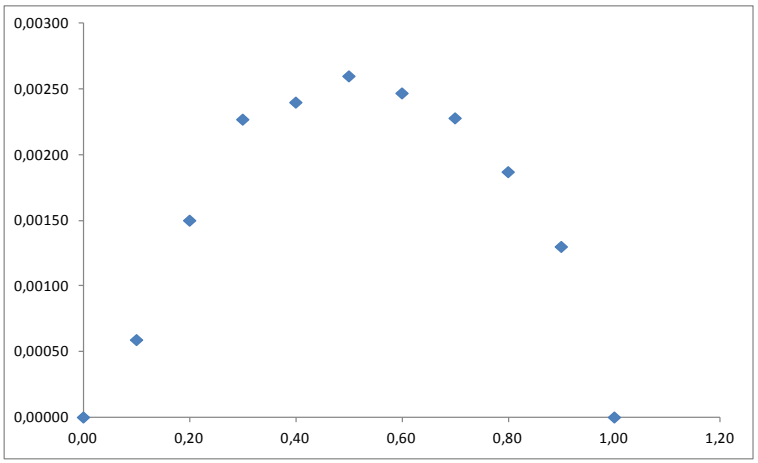

Figure S95: Job plot of **C_{70}@ Z6a**. The maximum is observed at $\chi = 0.5$ and $\Sigma c / c_{MAX} = 6.65$ both confirming 1:1 adduct.

Computational Details

Ab initio calculations were carried out by using the GAUSSIAN09 package.[11] DFT B97D Grimme's functional (including dispersion) was applied[12] because it provides a good description of the weak London forces in many systems, including similar corannulene-based hosts.[13] A split-valence triple-zeta basis set with polarization functions 6-311G(d,p) for all atoms.[14] Geometry full optimizations were performed in gas-phase without symmetry restrictions, and they were confirmed as minima by vibrational analysis.[15] Free energy was computed at 1 atm and 298 K. Then, energy was recalculated at previous optimized geometries with a more extended basis set including diffuse functions 6-311G+(d,p),[16] and was used to compute counterpoise correction to avoid basis set superposition error.[17] Solvent effects were taken into account by using PCM algorithm with toluene ($\varepsilon = 2.37$) as a solvent.[18] Ultra fine grid was used in all calculations. Initial geometries to be optimized were taken from crystal structures of **6b** and **4a**.

The interaction energy of a macromolecular system *AB* (being *A* the molecular tweezer and *B*, C_{60}) is calculated according to the equation:

$$\Delta E_{int}^{CP}(AB) = E_{AB}^{AB} - E_{A}^{AB} - E_{B}^{AB}$$

where superscript refers to the basis set used (that of the system AB) and the subscript indicates the geometry.

Non-Covalent Interaction (NCI) analysis was performed with NCIPLOT program[19] on both optimized adducts by using SCF densities. The cubes generated where visualized in VMD[20] and the gradient isosurface was plotted against the product of the sign (λ_2) and the electron-density function according to RGB scale where blue denotes strong attractive interactions, green for weak attractive interactions and red for repulsive interactions.

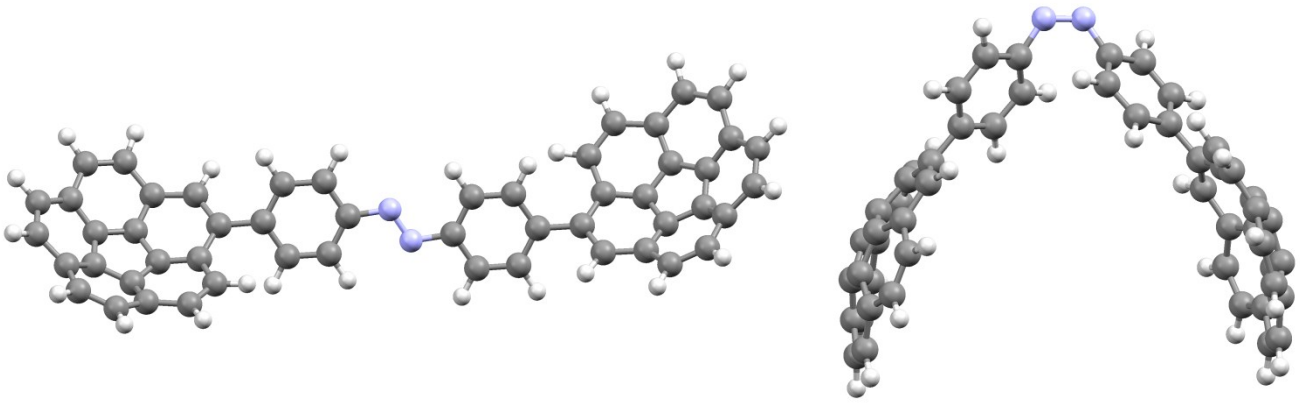

Figure S96. Optimized structure of **E6a** (left) and **Z6a** (right).

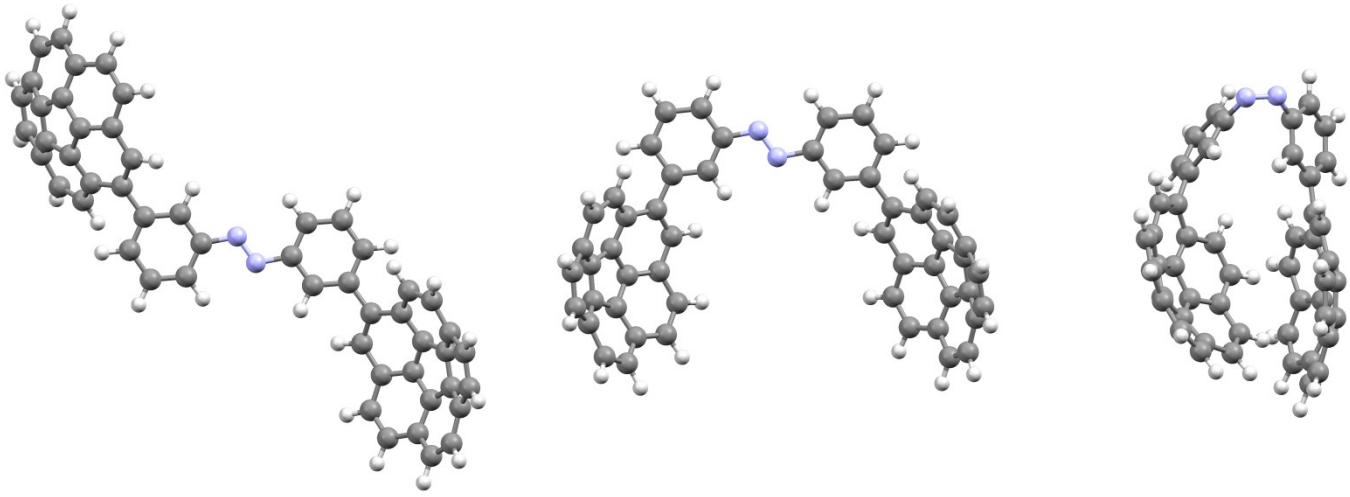

Figure S97. Optimized structure of **trans E6b** (left), **cis E6b** (center) and **Z6b** (right).

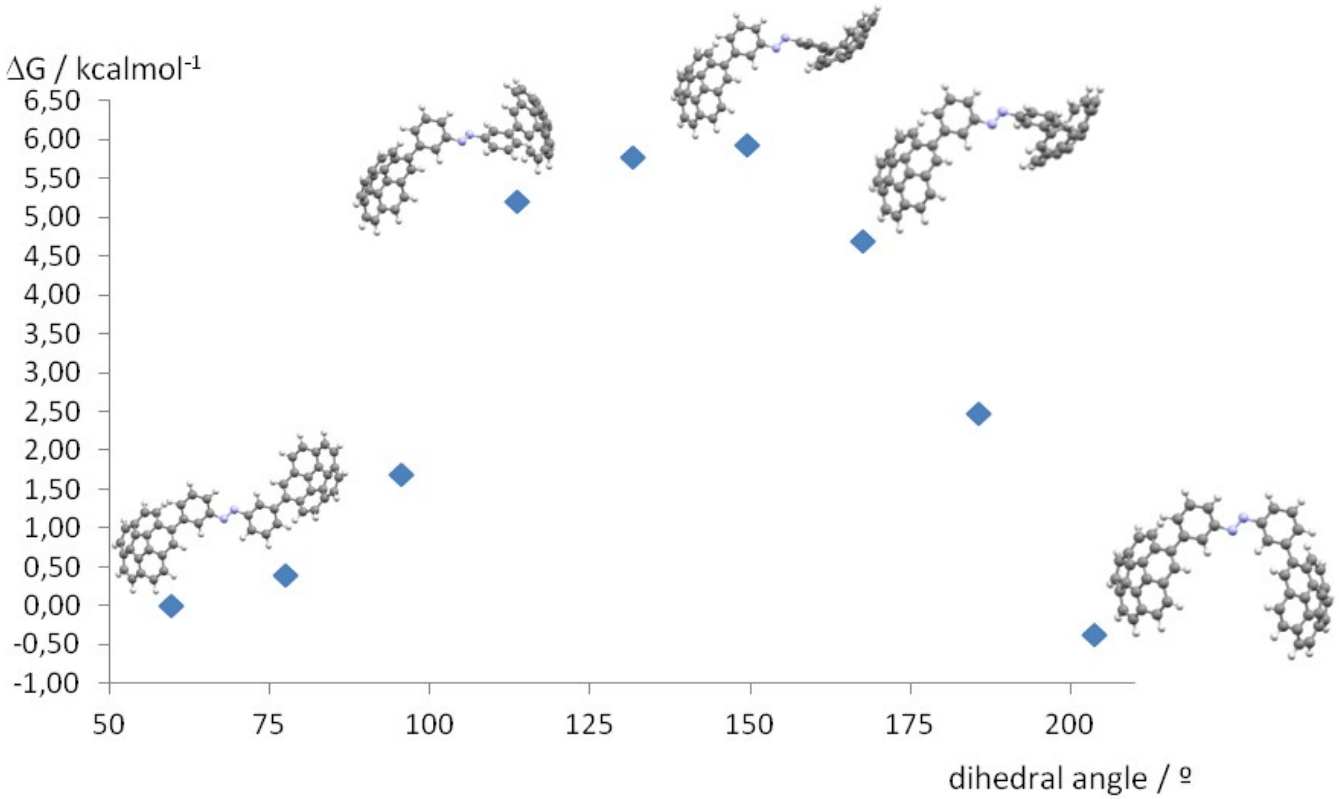

Figure S98. Energy profile for the rotation of N=N-C=CH dihedral angle in **E6b** from trans to cis configuration in toluene. Only 5 out of 9 conformations calculated are shown for clarity.

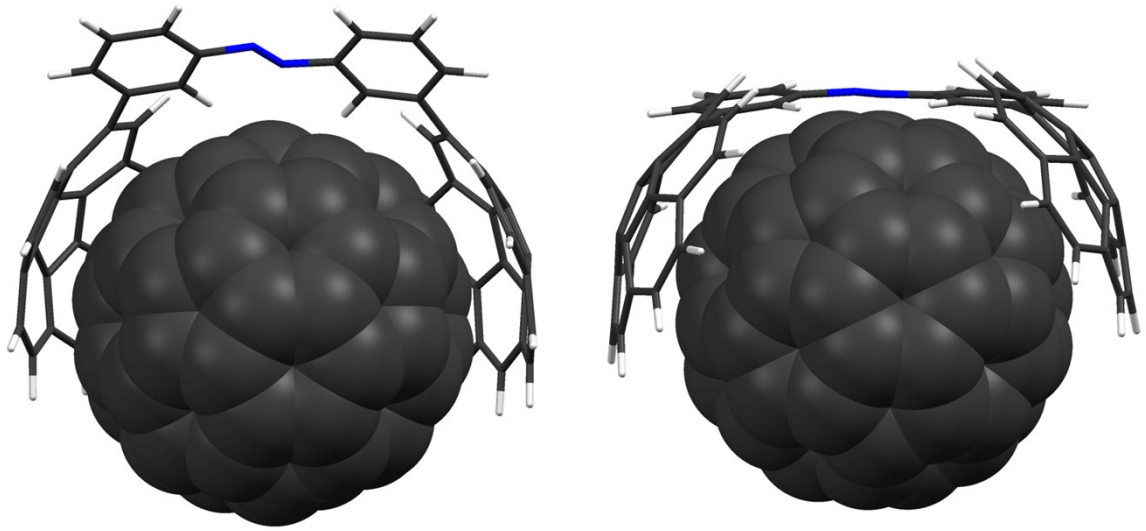

Figure S99. Optimized geometry of C_{60}**@E6b**. Side view (left) and top view (right).

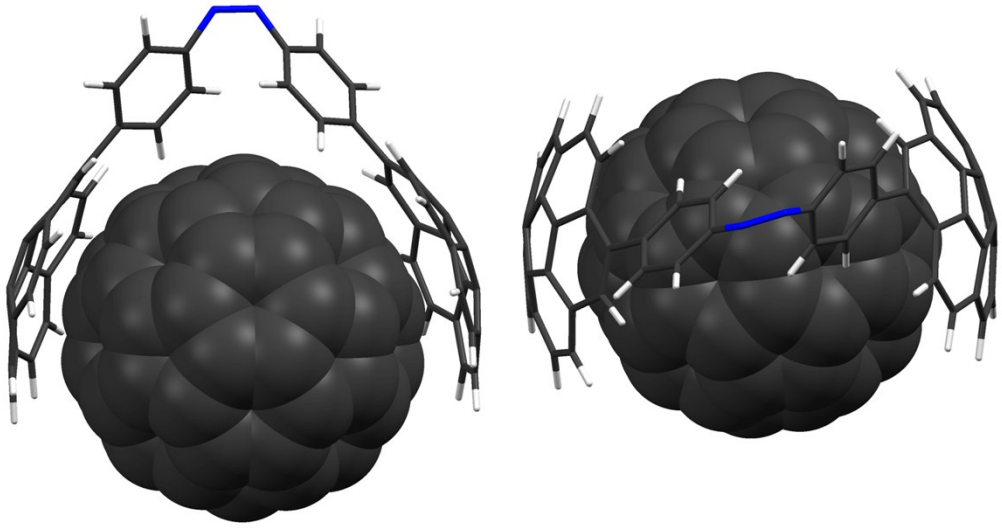

Figure S100. Optimized geometry of **C_{60}@Z6a**. Side view (left) and top view (right).

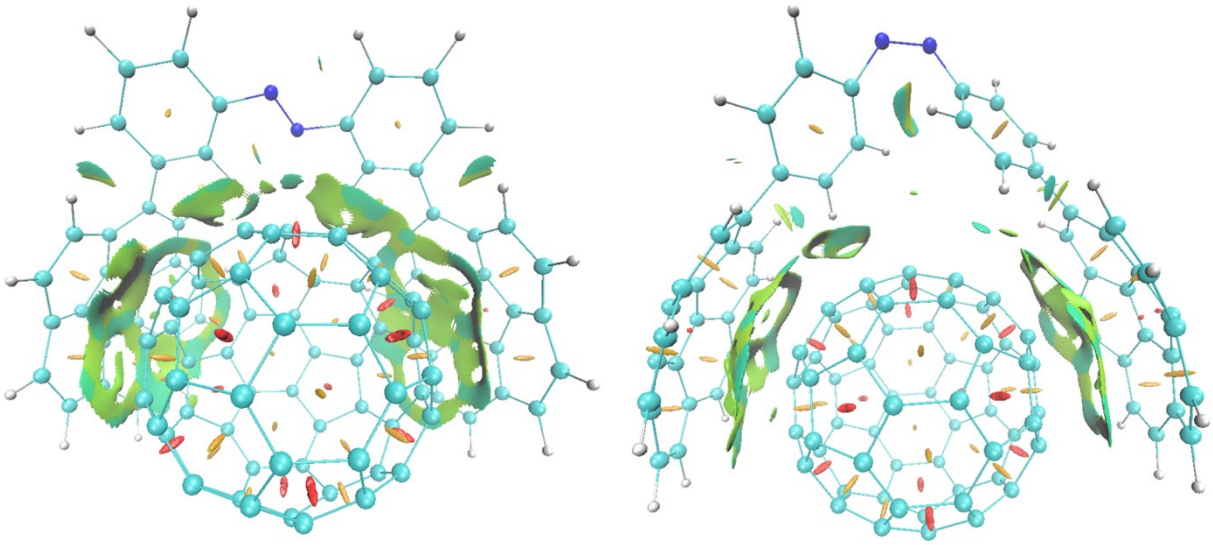

Figure S101. Gradient isosurfaces (s=0.3 a.u.) of **C_{60}@E6b** (left) and **C_{60}@Z6a** (right).

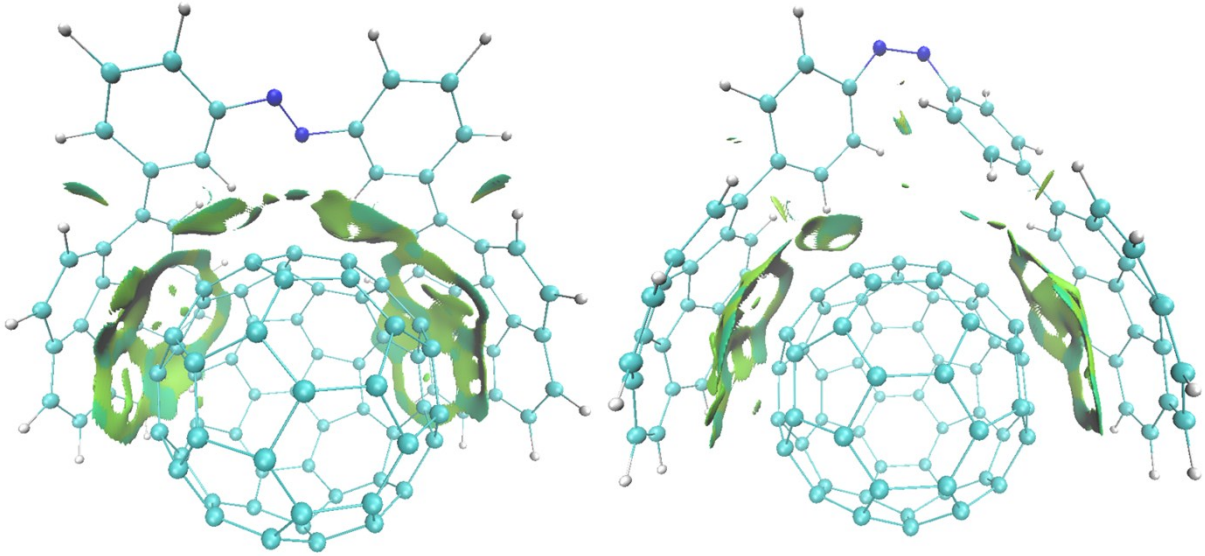

Figure S102. Gradient isosurfaces (s=0.3 a.u.) of **C_{60}@E6b** (left) and **C_{60}@Z6a** (right) with a density cutoff of 0.01 a.u. leaving weak attractive interactions only.

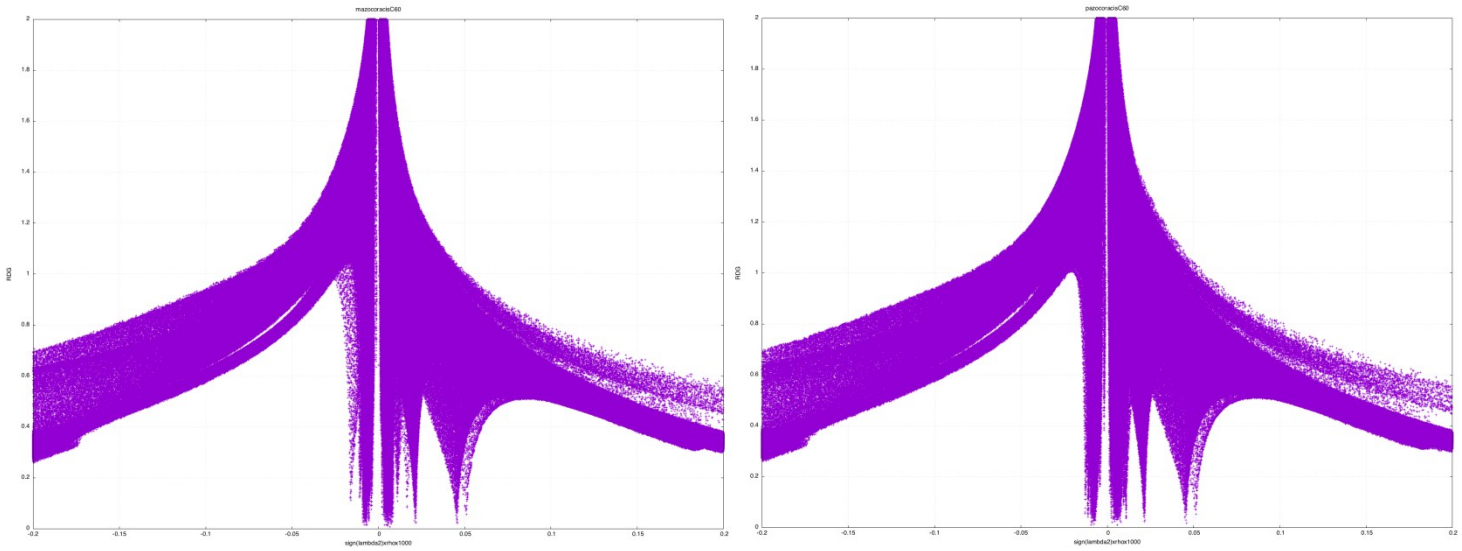

Figure S103. Plots of the reduced density gradient versus the electron density multiplied by the sign of the second Hessian eigenvalue (λ_2) of **C_{60}@E6b** (left) and **C_{60}@Z6a** (right).

X-Ray determination

Single crystals of compound **3a**, **4a**, **4b** and **6b** were grown from slow evaporation of a solution in DCM at room temperature, from slow diffusion of MeOH over a saturated solution in chloroform (**4a** and **4b**) at room temperature and by evaporation at 60 degrees of a solution in toluene, respectively.

Diffraction data were collected using an Oxford Diffraction Supernova diffractometer, equipped with an Atlas CCD area detector and a four-circle kappa goniometer. For the data collection Mo or Cu micro-focus sources with multilayer optics were used. Data integration, scaling and empirical absorption correction was carried out using the CrysAlis Pro program package.[21] The structure was solved using direct methods and refined by Full-Matrix-Least-Squares against F2 with SHELX[22] under OLEX2.[23] The non-hydrogen atoms were refined anisotropically and hydrogen atoms were placed at idealized positions and refined using the riding model. Graphics were made with OLEX2 and MERCURY.[24] Crystal data and particular details are given in Table S2. Due to the low quality of the crystal of **6b** some final parameters are bordering the standards (*i. e.* low number of observer reflections, GOF 0.789). Nevertheless the results of the determination confirm without any doubt the connectivity and the geometry of the molecule.

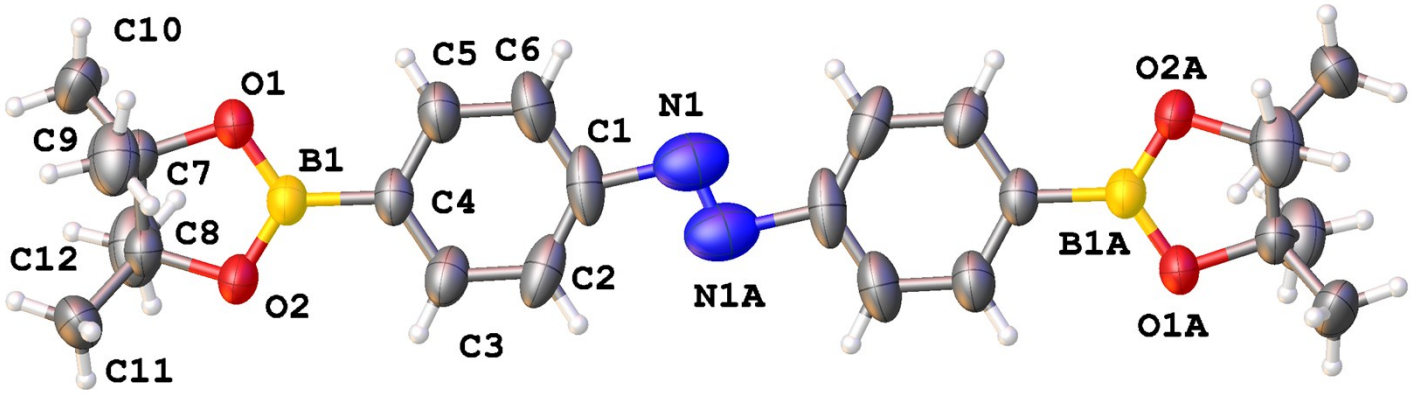

Figure S104. Crystal structure of compound **3a.**

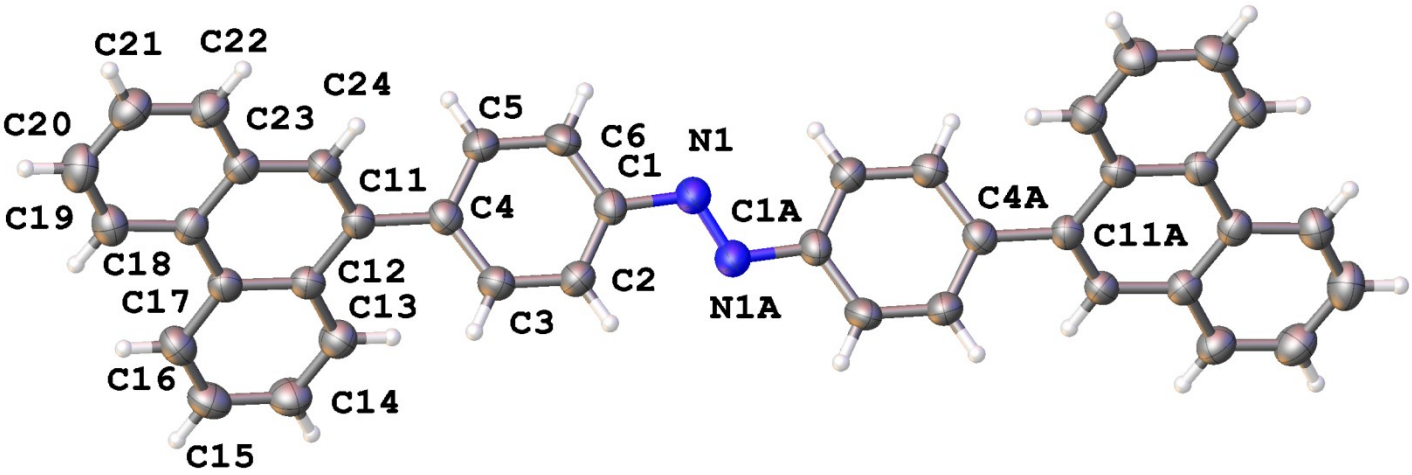

Figure S105. Crystal structure of compound **4a.**

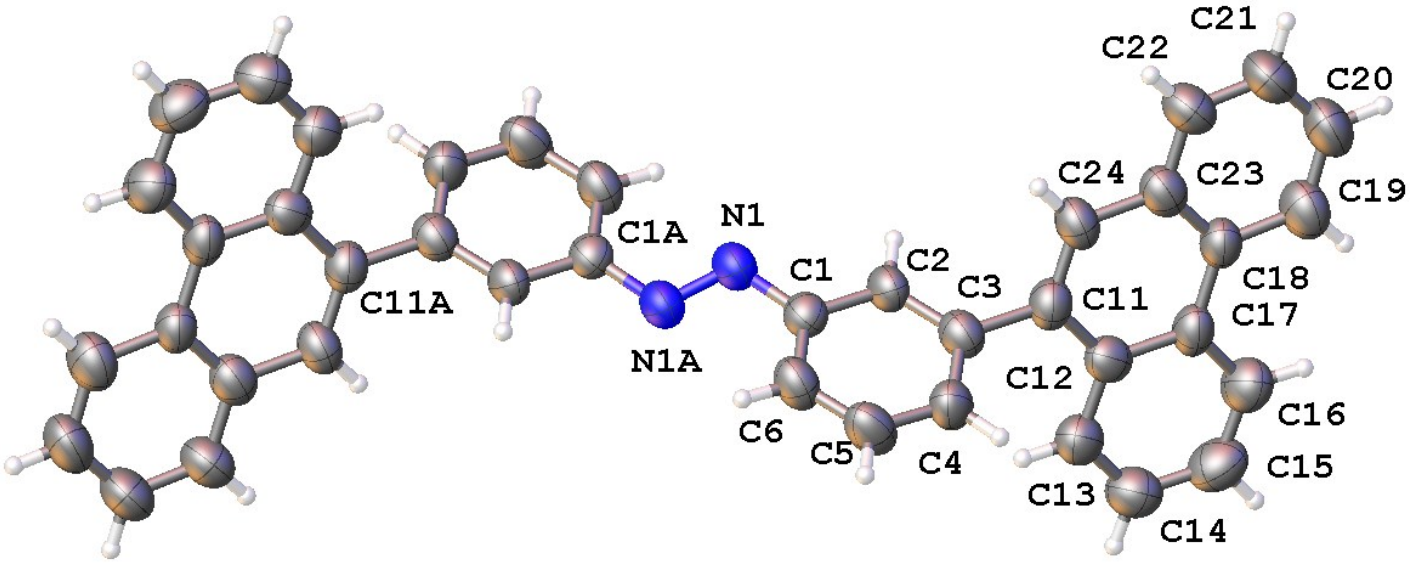

Figure S106. Crystal structure of compound **4b.**

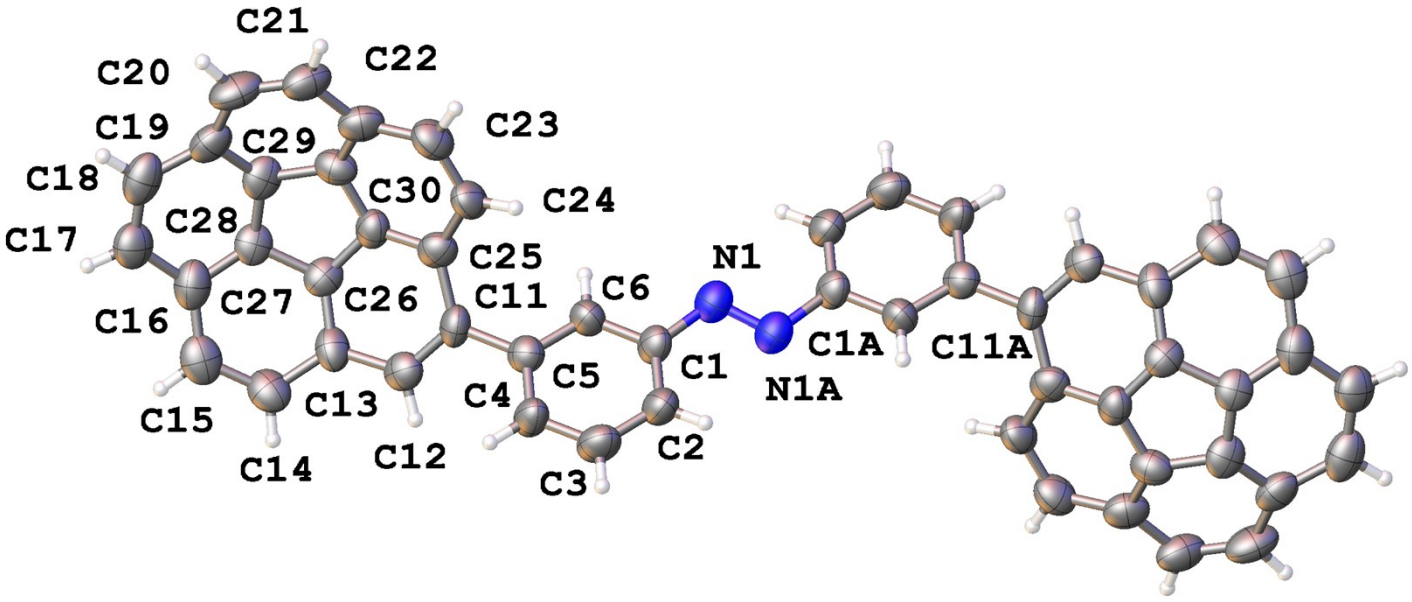

Figure S107. Crystal structure of compound **6b.**

Table S2. Crystal measurement and refinement data for the compounds studied by X-ray diffraction.

Identification code	**3a**	**4a**	**4b**	**6b**
Empirical formula	$C_{48}H_{64}B_4N_4O_8$	$C_{40}H_{26}N_2$	$C_{40}H_{26}N_2$	$C_{52}H_{26}N_2$
Formula weight	868.27	534.63	534.63	678.75
Temperature/K	293(2)	296	293(2)	293(2)
Crystal system	monoclinic	triclinic	monoclinic	monoclinic
Space group	$P2_1/n$	P-1	$P2_1/c$	$P2_1/c$
a/Å	6.4277(3)	3.9995(3)	11.0512(7)	9.1494(11)
b/Å	10.2330(4)	9.9251(9)	14.4682(12)	8.9306(13)
c/Å	18.9139(7)	17.4542(14)	8.5519(9)	20.285(3)
α/°	90	106.270(7)	90	90
β/°	94.954(4)	91.672(6)	91.007(7)	92.501(11)
γ/°	90	92.388(7)	90	90
Volume/Å^3	1239.41(9)	663.92(10)	1367.2(2)	1655.9(4)
Z	1	1	2	2
ρ_{calc}g/cm^3	1.163	1.337	1.299	1.361
μ/mm^{-1}	0.617	0.078	0.075	0.079
F(000)	464.0	280.0	560.0	704.0
Crystal size/mm^3	0.325 × 0.284 × 0.1048	0.3868 × 0.0963 × 0.0362	0.3206 × 0.0864 × 0.0451	0.2929 x 0.0722 x 0.0441
Radiation	CuKα (λ = 1.54184)	MoKα (λ = 0.71073)	MoKα (λ = 0.71073)	MoKα (λ = 0.71073)
2Θ range for data collection/°	9.386 to 149.726	4.28 to 59.414	4.638 to 59.546	40456 to 57.8
Index ranges	$-5 \le h \le 7$, $-12 \le k \le 8$, $-21 \le l \le 23$	$-4 \le h \le 5$, $-13 \le k \le 13$, $-21 \le l \le 13$	$-14 \le h \le 14$, $-19 \le k \le 14$, $-8 \le l \le 10$	$-9 \le h \le 12$, $-10 \le k \le 12$, $-24 \le l \le 25$
Reflections collected	4423	5196	7153	6366
Independent reflections	2453 [R_{int} = 0.0206, R_{sigma} = 0.0272]	3102 [R_{int} = 0.0392, R_{sigma} = 0.0916]	3229 [R_{int} = 0.0679, R_{sigma} = 0.1362]	3503 [R_{int} = 0.1600, R_{sigma} = 0.3566]
Data/restraints/parameters	2453/0/150	3102/0/191	3229/0/190	3503/0/245
Goodness-of-fit on F^2	1.032	0.977	0.982	0.789
Final R indexes [I>=2σ (I)]	R_1 = 0.0647, wR_2 = 0.1682	R_1 = 0.0569, wR_2 = 0.0989	R_1 = 0.0681, wR_2 = 0.1234	R_1 = 0.0828, wR_2 = 0.1367
Final R indexes [all data]	R_1 = 0.0894, wR_2 = 0.1883	R_1 = 0.1363, wR_2 = 0.1387	R_1 = 0.2398, wR_2 = 0.1838	R_1 = 0.3113, wR_2 = 0.2137
Largest diff. peak/hole / e Å^{-3}	0.50/-0.35	0.15/-0.20	0.14/-0.14	0.21/-0.17

References

[1] (a) , W. L. E. Armarego and C. L. L. Chai, *Purification of Laboratory Chemicals, Fifth Edition*, Butterworth-Heinemann Ed. 2003; (b) D. Bradley, G. Williams and M. Lawton, *J. Org. Chem.*, 2010, **75**, 8351-8354.

[2] (a) A. Suzuki and N. Miyaura, *Chem. Rev*., 1995, **95**, 2457-2483; (b) A. J. J. Lennox and G. C. Lloyd-Jones, *Chem. Soc. Rev.*, 2014, **43**, 412-443.

[3] K. Rück-Braun and B. Priewisch, *J. Org. Chem.,* 2005, **70**, 2350-2352.

[4] (a) D. Lentz, B. Topolinski, B. M. Schmidt, M. Kathan and S. I. Troyanov, *Chem. Commun.,* 2012, **48**, 6298-6300; (b) J. S. Siegel, A. M. Butterfield and B. Gilomen, *Org. Process Res. Dev.,* 2012, **16,** 664-676.

[5] (a) A. Defoin, *Synthesis*, 2004, **5**, 706-710; (b) U. Lüning and I. Köhl, *Synthesis,* 2014, **46**, 2376-2382; (c) J. Rebek, E. Busseron, J. Lux and M. Degardin, *Chem. Commun.,* 2013, **49**, 4842-4844; (d) H. A. Wegner and R. Reuter, *Chem. Eur. J.,* 2011, **17**, 2987-2995; (e) P. H. Lee, T. Ryu, J. Min, W. Choi and W. H. Jeon, *Org. Lett.,* 2014, **16**, 2810-2813; (f) T. M. Boller, J. M. Murphy, M. Hapke, T. Ishiyama, N. Miyaura and J. F. Hartwig, *J. Am. Chem. Soc.,* 2005, **127**, 14263−14278; (g) M. Beinhoff, W. Weigel, M. Jurczok, W. Rettig, C. Modrakowski, I. Brüdgam, H. Hartl and A. D. Schlüter, *Eur. J. Org. Chem.,* 2001, 3819-3829; (h) H. A. Wegner, L. T. Scott and A. de Meijere, *J. Org. Chem.,* 2003, **68**, 883-887.

[6] Due to low solubility, **Z6a** concentration was 10^{-5} M and, consequently, guest concentrations were lowered to 10^{-4}M.

[7] (a) L. Fielding, *Tetrahedron,* 2000, **56**, 6151-6170; (b) K. *J.* Hirose, *Incl. Phenom. Macrocycl. Chem.,* 2001, **39**, 193-209; (c) P. Thordarson, *Chem. Soc. Rev.,* 2011, **40**, 1305-1323.

[8] Total concentrations of Z isomers were divided by the appropriate number according to their E/Z ratio as depicted in Figure S75.

[9] P. Job, *Ann. Chim.,* 1928, **9**, 113-203.

[10] E. J. Olson and P. Bühlmann, *J. Org. Chem.,* 2011, **76**, 8406–8412.

[11] Gaussian 09, Revision E.01, M. J. Frisch, G. W. Trucks, H. B. Schlegel, G. E. Scuseria, M. A. Robb, J. R. Cheeseman, G. Scalmani, V. Barone, B. Mennucci, G. A. Petersson, H. Nakatsuji, M. Caricato, X. Li, H. P. Hratchian, A. F. Izmaylov, J. Bloino, G. Zheng, J. L. Sonnenberg, M. Hada, M. Ehara, K. Toyota, R. Fukuda, J. Hasegawa, M. Ishida, T. Nakajima, Y. Honda, O. Kitao, H. Nakai, T. Vreven, J. A. Montgomery, Jr., J. E. Peralta, F. Ogliaro, M. Bearpark, J. J. Heyd, E. Brothers, K. N. Kudin, V. N. Staroverov, R. Kobayashi, J. Normand, K. Raghavachari, A. Rendell, J. C. Burant, S. S. Iyengar, J. Tomasi, M. Cossi, N. Rega, J. M. Millam, M. Klene, J. E. Knox, J. B. Cross, V. Bakken, C. Adamo, J. Jaramillo, R. Gomperts, R. E. Stratmann, O. Yazyev, A. J. Austin, R. Cammi, C. Pomelli, J. W. Ochterski, R. L. Martin, K. Morokuma, V. G. Zakrzewski, G. A. Voth, P. Salvador, J. J. Dannenberg, S. Dapprich, A. D. Daniels, Ö. Farkas, J. B. Foresman, J. V. Ortiz, J. Cioslowski, and D. J. Fox, Gaussian, Inc., Wallingford CT, 2009.

[12] S. Grimme, *J. Comp. Chem.* 2006, **27**, 1787-1799.

[13] (a) A. Sygula and S. Saebø, *Int. J. Quantum Chem.* 2009, **109**, 65-72; (b) C. Muck-Lichtenfeld, S. Grimme, L. Kobryn and A. Sygula, *Phys. Chem. Chem. Phys.,* 2010, **12**, 7091-7097; (c) D. Josa, J. R. Otero and E. M. Cabaleiro Lago, *Phys. Chem. Chem. Phys.,* 2011, **13**, 21139-21145; (d) T. Janowski, P. Pulay, A. A. Sasith Karunarathna, A. Sygula and S. Saebø, *Chem. Phys. Lett.,* 2011, **512**, 155-160; (e) D. Josa, J. Rodríguez-Otero, E. M. Cabaleiro-Lago and M. Rellán-Piñeiro, *Chem. Phys. Lett.*, 2013, **557**, 170-175; (f) D. Josa, J. Rodríguez-Otero, E. M. Cabaleiro-Lago, L. A. Santos and T. C. Ramalho, *J. Phys. Chem. A,* 2014, **118**, 9521-9528.

[14] M. M. Francl, W. J. Pietro, W. J. Hehre, J. S. Binkley, D. J. DeFrees, J.A. Pople and M. S. Gordon, *J. Chem. Phys.*, 1982, **77**, 3654-3665.

[15] (a) R. Ditchfield, W. J. Hehre and J. A. Pople, *J. Chem. Phys.,* 1971, **54**, 724-728; (b) W. J. Hehre, R. Ditchfield and J. A. Pople, *J. Chem. Phys.,* 1972, **56**, 2257-2261; (c) P. C. Hariharan and J. A. Pople, *Theor. Chem. Acc.* 1973, **28**, 213-222; (d) P. C. Hariharan and J. A. Pople, *Mol. Phys.,* 1974, **27**, 209-214; (e) M. S. Gordon, *Chem. Phys. Lett.,* 1980, **76**, 163-168; (f) M. M. Francl, W. J. Pietro, W. J. Hehre, J. S. Binkley, D. J. DeFrees, J. A. Pople and M. S. Gordon, *J. Chem. Phys.,* 1982, **77**, 3654-3665; (g) R. C. Binning Jr. and L. A. Curtiss, *J. Comp. Chem.,* 1990, **11**, 1206-1216; (h) J.-P. Blaudeau, M. P. McGrath, L. A. Curtiss and L. Radom, *J. Chem. Phys.,* 1997, **107**, 5016-5021; (i) V. A. Rassolov, J. A. Pople, M. A. Ratner and T. L. Windus, *J. Chem. Phys.,* 1998, **109**, 1223-1229; (j) V. A. Rassolov, M. A. Ratner, J. A. Pople, P. C. Redfern and L. A. Curtiss, *J. Comp. Chem.,* 2001, **22**, 976-984.

[16] T. Clark, J. Chandrasekhar, G. W. Spitznagel and P. V. R. Schleyer, *J. Comp. Chem.,* 1983, **4**, 294-301.

[17] (a) S. F. Boys and F. Bernardi, *Mol. Phys.,* 1970, **19**, 553-566; (b) S. Simon, M. Duran and J. J. Dannenberg, *J. Chem. Phys.,* 1996, **105**, 11024-11031.

[18] J. Tomasi, B. Mennucci and R. Cammi, *Chem. Rev.,* 2005, **105**, 2999-3093.

[19] (a) W. Yang, E. R. Johnson, S. Keinan, P. Mori-Sánchez, J. Contreras-García and A. J. Cohen, *J. Am. Chem. Soc.,* 2010, **132**, 6498-6506; (b) W. Yang, J. Contreras-García, E. R. Johnson, S. Keinan, R. Chaudret, J.-P. Piquemal and D. N. Beratan, *J. Chem. Theory Comput.,* 2011, **7**, 625-632.

[20] W. Humphrey, A. Dalke and K. Schulten, `VMD -Visual Molecular Dynamics', *J. Mol. Graphics,* 1996, **14**, 33-38.

[21] CrysAlisPro-Data collection and integration software, version 1.171.37.35. Agilent Technologies UK Ltd, Oxford, UK, 2011.

[22] G. M. Sheldrick, *Acta Cryst.*, 2008, **A64**, 112-122.

[23] O. V. Dolomanov, L. J. Bourhis, R. J. Gildea, J. A. K. Howard and H. Puschmann, 'OLEX2: A complete structure solution, refinement and analysis program', *J. Appl. Cryst.,* 2009, **42**, 339-341.
[24] MERCURY: a) I. J. Bruno, J. C. Cole, P. R. Edgington, M. K. Kessler, C. F. Macrae, P. McCabe, J. Pearson and R. Taylor, *Acta Crystallogr.,* 2002, **B58**, 389-397; b) C. F. Macrae, P. R. Edgington, P. McCabe, E. Pidcock, G. P. Shields, R. Taylor, M. Towler and J. van de Streek, *J. Appl. Crystallogr.,* 2006, **39**, 453-457.